

California AHMCT Research Center  
University of California at Davis  
California Department of Transportation

**MODELING AND CONTROL  
OF  
MOBILE MANIPULATORS**

Jae H. Chung

AHMCT Research Report  
UCD-ARR-97-02-15-01

Final Report of Contract  
IA65X875 - T.O. 95-6

February 15, 1997

\* This work was supported by the California Department of Transportation (Caltrans)  
Advanced Highway Maintenance and Construction Technology Center at UC, Davis

## DISCLAIMER/DISCLOSURE

"The research reported herein was performed as part of the Advanced Highway Maintenance and Construction Technology Program (AHMCT), within the Department of Mechanical and Aeronautical Engineering at the University of California, Davis and the Division of New Technology and Materials Research at the California Department of Transportation. It is evolutionary and voluntary. It is cooperative venture of local, state and federal governments and universities"

"The contents of this report reflect the views of the author(s) who is (are) responsible for the facts and the accuracy of the data presented herein. The contents do not necessarily reflect the official views or policies of the STATE OF CALIFORNIA or FEDERAL HIGHWAY ADMINISTRATION and the UNIVERSITY OF CALIFORNIA. This report does not constitute a standard, specification, or regulation.

## ABSTRACT

A mobile manipulator is a robotic manipulator mounted upon a wheeled mobile platform. In recent years, interest in the area of mobile manipulators has increased significantly because of the mobility combined with the manipulation. Although significant amounts of research and development have been performed in the area of nonholonomic control of mobile robots and in the area of motion control of robotic manipulators, there is only limited literature available on control of mobile manipulators which combine those two functions.

There are several issues that contribute to the uniqueness of the mobile manipulator modeling and control problem. First, a wheeled mobile platform is subject to nonholonomic constraints. Therefore, the mobile manipulator which consists of a wheeled mobile platform and a robotic manipulator is also subject to nonholonomic constraints. Second, kinematic redundancy is created when a mobile platform and a multi-link manipulator are combined. Third, the mobile platform and the manipulator dynamically interact with each other.

This report is concerned with the modeling and control of mobile manipulators. The Lagrange-d'Alembert formulation is used to obtain a concise description of the dynamics of the system. Then, the solvability of tracking problems for a non-redundant mobile manipulators is investigated by using static input-output lin-

earization. Then, the complexity of the model is increased by introducing kinematic redundancy which is created when a multi-linked manipulator is used. The kinematic redundancy is resolved by decomposing the mobile manipulator into two subsystems; the mobile platform and the manipulator. Based on the redundancy resolution scheme, the nonlinear interaction control algorithm, in which the suitable controllers are designed for the two subsystems, is developed and applied to the redundant mobile manipulator.

When ideal kinematic constraints are violated due to wheel slip, modeling of wheeled mobile robots using a Lagrange-d'Alembert formulation is not valid. The wheel slip is modeled as a disturbance to the system and the tracking performance of the interaction controller is investigated in the presence of this disturbance.

## EXECUTIVE SUMMARY

A mobile manipulator is a robotic manipulator mounted upon a wheeled mobile platform. In recent years, interest in the area of mobile manipulators has increased significantly because of the mobility combined with the manipulation. Although significant amounts of research and development have been performed in the area of nonholonomic control of mobile robots and in the area of motion control of robotic manipulators, there is only limited literature available on control of mobile manipulators which combine those two functions.

There are several issues that contribute to the uniqueness of the mobile manipulator modeling and control problem. First, a wheeled mobile platform is subject to nonholonomic constraints. Therefore, the mobile manipulator which consists of a wheeled mobile platform and a robotic manipulator is also subject to nonholonomic constraints. Second, kinematic redundancy is created when a mobile platform and a multi-link manipulator are combined. Third, the mobile platform and the manipulator dynamically interact with each other.

This report discusses the modeling and control of mobile manipulators which consists of a robotic manipulator mounted upon a wheeled mobile platform. By neglecting slip of the wheeled platform's tires, nonholonomic constraints are introduced into the equations of motion which complicates the control problem. The dynamic

equations of the mobile manipulator are derived using the Lagrange-d'Alembert formulation. In this formulation, the equations of motion are projected onto the subspace of allowable motions. Then, the solvability of tracking problems for the mobile manipulator is investigated by using input-output feedback linearization. The feasibility of the control approach is demonstrated through computer simulation.

The complexity of the model is increased by introducing kinematic redundancy which is created when a multi-linked manipulator is used. The kinematic redundancy is resolved by decomposing the mobile manipulator into two subsystems; the mobile platform and the manipulator. According to the redundancy resolution scheme, the manipulator is commanded to follow the desired trajectory given in task space and the platform is responsible for positioning the manipulator at a specified point in the workspace to avoid singular configurations of the manipulator. This motivates the development of the interaction control algorithm in which two nonlinear controllers are designed for the subsystems based on the redundancy resolution scheme. The interaction controller consists of robust adaptive controller for the manipulator and nonlinear PD controller for the mobile platform. The simulation results demonstrate excellent tracking performance of the interaction controller.

While the interaction control algorithm represents the significant contributions to the area of the control of mobile manipulators subject to nonholonomic constraints and kinematic redundancy, consideration of wheel slip might be crucial for high load applications because wheel slip is expected to act as a disturbance to the system. The

dynamic equations of the wheeled mobile platform subject to wheel slip are derived and the interaction control is applied. The simulation results show degradation of tracking performance of the interaction controller in terms of convergence speed to the desired error bound. Our intention is to open up some potential problems of the interaction controller for high load and high speed applications of the mobile manipulators and suggest a robust control design for the platform as a part of future work.

# Contents

<b>List of Figures</b>	<b>x</b>
<b>1 Introduction</b>	<b>1</b>
1.1 Literature Search . . . . .	2
1.2 Stabilization of Mobile Robot as a Nonholonomic System . . . . .	3
1.3 Mobile Manipulators . . . . .	5
1.4 Discussion . . . . .	9
1.5 Preview of The report . . . . .	10
<b>2 Preliminaries</b>	<b>13</b>
2.1 Euler-Lagrange Equations . . . . .	14
2.2 Structural Properties . . . . .	16
2.3 Nonholonomic Constraints . . . . .	17
2.4 Control of Nonholonomic Systems . . . . .	22
<b>3 Non-redundant Mobile Manipulators</b>	<b>25</b>
3.1 Lagrange-d'Alembert Formulation . . . . .	26
3.2 Modeling of a Mobile Manipulator . . . . .	27
3.3 Control of the Mobile Manipulator . . . . .	34
3.4 Simulations . . . . .	39
<b>4 Interaction Control of Redundant Mobile Manipulators</b>	<b>59</b>
4.1 Redundancy Resolution . . . . .	60
4.2 Decentralization of Mobile Manipulator . . . . .	62
4.3 Modeling of the Mobile Manipulator . . . . .	63
4.4 Manipulability . . . . .	66
4.5 Nonlinear Controllers . . . . .	68
4.5.1 Robust Adaptive Control of Robotic Manipulator . . . . .	70
4.5.2 Nonlinear PD Control of Mobile Platform . . . . .	76
4.6 Interaction Control . . . . .	77

4.7	Simulations . . . . .	84
<b>5</b>	<b>Violation of Ideal Constraints</b>	<b>101</b>
5.1	Dynamic Modeling of Wheeled Mobile Robots . . . . .	102
5.2	Simulations . . . . .	107
<b>6</b>	<b>Conclusion</b>	<b>113</b>
6.1	Contributions of this Thesis . . . . .	113
6.2	Future Research . . . . .	115
<b>A</b>	<b>Sensors</b>	<b>123</b>
A.1	Angular Position Sensors . . . . .	123
A.1.1	Encoders . . . . .	124
A.1.2	Synchros . . . . .	124
A.1.3	Resolvers . . . . .	125
A.2	Angular Velocity Sensors . . . . .	125
A.2.1	DC Tachometer System . . . . .	125
A.3	Angular Acceleration Sensors . . . . .	126
A.3.1	Accelerometers . . . . .	126
A.3.2	Optical Gyros . . . . .	127

# List of Figures

2.1	A disk rolling on a horizontal plane . . . . .	19
3.1	Non-redundant mobile manipulator . . . . .	28
3.2	Structure of the control algorithm . . . . .	38
3.3	Simulation I - xy trajectory tracking in task space . . . . .	42
3.4	Simulation I - z trajectory tracking in task space . . . . .	42
3.5	Simulation I - xyz position error . . . . .	43
3.6	Simulation I - actuator torques of each wheel and the joint . . . . .	43
3.7	Simulation I - angular displacement of each wheel . . . . .	44
3.8	Simulation I - angular displacement of the joint . . . . .	44
3.9	Simulation I - heading angle of the platform . . . . .	45
3.10	Simulation II - xy trajectory tracking in task space . . . . .	46
3.11	Simulation II - z trajectory tracking in task space . . . . .	46
3.12	Simulation II - xyz position error . . . . .	47
3.13	Simulation II - actuator torques of each wheel and the joint . . . . .	47
3.14	Simulation II - angular displacement of each wheel . . . . .	48
3.15	Simulation II - angular displacement of the joint . . . . .	48
3.16	Simulation II - heading angle of the platform . . . . .	49
3.17	Simulation III - xy trajectory tracking in task space . . . . .	50
3.18	Simulation III - z trajectory tracking in task space . . . . .	50
3.19	Simulation III - xyz position error . . . . .	51
3.20	Simulation III - actuator torques of each wheel and the joint . . . . .	51
3.21	Simulation III - angular displacement of each wheel . . . . .	52
3.22	Simulation III - angular displacement of the joint . . . . .	52
3.23	Simulation III - heading angle of the platform . . . . .	53
3.24	Simulation IV - xy trajectory tracking in task space . . . . .	54
3.25	Simulation IV - z trajectory tracking in task space . . . . .	54
3.26	Simulation IV - xyz position error . . . . .	55
3.27	Simulation IV - actuator torques of each wheel and the joint . . . . .	55
3.28	Simulation IV - angular displacement of each wheel . . . . .	56

3.29	Simulation IV - angular displacement of the joint . . . . .	56
3.30	Simulation IV - heading angle of the platform . . . . .	57
4.1	The redundant mobile manipulator . . . . .	61
4.2	The adaptive controller . . . . .	71
4.3	The interaction control . . . . .	78
4.4	Simulation I - position error in task space . . . . .	88
4.5	Simulation I - actuator torque of each joint of the manipulator . . . . .	88
4.6	Simulation I - actuator torque of each wheel of the mobile platform . . . . .	89
4.7	Simulation I - angular displacement of each joint . . . . .	89
4.8	Simulation I - angular displacement of each wheel . . . . .	90
4.9	Simulation I - xy position of the platform . . . . .	90
4.10	Simulation I - heading angle of the platform . . . . .	91
4.11	Simulation II - position error in task space . . . . .	92
4.12	Simulation II - actuator torque of each joint of the manipulator . . . . .	92
4.13	Simulation II - actuator torque of each wheel of the mobile platform . . . . .	93
4.14	Simulation II - angular displacement of each joint . . . . .	93
4.15	Simulation II - angular displacement of each wheel . . . . .	94
4.16	Simulation II - xy position of the platform . . . . .	94
4.17	Simulation II - heading angle of the platform . . . . .	95
4.18	Simulation III - position error in task space . . . . .	96
4.19	Simulation III - actuator torque of each joint of the manipulator . . . . .	96
4.20	Simulation III - actuator torque of each wheel of the mobile platform . . . . .	97
4.21	Simulation III - angular displacement of each joint . . . . .	97
4.22	Simulation III - angular displacement of each wheel . . . . .	98
4.23	Simulation III - xy position of the platform . . . . .	98
4.24	Simulation III - heading angle of the platform . . . . .	99
5.1	Wheeled mobile robot . . . . .	103
5.2	Position error in task space . . . . .	110
5.3	Actuator torque of each joint of the manipulator . . . . .	110
5.4	Actuator torque of each wheel of the mobile platform . . . . .	111
5.5	Angular displacement of each joint of the manipulator . . . . .	111
5.6	XY position of the platform . . . . .	112
5.7	Heading angle of the platform . . . . .	112

# Chapter 1

## Introduction

Conventional robotic manipulators are mounted on a fixed base so that they can withstand the forces and torques applied to the base when they are subject to payloads. Tasks involving such a fixed-base manipulator must be carefully planned within the limited volume of the workspace so that they can be carried out in an efficient manner. Furthermore, the situation can become even more restrictive if a dexterous manipulation is required because the actual workspace, in general, is only a small portion of the total workspace.

In recent years, interest in the area of mobile manipulators has increased significantly in the industrial, space, and public service applications because the mobility combined with the dexterous manipulation provides increased efficiency and capabilities in various tasks (e.g., repair, material transfer and delivery, maintenance, or chemical handling etc). Although significant amounts of research and development

have been performed in the area of motion planning for mobile robots and in the area of control of robotic manipulators, very little has been reported on the topic of coupling these two functions for the purpose of developing an autonomous robot with combined large-scale-mobility and dexterous manipulation.

Mobile manipulators bring about a number of challenging problems in addition to simply increasing the structural complexity. First, a wheeled mobile robot introduces nonholonomic constraints to the equations of motion. Second, kinematic redundancy is created when a multi-link manipulator is mounted on a mobile robot. Third, the mobile platform and manipulator dynamically interact with each other. The objective of this research is to address the complexities of modeling and control of mobile manipulators.

## 1.1 Literature Search

The study of the modeling and control of mobile manipulators spans several different research domains. Major issues related to the topic of this research include the kinematic and dynamic modeling of a wheeled mobile platform subject to nonholonomic constraints, the coordination strategy of the mobile manipulator as a means of redundancy resolution, the dynamic interaction of the mobile platform and the manipulator, and the issues of the control of the mobile manipulator.

In the following sections, the previous work related to these issues is reviewed. The control and path planning problems of wheeled mobile robots have recently

drawn significant attention in the nonlinear control community because of their unique properties due to the presence of nonholonomic constraints. Therefore, a review on nonholonomic systems with emphasis on the control characteristics of wheeled mobile platforms is given in some detail. However, only limited literature is available on the control of a mobile manipulator although the advantages of a mobile manipulator over a fixed-base manipulator have been widely acknowledged.

A typical example of a nonholonomic system is a rigid disk rolling on a horizontal plane without slippage (Murray et al., 1994). Other examples of nonholonomic systems can be found in underwater vehicles (Nakamura and Mukherjee, 1993; Sordalen et al., 1993), robotic fingers (Kerr and Roth, 1986; Li and Canny, 1990), space manipulators (Vafa and Dubowsky, 1987; Nakamura and Mukherjee, 1989; Papadopoulos, 1993), falling cat and astronaut maneuvering (Kane and Scher, 1969; Kane, 1972; Fernandes et al., 1993). Also surveys of the recent developments in nonholonomic motion research and the nonholonomic behavior of robotic systems are given by Li and Canny (1993) and Murray et al. (1994).

## 1.2 Stabilization of Mobile Robot as a Nonholonomic System

Mechanical systems with nonholonomic constraints have the property that the number of independent position coordinates exceeds the number of independent ve-

locities. Typical examples are wheeled mobile robots in which the contacts between the wheels and the ground can be modeled as nonholonomic constraints, if wheel slip is neglected.

Most common objectives of the control of the mobile robots are motion planning and stabilization to an equilibrium state, the latter of which is pursued in this report. Brockett (1983) proved that the full state vector cannot be made asymptotically stable by using smooth time-invariant state-feedback control laws. Therefore, the control objectives cannot be solved using the well-established nonlinear control methods such as feedback linearization. Based on Brockett's theorem, new approaches have been developed to avoid violating his claim.

Samson and Ait-Abderrahin (1991) showed that there is no pure static state feedback law that stabilizes the system around a given terminal configuration which includes both position and orientation. Campion et al. (1991) and Samson and Ait-Abderrahin (1991) showed that feedback stabilization of the position of any mobile robot's point remains possible by using input-output linearization. Walsh et al. (1994) developed a new technique that gives an explicit control law which locally exponentially stabilizes the system to the desired trajectory. Pomet (1992a) used a time-varying state feedback control to stabilize a mobile robot to a point. Also, Pomet et al. (1992b) proposed a hybrid strategy to improve the convergence speed, in which a time-invariant feedback is used in the neighborhood of the desired point. Sarkar et al. (1994) investigated the trajectory tracking and path following problems of mobile

robots in the context of mechanical systems subject to rolling contacts. Jagannathan and Lewis (1994) showed that input-output feedback linearization with a suitable choice of a gradient-based control law can be used to solve the motion planning problem. Sordalen and Egeland (1995) demonstrated that global and asymptotical stability with exponential convergence is achieved about any desired configuration by using a nonsmooth, time-varying feedback control law which depends on a constant function except at predefined instants of time where the function is recomputed as a nonsmooth function of the state. D'Andrea-Novel et al. (1995) studied the tracking problem with stability of a reference trajectory, by means of linearizing static and dynamic state feedback laws. Also, they gave conditions to avoid possible singularities of the feedback law. Canudas de Wit and Sordalen (1992) proposed a piecewise smooth controller to render the origin exponentially stable for any initial condition. Using a two-wheeled model, they showed that the convergent speed is faster than those using time-varying feedback. Although the feedback law was not differentiable at some points, it was proven that the motion of the vehicle is smooth even when it passes the non-differentiable points.

### 1.3 Mobile Manipulators

Our use of the term "mobile manipulator" relates to terrestrial mobile manipulators which are typically an articulated manipulator mounted on a wheeled mobile vehicle. However, comparison to nonterrestrial mobile manipulators, namely under-

water vehicle and space manipulators, brings a useful insight with regard to certain issues such as the analysis of dynamic interactions or different bandwidths. However, this work does not consider the effects of gravity found in terrestrial applications.

First, the previous work on mobile manipulators which treats the dynamic interaction between a platform and a manipulator is discussed. Then, various control and coordination algorithms specifically developed for mobile manipulators using optimization methods are discussed. Lastly, control methods for space manipulators are reviewed with emphasis on how to compensate motion disturbances between the platform and the manipulator.

Wiens (1989) considered a single-linked manipulator on a planar mobile platform, and presented a technique for determining the dynamic coupling effect between the mobile platform and robotic arm manipulation. Jang and Wiens (1994) studied a similar model in Wiens (1989) and developed passive control systems (various spring-damper combinations) to reduce the dynamic coupling between the two subsystems. Using the technique which is an extension of the energy stability level concept, Ghamsepoor and Sepehri (1995) developed a means to quantify stability measures applicable to mobile manipulators. Joshi and Desrochers (1986) represented the motion due to the vehicle by an angular displacement (disturbance) to a two-linked arm. Their work took into account the effects of platform motion on the control of the robot arm relative to the platform. However, the control of the mobile platform was excluded. Liu and Lewis (1992) described a robust controller for a mobile robot by considering the

platform and the manipulator as two separate systems. Their model, used for simulation, consists of a two-link manipulator attached on a planar base in which the angular motion of the base is excluded, at least in their simulation, although it is included in the equations of motion. Dubowsky and Tanner (1987) studied the compensation of a dynamic disturbance caused by vehicle motion to a manipulator by deriving a set of linearized equations of motion for a 3-DOF planar manipulator atop a moving platform, and verified the efficacy of a dynamic compensation through simulation and experiments. Hootsmanns and Dubowsky (1991) derived the Mobile Manipulator Jacobian Transpose Algorithm with which a manipulator achieves a desired trajectory in the presence of dynamic disturbances from a softly-suspended platform. It was shown that, even with the limited sensing capability, the system is able to perform reasonably well with the proposed algorithm. However, only holonomic constraints are taken into account. Yamamoto and Yun (1994) studied a two-linked planar mobile manipulator subject to nonholonomic constraints and developed a coordination algorithm based on the concept of preferred operating region. However, if the manipulator reaches up to perform tasks in vertical coordinates, any motion from the mobile platform will not be able to bring the manipulator into the preferred operating region.

For the coordination and control of mobile manipulators, Seraji (1993) treated the base degrees-of-mobility equally with the arm degrees-of-manipulation, and solved the redundancy by introducing a user-defined additional task variable. Pin and Culioli

(1992) defined a weighted multi-criteria cost function which is then optimized using Newton's algorithm. Pin et al. (1994) formulated the coordination of mobility and manipulation as a nonlinear optimization problem. A general cost function for point-to-point motion in Cartesian space is defined and is minimized using the simulated annealing method. Miksch and Schroeder (1992) proposed a controller design for mobile manipulators. The controller consists of a feedforward part which executes an off-line optimization along the desired trajectory and a feedback part which realizes decoupling and compensation of the tracking errors. As a performance criteria to be minimized for the static optimization, they used the manipulability measure, joint ranges, kinetic energy of the system, and actuator torques. This approach is computationally expensive and is suitable for global motion planning in which the desired trajectory to be followed is precisely known a priori. Wang and Kumar (1993) solved the kinematic redundancy of a wheeled mobile manipulator with a local coordination technique which allocates the end-effector motion between the manipulator and the platform by specifying compliance functions for each joint.

There has been ample literature on space manipulators. There exist two basic approaches. The first controls the manipulator by assuming that the reaction wheels or jets can be used to maintain the position and the orientation of the platform (Longman et al., 1990). The other controls both end-effector motion and satellite attitude using only manipulator torques (Vafa and Dubowsky, 1987; Nakamura and Mukherjee, 1989; Umetani and Yoshida, 1989; Papadopoulos and Dubowsky, 1991;

Nenchev et al., 1992; Yamada, 1993). The work of Egeland and Sagli (1993) is an exception which is more efficient in terms of energy consumption than the first approach (Longman et al., 1990) and more flexible than the second approach (Vafa and Dubowsky, 1987; Nakamura and Mukherjee, 1989). In their algorithm, the manipulator with high bandwidth is commanded to keep track of a desired end-effector trajectory while the satellite with low bandwidth is controlled so that the manipulator is maintained near the center of the workspace. Therefore the concept used for the coordination of a manipulator and a platform is similar to Yamamoto and Yun (1994) in that both have used lowpass filtered inputs to a platform and have utilized similar redundancy resolution techniques although they differ on the design of the controllers. Spofford and Akin (1990) proposed a hybrid coordination algorithm which combines the reaction compensation method which does not deplete the fuel of the spacecraft and the pseudo-inverse method which assumes full actuation of the entire spacecraft/manipulator system. The transition between the two modes is determined based on a task-dependent potential function.

## 1.4 Discussion

The motivation for much of the previous work stems from identifying the stability criteria so that the vehicle does not overturn. The work addressing mobile manipulators, e.g., off-line optimization methods (Pin and Culioli, 1992; Pin et al., 1994; Miksch and Schroeder, 1992; Wang and Kumar, 1993), tends to focus on the method

to solve the redundancy created by the systems, and ignores the nonholonomic characteristic of the vehicle. The previous work (Wiens, 1989; Jang and Wiens, 1994; Ghamsepoor and Sepehri, 1995) on the dynamic interaction mostly focuses on identifying stability criteria of tip-over. The work reported in Joshi and Desrochers (1986), Liu and Lewis (1990), Hootsmanns and Dubowsky (1991) and Yamamoto and Yun (1994) analyzes the dynamic interaction in an explicit form. However, the models described in the work have only planar motion, so that the effectiveness of the control algorithms need to be validated using a spatial mobile manipulator model. In this report, we attempt to develop the nonlinear control algorithm for a general configuration of a spatial mobile manipulator subject to nonholonomic constraints and kinematic redundancy with model uncertainty such as parametric uncertainty and unmodeled dynamics. Also, the control of a realistic model of mobile manipulator subject to wheel slip is investigated.

## 1.5 Preview of The report

In Chapter 2, some basic properties of robotic manipulators and nonholonomic systems are reviewed.

The actual research work begins in Chapter 3 with the modeling and control of a spatial mobile manipulator subject to nonholonomic constraints. First, the Lagrange-d'Alembert formulation is employed in modeling the nonholonomic system. Then, a nonlinear control law is derived based on the feedback linearization method.

In Chapter 4 the interaction control algorithm is developed for a general configuration of spatial mobile manipulator subject to nonholonomic constraints, kinematic redundancy and motion disturbance. First, coordination strategies are discussed as a means of resolving the kinematic redundancy created by combining a mobile platform with a multi-link manipulator. Second, based on the redundancy resolution schemes, the interaction control law is proposed, in which the controller is designed for each of two primary subsystems; the mobile platform and the multi-link manipulator.

In Chapter 5, a dynamic vehicle model is derived and the interaction controller, designed in Chapter 4, is tested for the redundant mobile manipulator.

Chapter 6 gives a brief summary of this report and conclusions. As in most studies, this work has answered some questions and has raised a wealth of additional questions. Accordingly, Chapter 6 also presents a number of issues that can be the subject of future work.

## Chapter 2

### Preliminaries

Typically, a mobile manipulator consists of a mobile robot and a robotic manipulator. These mechanical systems differ substantially in their task assignments and dynamic characteristics. Hence, the study of the modeling and control of mobile manipulators spans different research domains. In this chapter, some areas of robotics which are relevant to the current research are presented. First, Euler-Lagrange equations of motion are reviewed (Haug, 1989; Greenwood, 1988). Then, several important properties of robotic manipulators for control applications are stated. Also, a short description of nonholonomic systems is given. The detailed derivation of the motion equations of mobile manipulators is left to the following chapter.

## 2.1 Euler-Lagrange Equations

A standard method for deriving the dynamic equations of mechanical systems is via the so-called Euler-Lagrange equations which are expressed as

$$\frac{d}{dt} \frac{\partial L}{\partial \dot{q}} - \frac{\partial L}{\partial q} = \tau \quad (2.1)$$

where  $q = (q_1, \dots, q_n)^T$  is a set of generalized coordinates for the system,  $L$ , the Lagrangian, is the difference,  $K - V$ , between the kinetic energy  $K$  and the potential energy  $V$ , and  $\tau = (\tau_1, \dots, \tau_n)^T$  is the vector of generalized forces acting on the system. An important special case arises when the potential energy  $V = V(q)$  is independent of  $\dot{q}$ , and the kinetic energy is a quadratic function of the vector  $\dot{q}$  of the form

$$\begin{aligned} K &= \frac{1}{2} \sum_{i,j}^n m_{ij}(q) \dot{q}_i \dot{q}_j \\ &= \frac{1}{2} \dot{q}^T M(q) \dot{q} \end{aligned} \quad (2.2)$$

where the  $n \times n$  inertia matrix  $M(q)$  is symmetric and positive definite for each  $q \in \mathbb{R}^n$ . The generalized coordinates in this case are the joint positions.

The Euler-Lagrange equations for such a system can be derived as follows. Since

$$L = \frac{1}{2} \sum_{i,j}^n m_{ij}(q) \dot{q}_i \dot{q}_j - V(q), \quad (2.3)$$

we have

$$\frac{\partial L}{\partial \dot{q}_k} = \sum_j m_{kj}(q) \dot{q}_j \quad (2.4)$$

and

$$\begin{aligned}\frac{d}{dt} \frac{\partial L}{\partial \dot{q}_k} &= \sum_j m_{kj}(q) \ddot{q}_j + \sum_j \frac{d}{dt} m_{kj}(q) \dot{q}_j \\ &= \sum_j m_{kj}(q) \ddot{q}_j + \sum_{i,j} \frac{\partial m_{kj}}{\partial q_i} \dot{q}_i \dot{q}_j.\end{aligned}\quad (2.5)$$

Also

$$\frac{\partial L}{\partial q_k} = \frac{1}{2} \sum_{i,j} \frac{\partial m_{ij}}{\partial q_k} \dot{q}_i \dot{q}_j. \quad (2.6)$$

Thus, the Euler-Lagrange equations can be written as

$$\sum_j m_{kj} \ddot{q}_j + \sum_{i,j} \left( \frac{\partial m_{kj}}{\partial q_i} - \frac{1}{2} \frac{\partial m_{ij}}{\partial q_k} \dot{q}_i \dot{q}_j \right) - \frac{\partial V}{\partial q_k} = \tau_k, \quad k = 1, \dots, n. \quad (2.7)$$

By interchanging the order of summation in the second term above and by taking advantage of the symmetry of the inertia matrix, we can show that

$$\sum_{i,j} \left( \frac{\partial m_{kj}}{\partial q_i} - \frac{1}{2} \frac{\partial m_{ij}}{\partial q_k} \dot{q}_i \dot{q}_j \right) = \sum_{i,j} \frac{1}{2} \left( \frac{\partial m_{kj}}{\partial q_i} + \frac{\partial m_{ki}}{\partial q_j} - \frac{\partial m_{ij}}{\partial q_k} \right) \dot{q}_i \dot{q}_j. \quad (2.8)$$

The coefficients

$$c_{ijk} = \sum_{i=1}^n \frac{1}{2} \left( \frac{\partial m_{kj}}{\partial q_i} + \frac{\partial m_{ki}}{\partial q_j} - \frac{\partial m_{ij}}{\partial q_k} \right) \quad (2.9)$$

are known as Christoffel symbols of the first kind. If we set

$$\phi_k = \frac{\partial P}{\partial q_k}, \quad (2.10)$$

then we can write the Euler-Lagrange equations, Eq. (2.7), as

$$\sum_j m_{kj}(q) \ddot{q}_j + \sum_{i,j} c_{ijk}(q) \dot{q}_i \dot{q}_j + \phi_k(q) = \tau_k, \quad k = 1, \dots, n. \quad (2.11)$$

In the above equation, there are three types of terms. The first type involve the second derivative of the generalized coordinates. The second type are quadratic terms in the first derivatives of  $q$ , where the coefficients may depend on  $q$ . These are further classified into two types. Terms involving a product of the type  $\dot{q}_i^2$  are called centrifugal, while those involving a product of the type  $\dot{q}_i\dot{q}_j$ , where  $i \neq j$ , are called Coriolis terms. The third type of terms are those involving only  $q$  but not its derivatives. Clearly the latter arise from differentiating the potential energy. It is common to write Eq. (2.11) in matrix form as

$$M(q)\ddot{q} + C(q, \dot{q})\dot{q} + G(q) = \tau \quad (2.12)$$

where the  $kj$ th element of the matrix  $C(q, \dot{q})$  is defined as

$$c_{kj} = \sum_{i=1}^n c_{ijk}(q)\dot{q}_i = \sum_{i=1}^n \frac{1}{2} \left( \frac{\partial m_{kj}}{\partial q_i} + \frac{\partial m_{ki}}{\partial q_j} - \frac{\partial m_{ij}}{\partial q_k} \right) \dot{q}_i. \quad (2.13)$$

## 2.2 Structural Properties

Although the equations of motion Eq. (2.12) are complex, nonlinear equations for all but the simplest robots, they have several fundamental properties which can be exploited to facilitate control system design. These properties are stated as follows:

*Property 1.* The inertia matrix  $M(q)$  is symmetric, positive definite, and both  $M(q)$  and  $M(q)^{-1}$  are uniformly bounded as a function of  $q \in \mathbb{R}^n$ . Strictly speaking, boundedness of the inertia matrix requires, in general, that all joints be revolute.

*Property 2.* There is an independent control input for each degree of freedom.

*Property 3.* All of the constant parameters of interest such as link masses, moments of inertias, etc., appear as coefficients of known functions of the generalized coordinates. By defining each coefficient as a separate parameter, a linear relationship results so that we may write the dynamic equations, Eq. (2.12), as

$$M(q)\ddot{q} + C(q, \dot{q})\dot{q} + G(q) = Y(q, \dot{q}, \ddot{q})a = \tau \quad (2.14)$$

where  $Y(q, \dot{q}, \ddot{q})$  is an  $n \times r$  matrix of known functions, known as the regressor, and  $a$  is an  $r$ -dimensional vector of parameters.

*Property 4.* Define the matrix

$$N(q, \dot{q}) = \dot{M}(q) - 2C(q, \dot{q}). \quad (2.15)$$

Then  $N(q, \dot{q})$  is skew symmetric, i.e. the components  $n_{jk}$  of  $N$  satisfy  $n_{jk} = -n_{kj}$ .

*Property 5.* The dynamic equations (2.12) of a rigid robot define a passive mapping  $\tau \rightarrow \dot{q}$ , i.e.

$$\langle \dot{q} | \tau \rangle_T = \int_0^T \dot{q}^T \tau dt \geq -\beta \quad (2.16)$$

for some  $\beta > 0$ , for all  $T$ .

## 2.3 Nonholonomic Constraints

A holonomic system is a dynamic system that is subjected to holonomic constraints. Holonomic constraints in a mechanical system are characterized by algebraic equations in terms of position variables (or can be integrated to position-level

equations if initially described by velocity-level equations). Mechanical systems with holonomic constraints are typically treated by eliminating certain variables (generalized coordinates) from the equations of motion. The elimination process requires solving certain components of variables in terms of the other variables. Assuming the holonomic constraints are independent and continuously differentiable, the elimination is analytically possible.

Alternatively, holonomic constraints may be differentiated once with respect to time and can be represented at the velocity level, in the same form as nonholonomic constraints are represented.

Since we are working with mechanical systems, we will assume the existence of a Lagrangian function  $L(q, \dot{q})$ . In the absence of constraints, the robot's dynamic equations can be derived from the Euler-Lagrange equations (see Eq. (2.1)). Given  $k$  such constraints, we can write them as a vector-valued set of  $k$  equations:

$$C_j^i(q)\dot{q} = 0, \quad i = 1, \dots, k \quad (2.17)$$

where  $C(q) \in \mathbb{R}^{k \times n}$  represents a set of  $k$  velocity constraints. A constraint of this form is called a Pfaffian constraint. We assume that the constraints are pointwise linearly independent and hence that  $C(q)$  has full row rank. This class of constraints includes nonholonomic constraints. Nonholonomic systems most commonly arise in finite dimensional mechanical systems where constraints are imposed on the motion that are not integrable, i.e. the constraints cannot be written as time derivatives of some function of the generalized coordinates. Such constraints can usually be

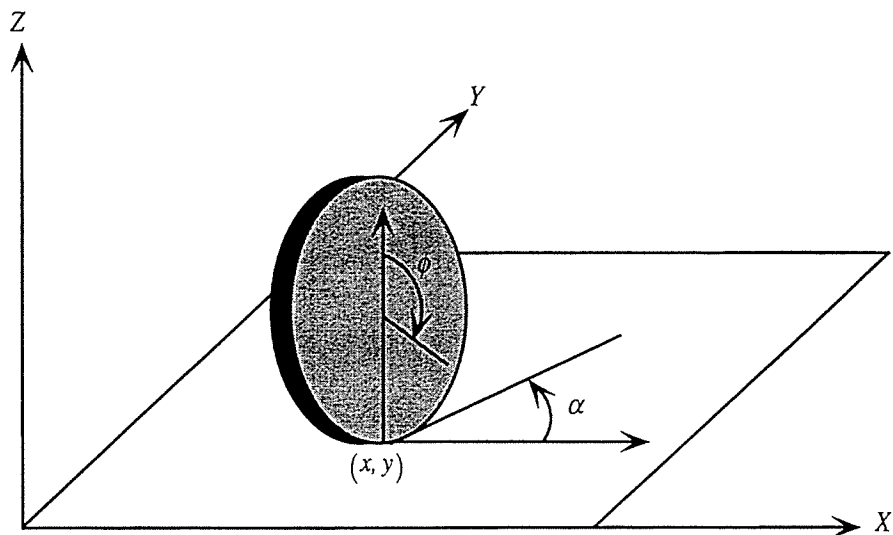


Figure 2.1: A disk rolling on a horizontal plane

expressed in terms of a nonintegrable linear velocity relationship. In other words, a Pfaffian constraint which is not integrable is an example of a nonholonomic constraint.

As an example of a nonholonomic constraint, consider a rolling disk without slipping on the horizontal plane as shown in Figure 2.1. Let us define the configuration vector as

$$q = \begin{bmatrix} x \\ y \\ \alpha \\ \phi \end{bmatrix} \quad (2.18)$$

where  $x$  and  $y$  give the location of the point of contact,  $\phi$  is the angle of rotation with respect to the perpendicular axis through its center, and  $\alpha$  is the angle between the

yz plane and the plane of the disk. The requirement of rolling without slipping can be written as a set of nonintegrable velocity constraints as follows:

$$\dot{x} - r\dot{\phi}\sin\alpha = 0 \quad \text{and} \quad (2.19)$$

$$\dot{y} - r\dot{\phi}\cos\alpha = 0. \quad (2.20)$$

Alternatively, the velocity constraints can be rewritten in the form of Eq. (2.17) as

$$C(q)\dot{q} = \begin{bmatrix} 1 & 0 & 0 & -r\sin\alpha \\ 0 & 1 & 0 & -r\cos\alpha \end{bmatrix} \dot{q} = 0. \quad (2.21)$$

Eqs. (2.19) and (2.20), the equations of constraint, are independent. Thus, since there are four coordinates and two equations of constraint, the system has only two degrees of freedom. Particularly, note that at a given configuration  $q$ , only those motions which satisfy the instantaneous nonholonomic constraints are feasible, which is given by the null space of the constraint matrix,  $C(q)$ .

The constraints can be incorporated into the dynamics through the use of Lagrange multipliers. That is, Eq. (2.1) is modified by adding a force of constraint with an unknown multiplier,  $\lambda$  defined as

$$\lambda = \begin{bmatrix} \lambda_h^T \\ \lambda_n^T \end{bmatrix} \quad (2.22)$$

where  $\lambda_h$  is the  $l$  vector of constraint force associated with the holonomic constraints, and  $\lambda_n$  is the  $m$  vector of constraint force associated with the nonholonomic constraints.

Then, Eq. (2.1) can be rewritten as

$$\frac{d}{dt} \frac{\partial L}{\partial \dot{q}} - \frac{\partial L}{\partial q} + C^T(q)\lambda - \tau = 0 \quad (2.23)$$

where

$$C(q) = \begin{bmatrix} C_h(q) \\ C_n(q) \end{bmatrix}. \quad (2.24)$$

In Eq. (2.24),  $C_h$  represents  $l$  holonomic constraints and  $C_n$  is a  $m \times n$  nonholonomic constraint matrix. Note, as mentioned earlier in this section, that in the presence of  $l$  holonomic constraints, we, in principle, may eliminate  $l$  Lagrange coordinates from the equations of motion, and at the same time eliminate the constraint force vector  $\lambda_h$ . The elimination process requires solving  $l$  Lagrange coordinates in terms of the others from the holonomic constraint equations.

We can derive an explicit formula for the Lagrange multipliers. The equations of motion can be written as

$$M(q)\ddot{q} + N(q, \dot{q}) + C^T(q)\lambda = \tau \quad (2.25)$$

where  $\tau$  corresponds to the vector of external forces and  $N(q, \dot{q})$  includes nonconservative forces as well as gravitational forces. It can be shown that by differentiating the constraint Eq. (2.17) and substituting the resulting equation into Eq. (2.25), the Lagrange multiplier is written as

$$\lambda = (CM^{-1}C^T)^{-1}(CM^{-1}(\tau - N) + \dot{C}\dot{q}) \quad (2.26)$$

where the configuration dependent matrix is full rank if the constraints are independent. The equations of motion are now given by Eq. (2.25) with the Lagrange multiplier defined in Eq. (2.26).

## 2.4 Control of Nonholonomic Systems

The models of the nonholonomic systems can be classified into kinematic models and dynamic models. These two models possess similar state-space structure as follows:

### Kinematic Models

$$\dot{x} = g_1(x)u_1 + \cdots + g_m(x)u_m, \quad (2.27)$$

where  $x$  is the state vector,  $u_i$ ,  $i = 1, \dots, m$ , are the controls, and  $g_i$  are smooth, linearly independent vector fields on  $\mathbb{R}^n$ .

### Dynamic Models

$$\dot{x} = g_1(x)v_1 + \cdots + g_m(x)v_m, \quad (2.28)$$

$$\dot{v}_i^{r_i} = u_i, \quad i = 1, \dots, m, \quad (2.29)$$

where  $x$  is the state vector,  $v_i$  is a  $m \times 1$  vector and  $r_i$  denote the order of time differentiation.

The controls of kinematic models are velocity variables while those of dynamic models are generalized force variables. Note that Eq. (2.27) is actually the kinematic constraints on the motion.

The most common control objectives of nonholonomic systems can be categorized into two areas: path planning and stabilization to an equilibrium state. Path planning problems are concerned with finding a path that connects an initial configuration to the final configuration and satisfies all the holonomic and nonholonomic conditions for the system. Stabilization problems are concerned with constructing a feedback controller that drives the system to the desired target while maintaining the boundedness of all the states.

## Chapter 3

# Non-redundant Mobile

# Manipulators

The objective of this chapter is to discuss modeling and control of a non-redundant spatial mobile manipulator. A wheeled mobile robot introduces nonholonomic constraints to the equations of motion when wheel slip is neglected. Therefore, the mobile manipulator which consists of a wheeled mobile platform and a robotic manipulator is also subject to nonholonomic constraints. We begin by deriving the dynamic equations of the mobile manipulator using the Lagrange-d'Alembert formulation which represents the motion of the system by projecting the equations of motion onto the subspace of allowable motions. Then, the solvability of tracking problems for non-redundant mobile manipulators is investigated by using static feedback linearization.

### 3.1 Lagrange-d'Alembert Formulation

The Lagrange-d'Alembert formulation of the dynamics represents the motion of the system by projecting the equations of motion onto the subspace of allowable motions. In doing so, it is possible to get a concise description which is in a form well suited for closed-loop control.

Let the virtual displacement  $\delta q$  be a vector which satisfies  $C(q)\delta q = 0$ . D'Alembert's principle states that the forces of constraint do no virtual work. Hence,  $(C^T(q)\lambda) \cdot \delta q = 0$  for  $C(q)\delta q = 0$ . Since  $(C^T(q)\lambda) \cdot \delta q = 0$ , Eq. (2.23) becomes

$$\left( \frac{d}{dt} \frac{\partial L}{\partial \dot{q}} - \frac{\partial L}{\partial q} - \tau \right) \cdot \delta q = 0 \quad (3.1)$$

where

$$C(q)\delta q = 0. \quad (3.2)$$

Eqs. (3.1) and (3.2) are called the Lagrange-d'Alembert equations. In the case where the constraint is integrable, these equations agree with those obtained by substituting the constraint into the Lagrangian and then using the unconstrained version of Lagrange's equations. If  $q = (q_1, q_2) \in \mathbb{R}^{n-k} \times \mathbb{R}^k$  and the constraints have the form  $\dot{q}_1 = A(q)\dot{q}_2$ , then the equations of motion can be written as

$$\left( \frac{d}{dt} \frac{\partial L}{\partial \dot{q}_1} - \frac{\partial L}{\partial q_1} - \tau_1 \right) + A^T \left( \frac{d}{dt} \frac{\partial L}{\partial \dot{q}_2} - \frac{\partial L}{\partial q_2} - \tau_2 \right) = 0. \quad (3.3)$$

This reduction process of the motion equations is illustrated in modeling the mobile manipulator.

### 3.2 Modeling of a Mobile Manipulator

The mobile manipulator to be considered is supported by two independently driven wheels with a common platform-fixed axis and two passive, self-aligning wheels. The wheeled platform is modeled as a nonholonomic system in which slip is neglected due to slow motions. Therefore, the wheeled platform consists of three degrees-of-freedom which are reduced to two degrees-of-freedom due to the no-slip condition. The following notation is used in deriving the equations of motion:

$q_1$ : the angular displacement of the right driving wheel,

$q_2$ : the angular displacement of the left driving wheel,

$q_3$ : the joint angle of the manipulator,

$\theta$ : the heading angle of the platform,

$m_p$ : the mass of the platform,

$m_m$ : the mass of the manipulator,

$m_w$ : the mass of the each driving wheel,

$I_p$ : the moment of inertia of the platform,

$I_m$ : the moment of inertia of the manipulator,

$I_w$ : the moment of inertia of the each driving about the center of the mass,

$I_d$ : the moment of inertia of the wheel about the wheel diameter,

$P_w$ : the mid-point of the wheel base line,

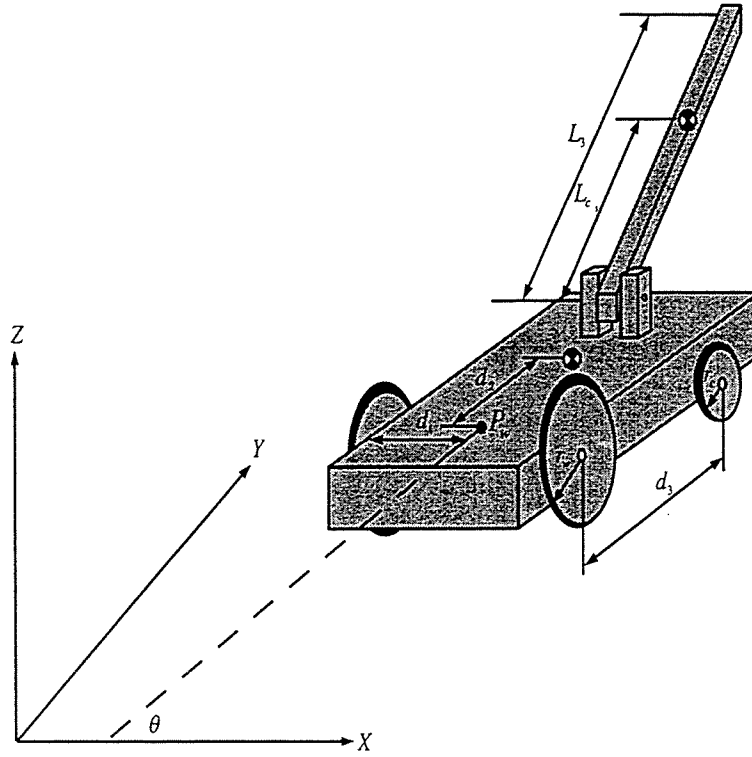


Figure 3.1: Non-redundant mobile manipulator

$d_1$ : the half length of the base line, and

$d_2$ : the distance between the center of mass and  $P_w$ .

The mobile platform is subject to one holonomic constraint and two nonholonomic constraints written as

$$\theta = h(q_1 - q_2), \quad (3.4)$$

$$\dot{y}_w \cos \theta - \dot{x}_w \sin \theta = 0, \quad \text{and} \quad (3.5)$$

$$\dot{x}_w \cos \theta + \dot{y}_w \sin \theta = \frac{1}{2} r_w (\dot{q}_1 + \dot{q}_2) \quad (3.6)$$

where  $x_w$  and  $y_w$  denote the position coordinates of  $P_w$ .

We may write Eqs. (3.5) and (3.6) in the form of Eq. (2.17) with a vector  $q$  defined as

$$q = \begin{bmatrix} q_1 \\ q_2 \\ q_3 \\ x_w \\ y_w \end{bmatrix} \quad (3.7)$$

and  $C(q)$  is given by

$$C(q) = \begin{bmatrix} 0 & 0 & 0 & -\sin \theta & \cos \theta \\ \frac{1}{2}r_w & \frac{1}{2}r_w & 0 & -\cos \theta & -\sin \theta \end{bmatrix}. \quad (3.8)$$

Eq. (3.5) is rewritten as

$$\dot{x}_w \sin \theta = \dot{y}_w \cos \theta \quad (3.9)$$

and substituting Eq. (3.9) into Eq. (3.6) and rearranging the resulting equations gives a set of velocity constraints

$$\dot{x}_w = d_1 h(\dot{q}_1 + \dot{q}_2) \cos \theta \quad \text{and} \quad (3.10)$$

$$\dot{y}_w = d_1 h(\dot{q}_1 + \dot{q}_2) \sin \theta. \quad (3.11)$$

Now  $C(q)$  is rearranged as

$$C(q) = [C_1(q) \ C_2(q)] \quad (3.12)$$

where

$$C_1(q) = \begin{bmatrix} 0 & 0 & 0 \\ \frac{1}{2}r_w & \frac{1}{2}r_w & 0 \end{bmatrix}, \quad (3.13)$$

$$C_2(q) = \begin{bmatrix} -\sin \theta & \cos \theta \\ -\cos \theta & -\sin \theta \end{bmatrix} \quad (3.14)$$

and  $C_2(q) \in \mathbf{R}^{2 \times 2}$  which is invertible.

The kinetic energies of the platform, and of the manipulator, are as follows (see Figure 3.1):

$$\begin{aligned} T_1 = & \frac{1}{2}m_p(\dot{x}_w^2 + \dot{y}_w^2) + \\ & \frac{1}{2}(2m_w)(\dot{x}_w^2 + \dot{y}_w^2) + \\ & \frac{1}{2}I_w(\dot{q}_1^2 + \dot{q}_2^2) + \\ & m_p \left( \frac{r}{2d_1} \right) d_2(\dot{q}_1 - \dot{q}_2)(\dot{y}_w \cos \theta - \dot{x}_w \sin \theta) + \\ & \frac{1}{2}I_p \left( \frac{r}{2d_1} \right)^2 (\dot{q}_1 - \dot{q}_2)^2 + \\ & \frac{1}{2}(2m_w d_1^2) \left( \frac{r}{2d_1} \right)^2 (\dot{q}_1 - \dot{q}_2)^2 \quad \text{and} \end{aligned} \quad (3.15)$$

$$\begin{aligned} T_2 = & \frac{1}{2}m_m v_0^2 + \\ & \frac{1}{2}[I_x \omega_x^2 + I_y \omega_y^2 + I_z \omega_z^2 - 2I_{xz} \omega_x \omega_z - 2I_{xy} \omega_x \omega_y - 2I_{yz} \omega_y \omega_z] + \\ & m_m [v_0 x(\omega_y \bar{z} - \omega_z \bar{y}) + v_0 y(\omega_z \bar{x} - \omega_x \bar{z}) + v_0 z(\omega_x \bar{y} - \omega_y \bar{x})] \end{aligned} \quad (3.16)$$

where

$$\bar{x} = \bar{z} = 0,$$

$$\bar{y} = L_{c_1},$$

$$I_y = 0,$$

$$\omega_x = \dot{q}_3,$$

$$\omega_y = \dot{\theta} \sin q_3,$$

$$\omega_z = \dot{\theta} \cos q_3,$$

$$\dot{x}_m = \dot{x}_w^2 - d_3 \dot{\theta} \sin \theta,$$

$$\dot{y}_m = \dot{y}_w^2 + d_3 \dot{\theta} \cos \theta,$$

$$v_0 = \dot{x}_m^2 + \dot{y}_m^2,$$

$$v_{0x} = \dot{x}_w \sin \theta - \dot{y}_w \cos \theta - d_3 \dot{\theta},$$

$$v_{0y} = (\dot{x}_w \cos \theta + \dot{y}_w \sin \theta) \cos q_3, \text{ and}$$

$$v_{0z} = -(\dot{x}_w \cos \theta + \dot{y}_w \sin \theta) \sin q_3.$$

The potential energy is written as

$$V = m_1 g (r_c + e + L_0 + \bar{y} \sin q_1). \quad (3.17)$$

The Lagrangian for the mobile manipulator is simply  $L(q, \dot{q}) = T_1(q, \dot{q}) + T_2(q, \dot{q}) - V(q)$ .

Now, we derive the equations of motion using the Lagrange-d'Alembert formulation. Let  $\delta q = (\delta q_1 \delta q_2 \delta q_3 \delta x_w \delta y_w)$  represent a virtual displacement of the system.

We obtain Eq. (3.1) with the set of velocity constraints as

$$\begin{bmatrix} 0 & 0 & 0 & -\sin \theta & \cos \theta \\ \frac{1}{2}r_w & \frac{1}{2}r_w & 0 & -\cos \theta & -\sin \theta \end{bmatrix} \delta q = 0. \quad (3.18)$$

Solving Eq. (3.18) for  $\delta x_w$  and  $\delta y_w$  gives

$$\delta x_w = \frac{1}{2}r_w(\delta q_1 + \delta q_2) \cos \theta \quad \text{and} \quad (3.19)$$

$$\delta y_w = \frac{1}{2}r_w(\delta q_1 + \delta q_2) \sin \theta. \quad (3.20)$$

We redefine  $\delta q$  as  $\delta q_u = (\delta q_1 \ \delta q_2 \ \delta q_3)$  and  $\delta q_c = (\delta x_w \ \delta y_w)$  where  $\delta q_u$  is unconstrained and  $\delta q_c$  is constrained. Using Eq. (3.12) and  $\delta q = (\delta q_u \ \delta q_c)$ , we obtain

$$\delta q_c = -C_c^{-T}(q)C_u(q)\delta q_u. \quad (3.21)$$

It can be shown that the equations of motion become

$$\left( \frac{d}{dt} \frac{\partial L}{\partial \dot{q}_u} - \frac{\partial L}{\partial q_u} - \tau_u \right) - C_u^T C_c^{-T} \left( \frac{d}{dt} \frac{\partial L}{\partial \dot{q}_c} - \frac{\partial L}{\partial q_c} - \tau_c \right) = 0. \quad (3.22)$$

Substituting the Lagrangian  $L(q, \dot{q})$  into Eq. (3.22), the equations of motion of the mobile manipulator can be written as

$$M\ddot{q}_u + N + G = \tau_u \quad (3.23)$$

where

$$M = \begin{bmatrix} I_{v_1} + I_{m_1} & I_{v_2} + I_{m_2} & I_{m_3} \\ I_{v_2} + I_{m_2} & I_{v_1} + I_{m_1} & I_{m_3} \\ I_{m_3} & I_{m_3} & I_{m_4} \end{bmatrix},$$

$$N = \begin{bmatrix} n_1 \\ n_2 \\ n_3 \end{bmatrix},$$

$$G = \begin{bmatrix} 0 \\ 0 \\ m_m g L_{c_3} \cos q_3 \end{bmatrix},$$

$$\tau_u = \begin{bmatrix} \tau_{q_1} \\ \tau_{q_2} \\ \tau_{q_3} \end{bmatrix},$$

$$I_{v_1} = (I_p + 2I_d)h^2 + I_w + (m_p + 4m_w)d_1^2 h^2,$$

$$I_{v_2} = (I_p + 2I_d)h^2 + m_p d_1^2 h^2,$$

$$I_{m_1} = \frac{1}{2}h^2(1 + \cos(2q_3)) + m_m h^2(d_1^2 + d_3^2 + 2d_3 L_{c_3} \cos q_3),$$

$$I_{m_2} = -\frac{1}{2}h^2(1 + \cos(2q_3)) + m_m h^2(d_1^2 - d_3^2 - 2d_3 L_{c_3} \cos q_3),$$

$$I_{m_3} = -m_m d_1 h L_{c_3} \sin q_3,$$

$$I_{m_4} = I_m,$$

$$n_1 = -m_p d_1 d_2 h^2 \dot{\theta} \dot{q}_1 + m_p d_1 d_2 h^2 \dot{\theta} \dot{q}_2 - m_m d_1 d_3 h^2 \dot{\theta} \dot{q}_1 + m_m d_1 d_3 h^2 \dot{\theta} \dot{q}_2 -$$

$$m_m d_1 h^2 L_{c_3} \dot{\theta} \dot{q}_1 \cos q_3 + m_m d_1 h^2 L_{c_3} \dot{\theta} \dot{q}_2 \cos q_3 - m_m d_1 h L_{c_3} \dot{q}_3^2 \cos q_2 +$$

$$2m_m h^2 d_3 L_{c_3} \dot{q}_1 \dot{q}_2 \sin q_3$$

$$n_2 = -m_p d_1 d_2 h^2 \dot{\theta} \dot{q}_1 + m_p d_1 d_2 h^2 \dot{\theta} \dot{q}_2 - m_m d_1 d_3 h^2 \dot{\theta} \dot{q}_1 + m_m d_1 d_3 h^2 \dot{\theta} \dot{q}_2 +$$

$$m_m d_1 h^2 L_{c_3} \dot{\theta} \dot{q}_1 \cos q_3 - m_m d_1 h^2 L_{c_3} \dot{\theta} \dot{q}_2 \cos q_3 + m_m d_1 h L_{c_3} \dot{q}_3^2 \cos q_2 - 2m_m h^2 d_3 L_{c_3} \dot{q}_1 \dot{q}_2 \sin q_3$$

$$n_3 = m_m h^2 d_3 L_{c_3} \dot{q}_1^2 \sin q_3 - 2m_m h^2 d_3 L_{c_3} \dot{q}_1 \dot{q}_2 \sin q_3 + m_m h^2 d_3 L_{c_3} \dot{q}_2^2 \sin q_3 + \frac{1}{2} I_m h^2 d_3 \dot{q}_1^2 \sin(2q_3) - I_m h^2 \dot{q}_1 \dot{q}_2 \sin(2q_3) + \frac{1}{2} I_m h^2 d_3 \dot{q}_2^2 \sin(2q_3)$$

$$G_1 = G_2 = 0,$$

$$G_3 = m_m g L_{c_3} \cos q_3, \text{ and}$$

$$h = r/(2d_1).$$

### 3.3 Control of the Mobile Manipulator

In this section, we derive the control law for the spatial mobile manipulator based on the model obtained using Eq. (3.22).

We first rewrite Eq. (3.23) as

$$\ddot{q}_u = H + M^{-1} \tau_u \quad (3.24)$$

where

$$H = -M^{-1} N - M^{-1} F. \quad (3.25)$$

Now, the state variables are defined as

$$x = \begin{bmatrix} q_1 \\ q_2 \\ q_3 \\ \dot{q}_1 \\ \dot{q}_2 \\ \dot{q}_3 \end{bmatrix} = \begin{bmatrix} x_1 \\ x_2 \\ x_3 \\ \dot{x}_4 \\ \dot{x}_5 \\ \dot{x}_6 \end{bmatrix}. \quad (3.26)$$

Eqs. (3.24) and (3.26) can be used to write

$$\dot{x} = f(x) + g(x)\tau_u \quad (3.27)$$

where

$$f(x) = \begin{bmatrix} x_4 \\ x_5 \\ x_6 \\ H_{3 \times 1} \end{bmatrix} \quad \text{and} \quad (3.28)$$

$$g(x) = \begin{bmatrix} 0_{3 \times 3} \\ M_{3 \times 3}^{-1} \end{bmatrix}. \quad (3.29)$$

Now we select the output associated with Eq. (3.27),  $y = f(q)$ , as

$$x = \begin{bmatrix} p_{e_x} \\ p_{e_y} \\ p_{e_z} \end{bmatrix} = \begin{bmatrix} x_w + L_3 \cos q_3 \cos \theta \\ y_w + L_3 \cos q_3 \sin \theta \\ r_c + e + L_0 + L_3 \sin q_3 \end{bmatrix}. \quad (3.30)$$

Then, differentiating each element of  $y$  twice allows terms involving elements of  $t$  to appear. Thus, the first and second derivative of the output can be written as

$$\dot{y} = J(q)\dot{q} \quad \text{and} \quad (3.31)$$

$$\ddot{y} = J(q)\ddot{q} + \dot{J}(q)\dot{q} \quad (3.32)$$

where

$$J = \begin{bmatrix} h(d_1 \cos \theta - L_3 \cos q_3 \sin \theta) & h(d_1 \cos \theta + L_3 \cos q_3 \sin \theta) & -L_3 \sin q_3 \cos \theta \\ h(d_1 \sin \theta + L_3 \cos q_3 \cos \theta) & h(d_1 \sin \theta - L_3 \cos q_3 \cos \theta) & -L_3 \sin q_3 \cos \theta \\ 0 & 0 & L_3 \cos q_3 \end{bmatrix}.$$

If the objective is to move the platform along prescribed trajectories, input-output linearization can be applied, where the number of outputs equals the number of independent control inputs. The particular formulation of the control problem depends on the available control inputs as well as the output variables to be controlled. In this case input-output linearization is achieved by a static state-feedback. An outer feedback loop is provided for asymptotic stability.

Now, substituting Eq. (3.24) into Eq. (3.32), we can rewrite Eq.(3.32) as

$$\ddot{y} = J(H + M^{-1}\tau_u) + \dot{J}\dot{q}_u. \quad (3.33)$$

Then, the input-output description of the system Eq.(3.27) can be linearized to cancel the nonlinearities in Eq. (3.33) using the following feedback:

$$\tau_u = F(x) + G(x)u \quad (3.34)$$

where

$$F(x) = -MJ^{-1}\dot{J}\dot{q} - MH \quad \text{and} \quad (3.35)$$

$$G(x) = MJ^{-1}. \quad (3.36)$$

Thus, the combined system Eqs. (3.33) - (3.36) reduces to

$$\ddot{y} = u. \quad (3.37)$$

The term  $u$  represents a new input to the system which is yet to be chosen. Eq. (3.37) is known as the double integrator system as it represents  $n$  uncoupled double integrators. After applying the nonlinear feedback Eq. (3.37), we convert the system into a linear system as

$$\dot{\zeta} = A\zeta + Bu \quad (3.38)$$

$$y = \Gamma\zeta \quad (3.39)$$

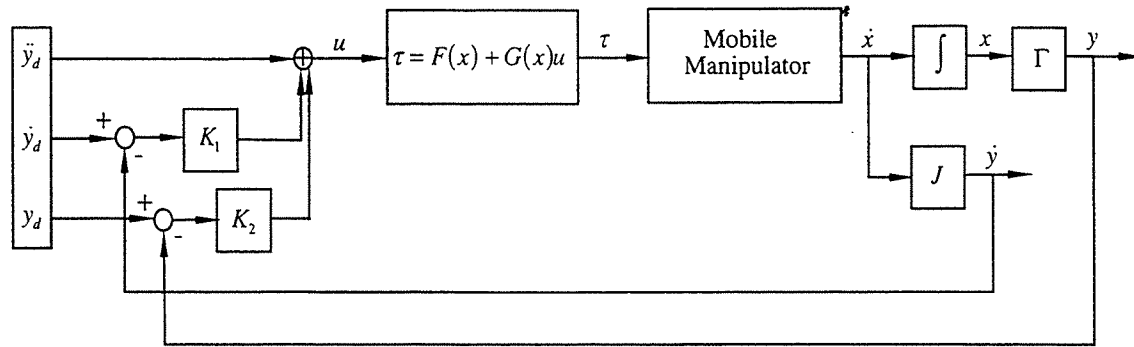


Figure 3.2: Structure of the control algorithm

where

$$A = \begin{bmatrix} 0 & 1 & 0 \\ 0 & 0 & 1 \\ 0 & 0 & 0 \end{bmatrix}, \quad B = \begin{bmatrix} 0 \\ 0 \\ 1 \end{bmatrix}, \quad \text{and } \Gamma = (1 \ 0 \ 0), \quad (3.40)$$

and  $\zeta$  are the new state variables.

Control system design of the mobile manipulator is then equivalent to a design problem of decoupled linear subsystems described by Eqs. (3.38) and (3.39). The system (3.38) and (3.39) can be represented by the block diagram of Figure 3.2. Since these linear systems are controllable, their eigenvalues can be placed anywhere by using a constant feedback

$$u = \ddot{y}_d + K_1(\dot{y}_d - \dot{y}) + K_2(y_d - y) \quad (3.41)$$

where  $K_1$  and  $K_2$  are the diagonal gain matrices. Then, the tracking error dynamics can be described as follows:

$$\ddot{e}(t) + K_1\dot{e}(t) + K_2e(t) = 0. \quad (3.42)$$

### 3.4 Simulations

In this section we use a single-link mobile manipulator as our simulation example (see Figure 3.1). The following parameters are used in the simulation:

$m_p = 100kg$ ,  $m_m = 10kg$ ,  $m_w = 8kg$ ,  $I_p = 8kg \cdot m^2$ ,  $I_m = 0.2kg \cdot m^2$ , and  $I_w = 0.1kg \cdot m^2$

For each simulation, the mobile manipulator is initially at rest, and the desired trajectory and its initial end-effector position are as follows:

#### Simulation I

- The desired trajectory:

$$x_d(t) = 0.6$$

$$y_d(t) = t$$

$$z_d(t) = 0.41$$

- The initial position of the end-effector: (0.3, 0, 0.35)

#### Simulation II

- The desired trajectory:

$$x_d(t) = 0.57 + t$$

$$y_d(t) = 0.15$$

$$z_d(t) = 0.3 + 0.1 \sin\left(\frac{\pi}{2}t\right)$$

- The initial position of the end-effector: (0.2, 0, 0.35)

### Simulation III

- The desired trajectory:

$$x_d(t) = 3 + \sin t$$

$$y_d(t) = 3 + \cos t$$

$$z_d(t) = 0.3 + 0.1 \sin\left(\frac{\pi}{2}t\right)$$

- The initial position of the end-effector: (2.7, 3.8, 0.35)

### Simulation IV

- The desired trajectory:

$$x_d(t) = 3 + t$$

$$y_d(t) = 3 + 0.1 \cos t$$

$$z_d(t) = 0.3 + 0.1 \sin\left(\frac{\pi}{2}t\right)$$

- The initial position of the end-effector: (2.7, 3.8, 0.35)

Four different desired trajectories are applied in simulation to the mobile manipulator. We use a straight line trajectory in simulation I and sinusoidal trajectories in simulation II, III and IV. The corresponding motion of the end-point, the heading angle, the angular displacement of each wheel, the angular displacement of each joint, and control inputs are plotted in Figure 3.3 - 3.30. In each simulation, the end point of the mobile manipulator is commanded to follow the desired trajectory. Initially,

the end point is not on the specified initial position in each simulation. Note that for each simulation, the heading angle is set to be zero. The same feedback gains are chosen to investigate the performance of the designed controller for the different trajectories. The natural choices for the feedback gains are  $K_1 = \text{diag}(2\omega_1, 2\omega_2, 2\omega_3)$  and  $K_2 = \text{diag}(\omega_1^2, \omega_2^2, \omega_3^2)$  respectively, which results in a decoupled closed loop system with each joint response equal to the response of a critically damped linear second order system with natural frequency  $\omega_i$ ,  $i = 1, \dots, 3$ . The feedback gains are initialized to  $K_1 = \text{diag}(10, 10, 10)$  and  $K_2 = \text{diag}(25, 25, 25)$ . Note that in each case, the steady state error goes to zero in 3 seconds and the control inputs are smooth. Simulation results demonstrate the effectiveness of the proposed control scheme.

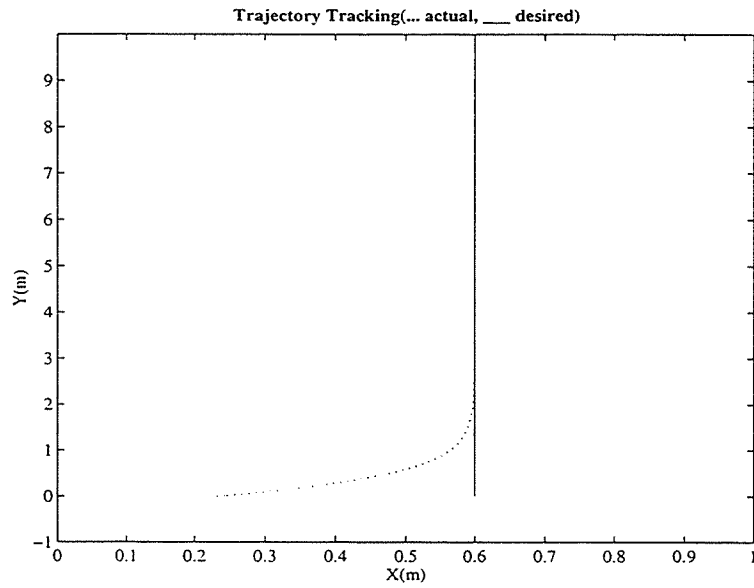


Figure 3.3: Simulation I - xy trajectory tracking in task space

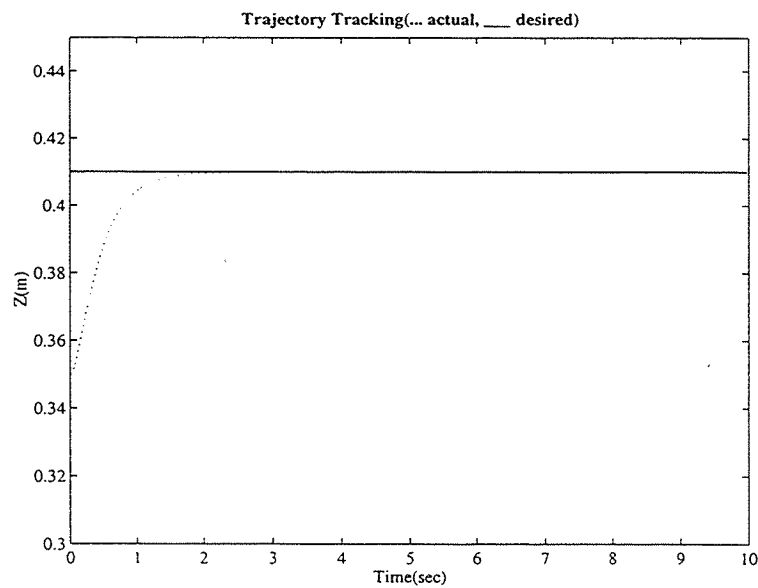


Figure 3.4: Simulation I - z trajectory tracking in task space

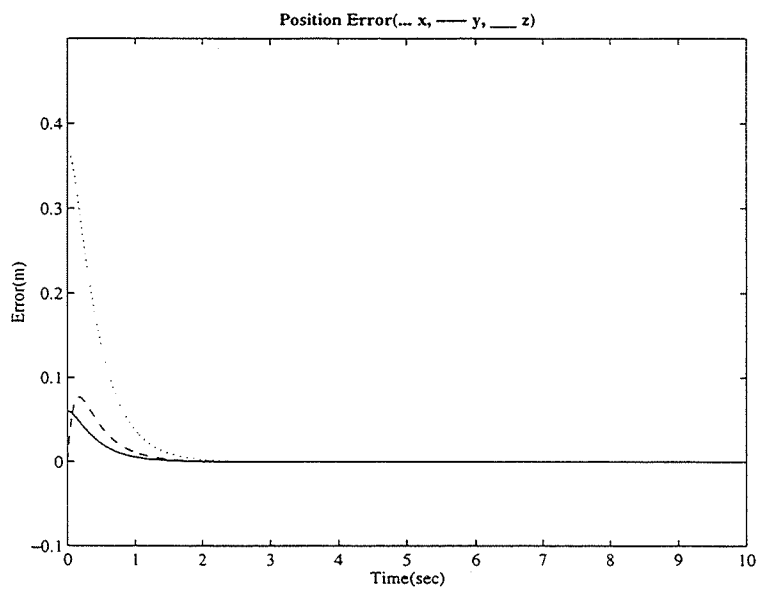


Figure 3.5: Simulation I - xyz position error

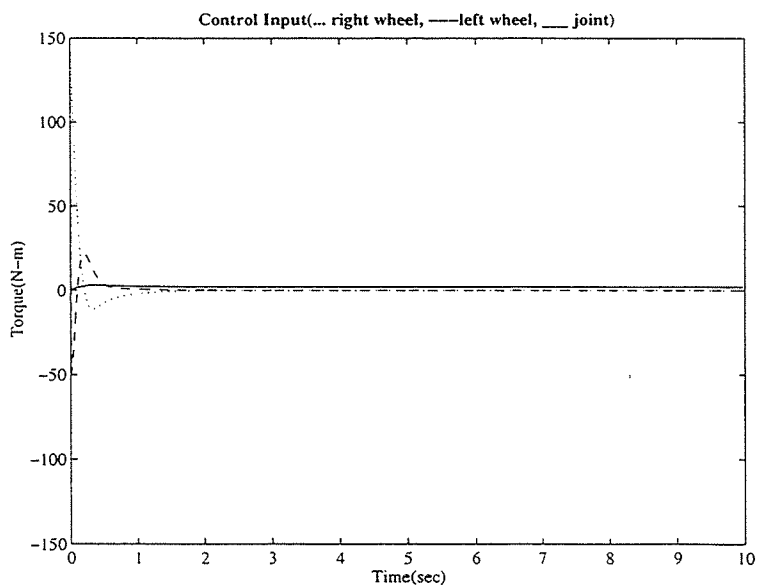


Figure 3.6: Simulation I - actuator torques of each wheel and the joint

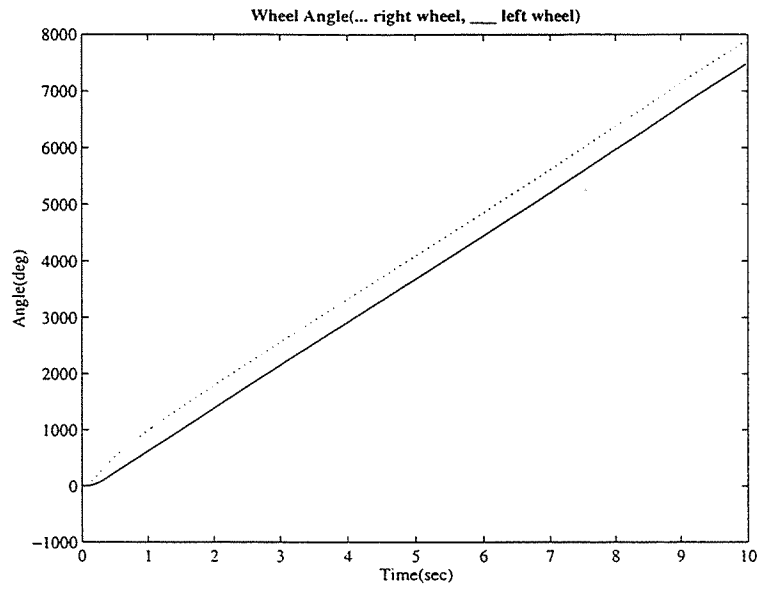


Figure 3.7: Simulation I - angular displacement of each wheel

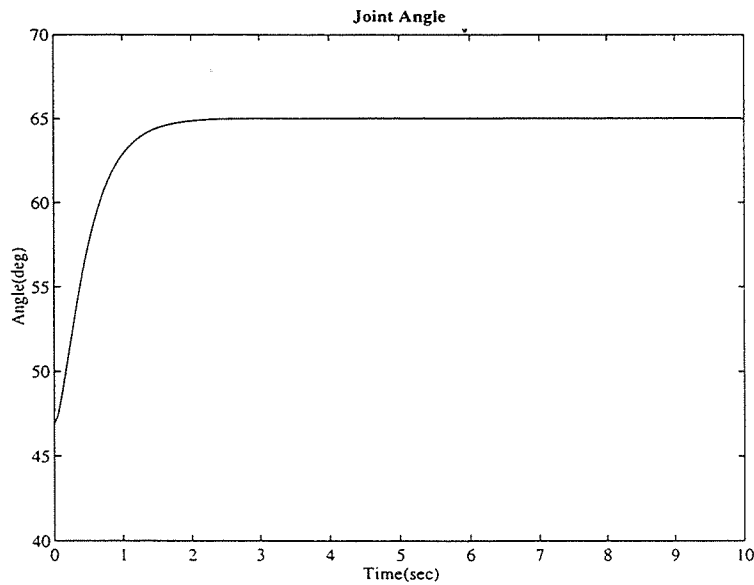


Figure 3.8: Simulation I - angular displacement of the joint

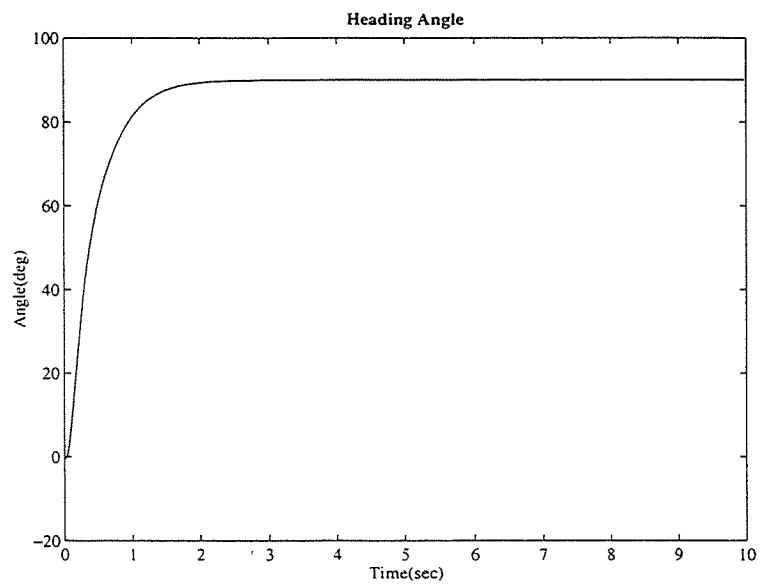


Figure 3.9: Simulation I - heading angle of the platform

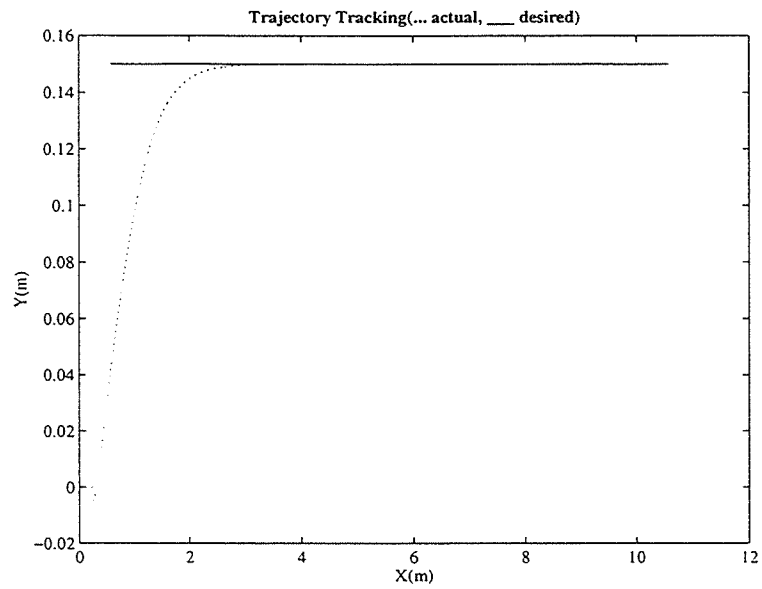


Figure 3.10: Simulation II - xy trajectory tracking in task space

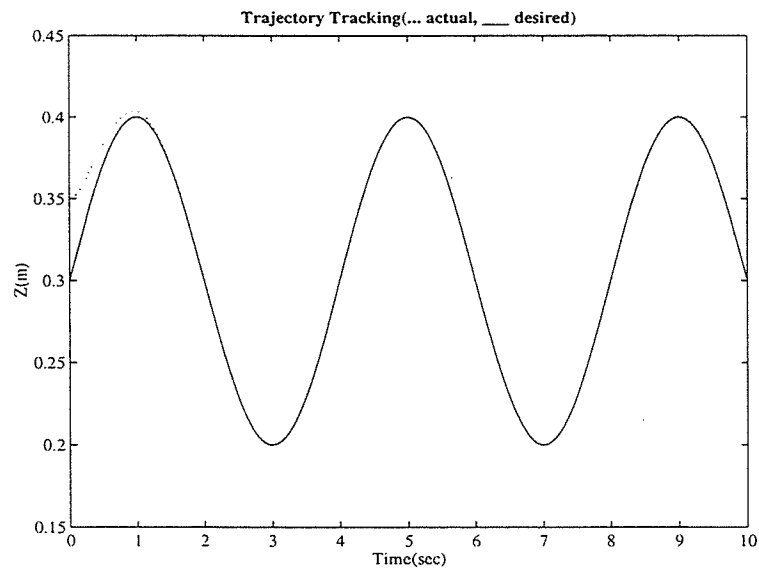


Figure 3.11: Simulation II - z trajectory tracking in task space

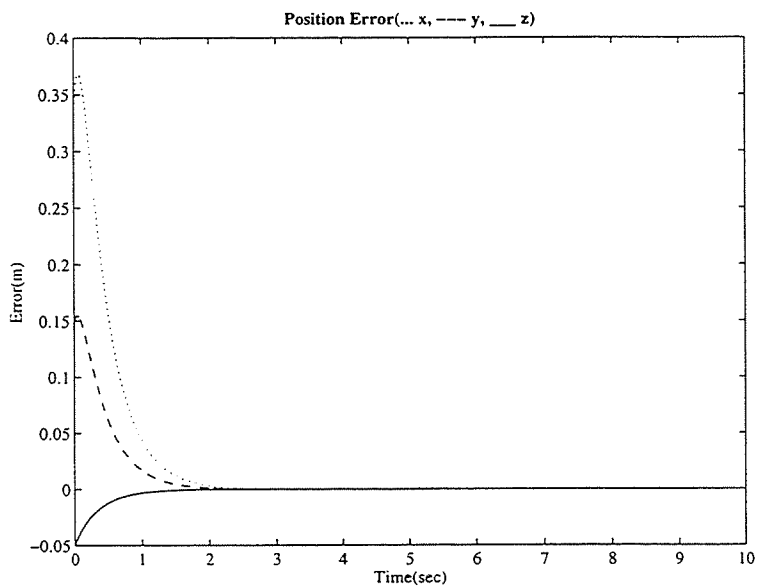


Figure 3.12: Simulation II - xyz position error

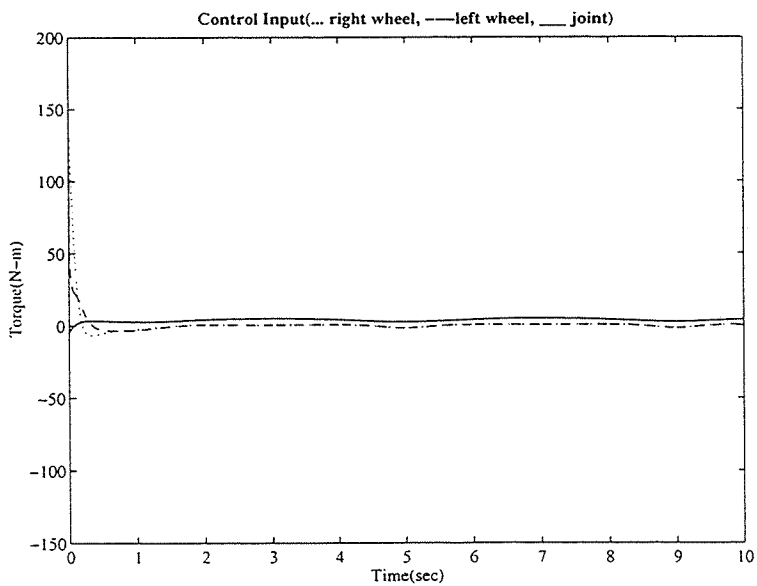


Figure 3.13: Simulation II - actuator torques of each wheel and the joint

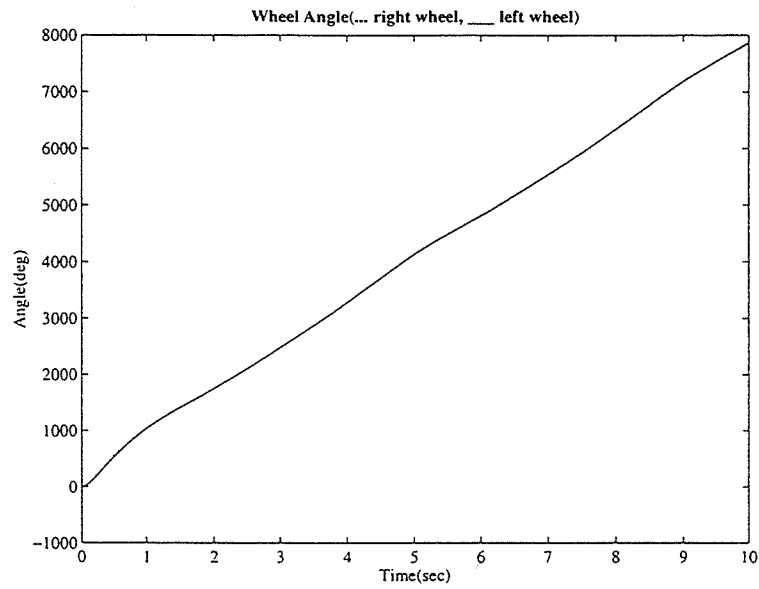


Figure 3.14: Simulation II - angular displacement of each wheel

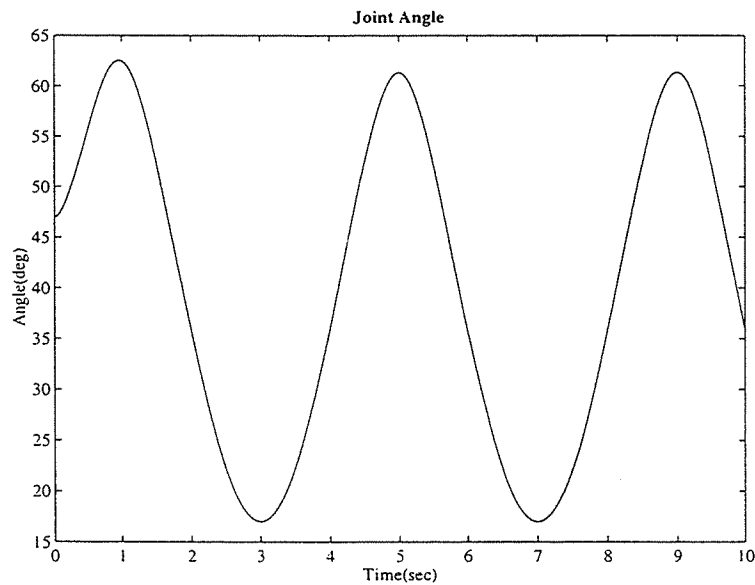


Figure 3.15: Simulation II - angular displacement of the joint

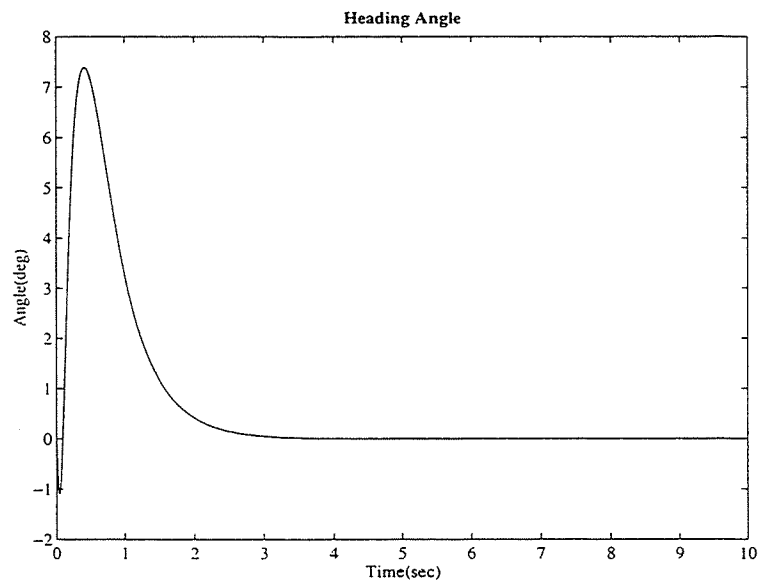


Figure 3.16: Simulation II - heading angle of the platform

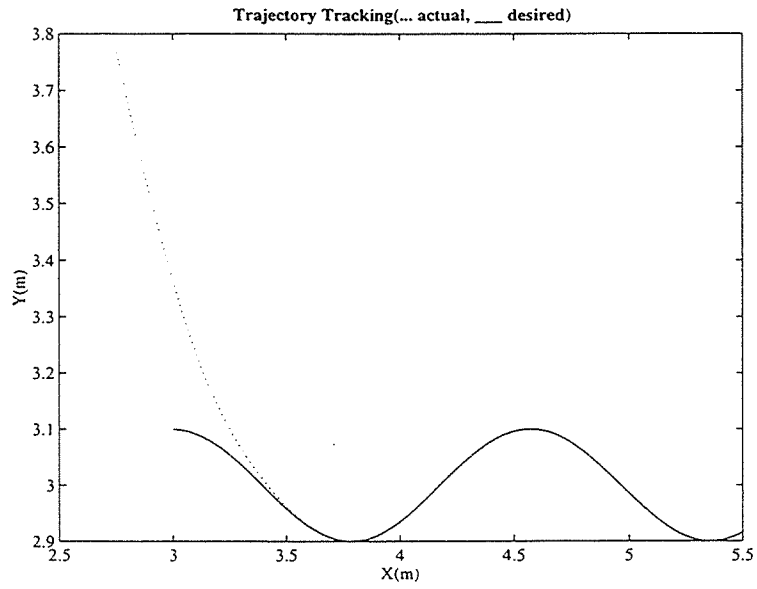


Figure 3.17: Simulation III - xy trajectory tracking in task space

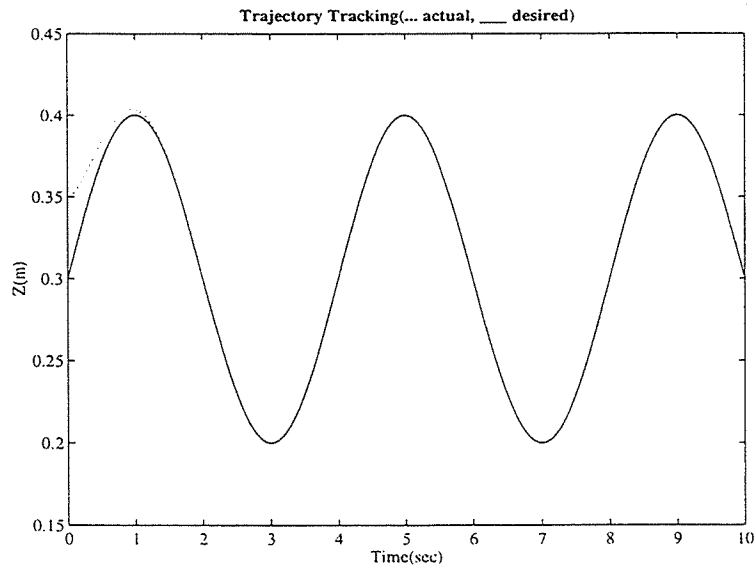


Figure 3.18: Simulation III - z trajectory tracking in task space

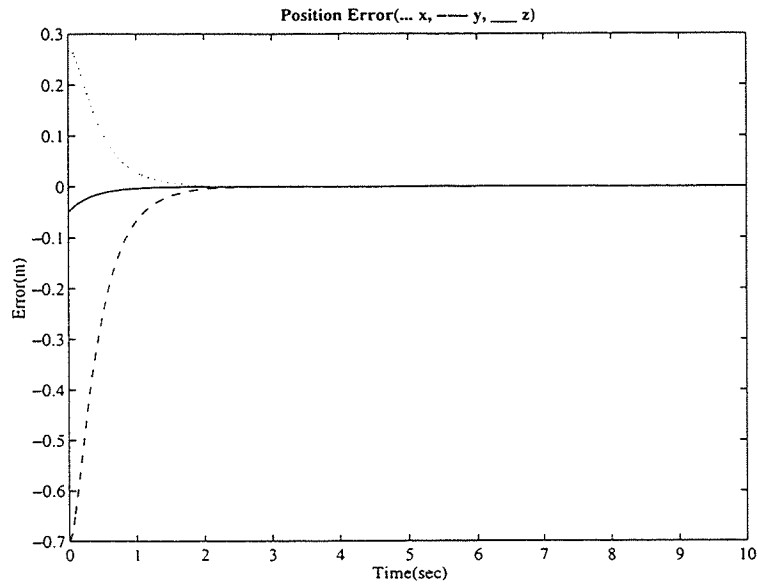


Figure 3.19: Simulation III - xyz position error

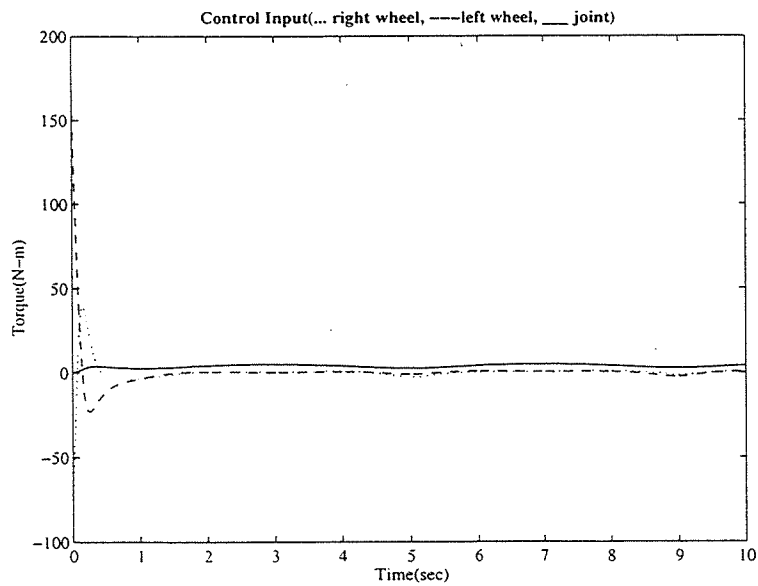


Figure 3.20: Simulation III - actuator torques of each wheel and the joint

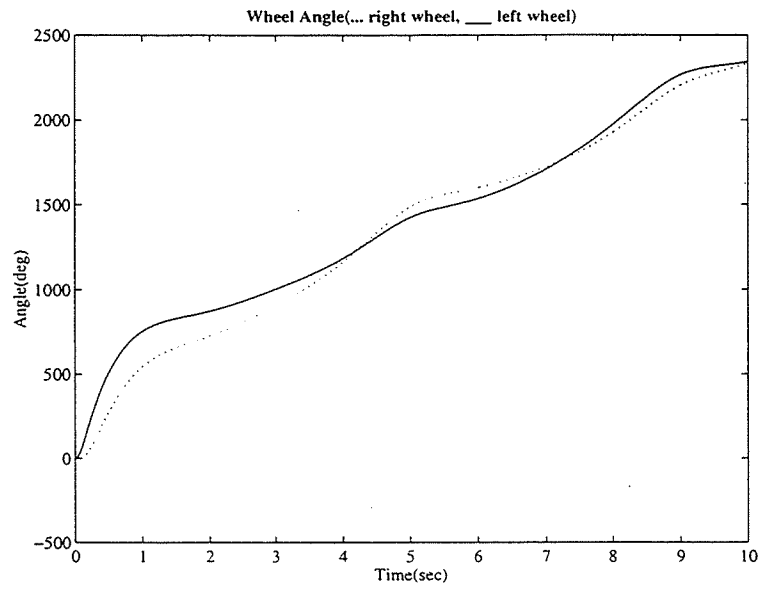


Figure 3.21: Simulation III - angular displacement of each wheel

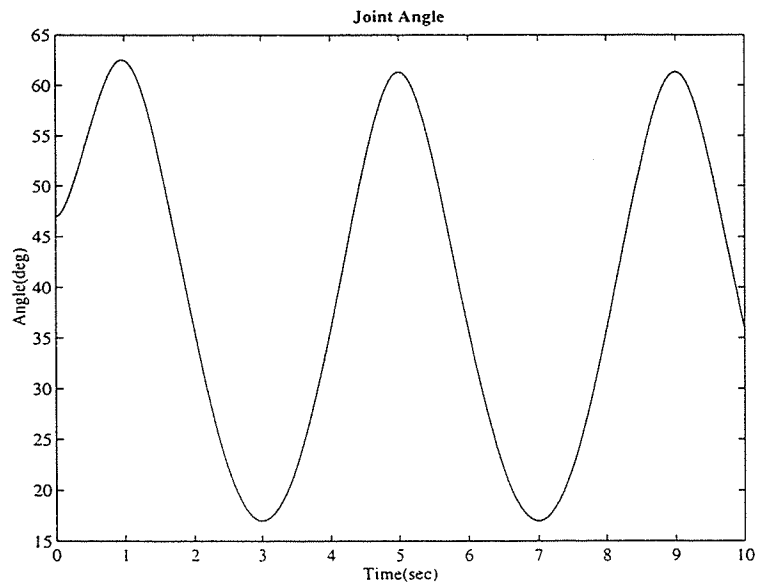


Figure 3.22: Simulation III - angular displacement of the joint

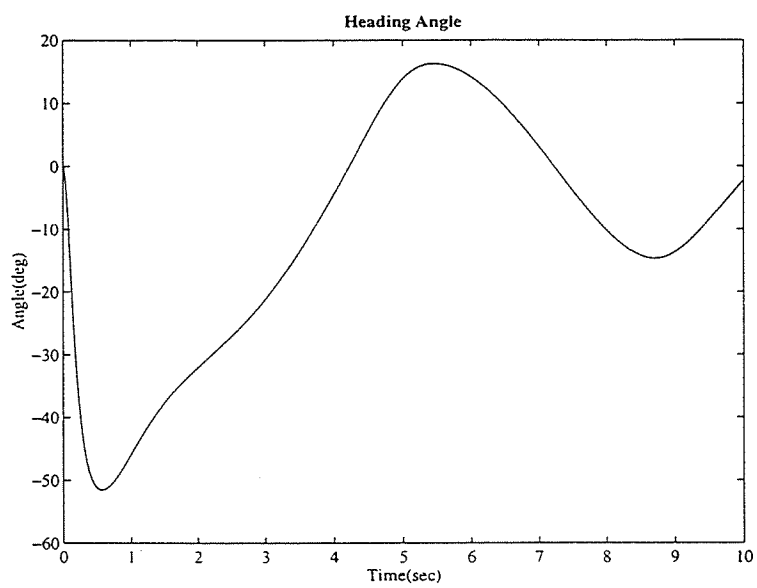


Figure 3.23: Simulation III - heading angle of the platform

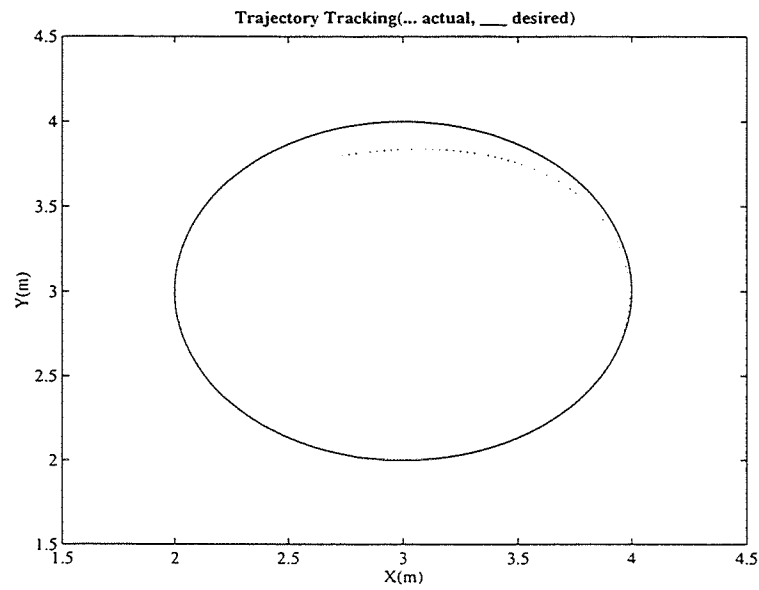


Figure 3.24: Simulation IV - xy trajectory tracking in task space

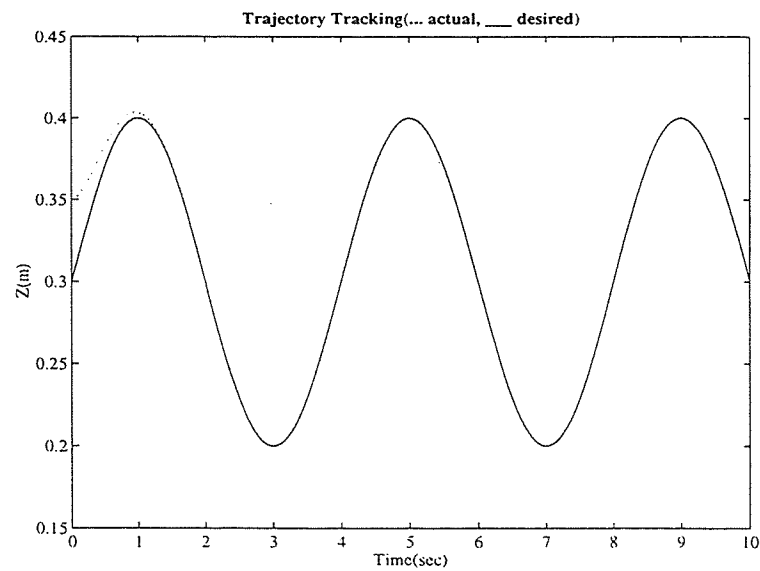


Figure 3.25: Simulation IV - z trajectory tracking in task space

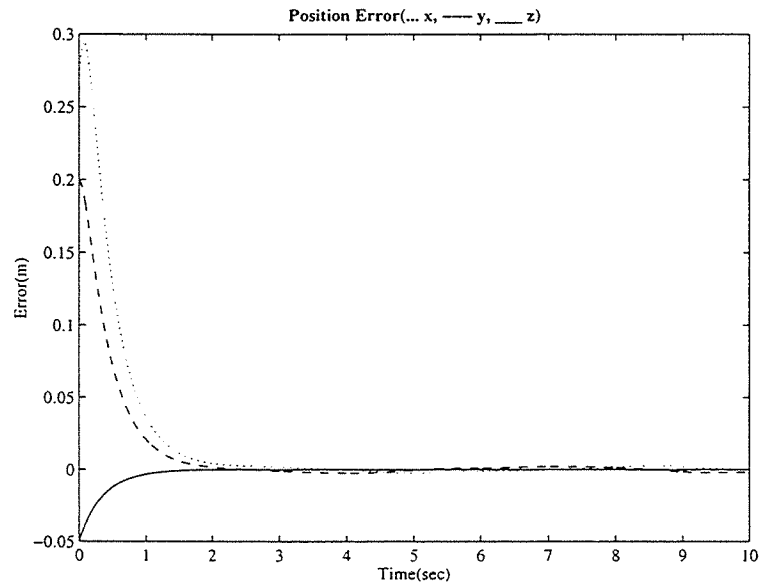


Figure 3.26: Simulation IV - xyz position error

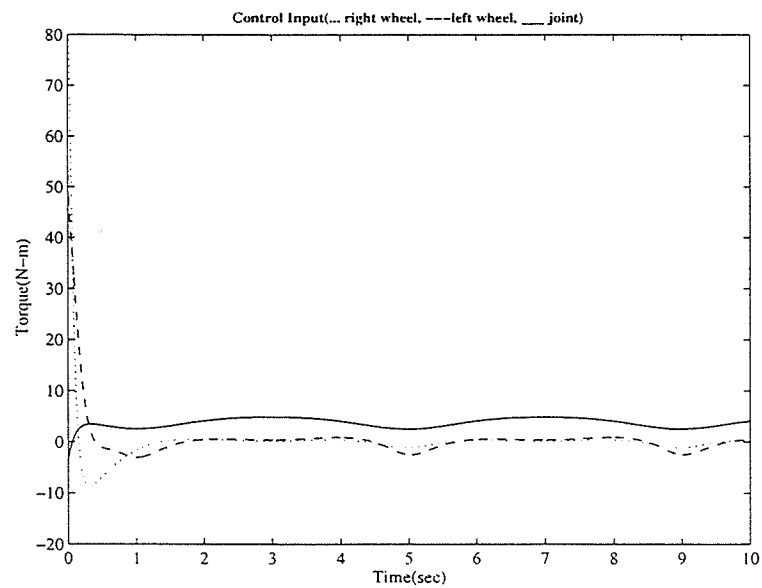


Figure 3.27: Simulation IV - actuator torques of each wheel and the joint

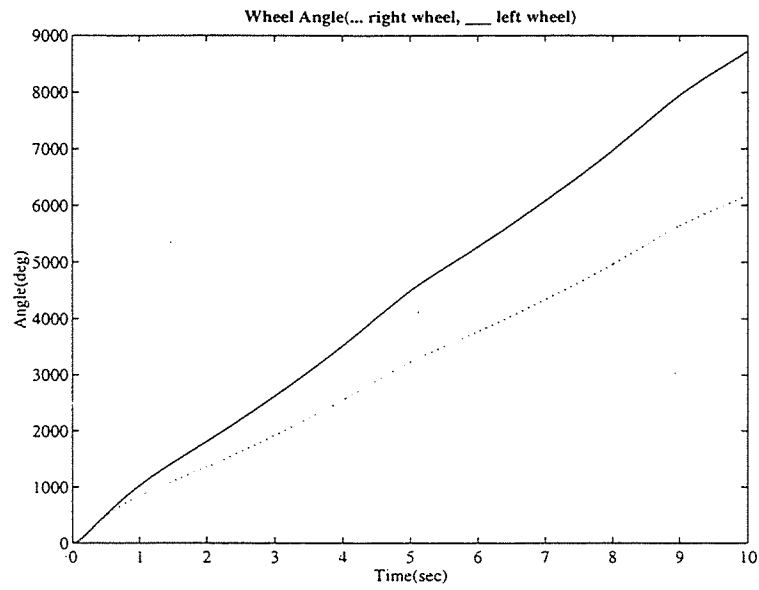


Figure 3.28: Simulation IV - angular displacement of each wheel

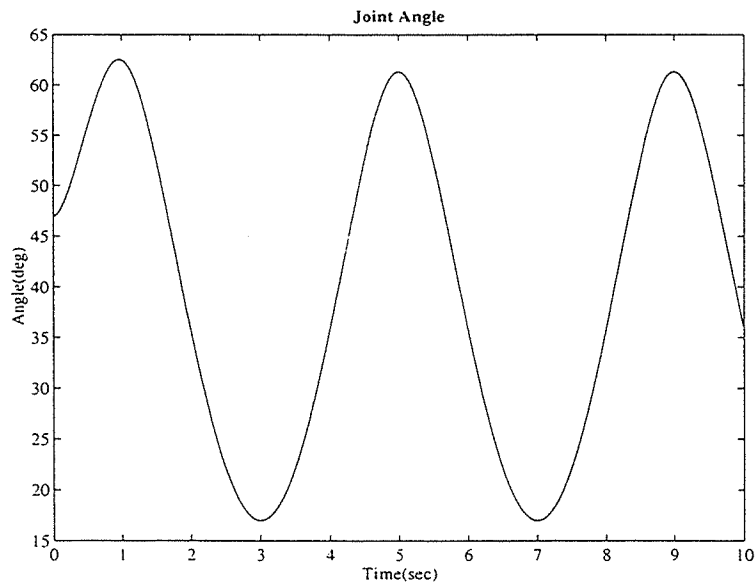


Figure 3.29: Simulation IV - angular displacement of the joint

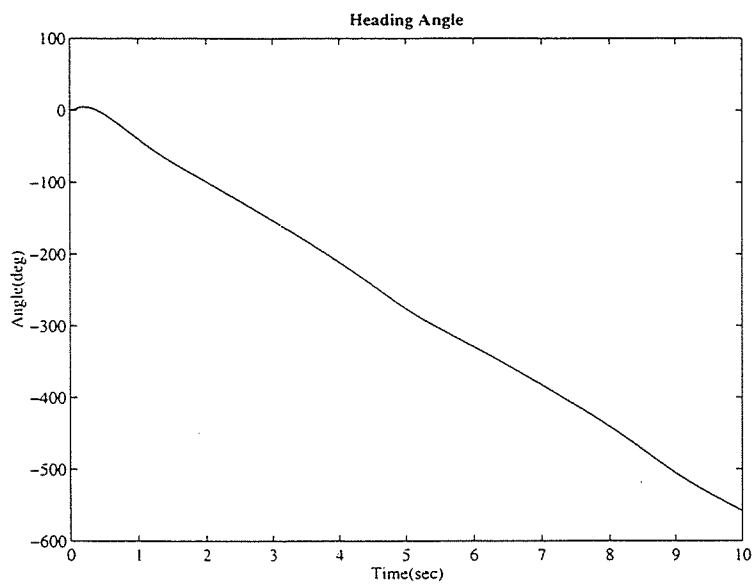


Figure 3.30: Simulation IV - heading angle of the platform

## Chapter 4

# Interaction Control of Redundant Mobile Manipulators

In the previous chapter, an input-output linearizing controller was designed for a single-link mobile manipulator. In order to increase the dexterity of the mobile manipulator, a multi-link manipulator is employed as shown in Figure 4.1. Therefore, kinematic redundancy is introduced to the system in addition to nonholonomic constraints. First, the coordination strategy of the mobile manipulator as a means of redundancy resolution is discussed. Then, a novel nonlinear interaction controller is developed for the mobile manipulator subject to kinematic redundancy and nonholonomic constraints.

## 4.1 Redundancy Resolution

In order to perform a variety of tasks which require sophisticated mechanical motion in an unstructured, dynamically varying environment, a robot must have enough degrees of freedom to accomplish those tasks. In order to increase the performance capability of a mobile manipulator, it might be desirable to introduce some kinematic redundancy. Any robotic mechanism is kinematically redundant with  $m < n$ ,  $m$  denoting the number of task variables and  $n$  the number of the degrees-of-freedom. The difference  $n - m$  is termed the degree of redundancy.

A robotic mechanism has certain configurations in which it can no longer move its end effector to change position or orientation in certain directions. These configurations are called singular configurations. Some joint velocities would become excessively large trying to maintain the desired trajectory. In the robotics literature, the manipulability measure is often used as a quantitative measure of the capability of a manipulator to move its end effector freely in any direction. This measure can also be regarded as an index of the distance from singular configurations. However, this criterion cannot be applied directly to a spatial mobile manipulator without additional considerations and modifications.

Egeland and Sagli (1993) studied coordination of motion in a space/manipulator system. They proposed that the manipulator with high bandwidth be commanded to keep track of a desired end-effector trajectory while the satellite with low bandwidth be controlled so that the manipulator is maintained near the center of the workspace.

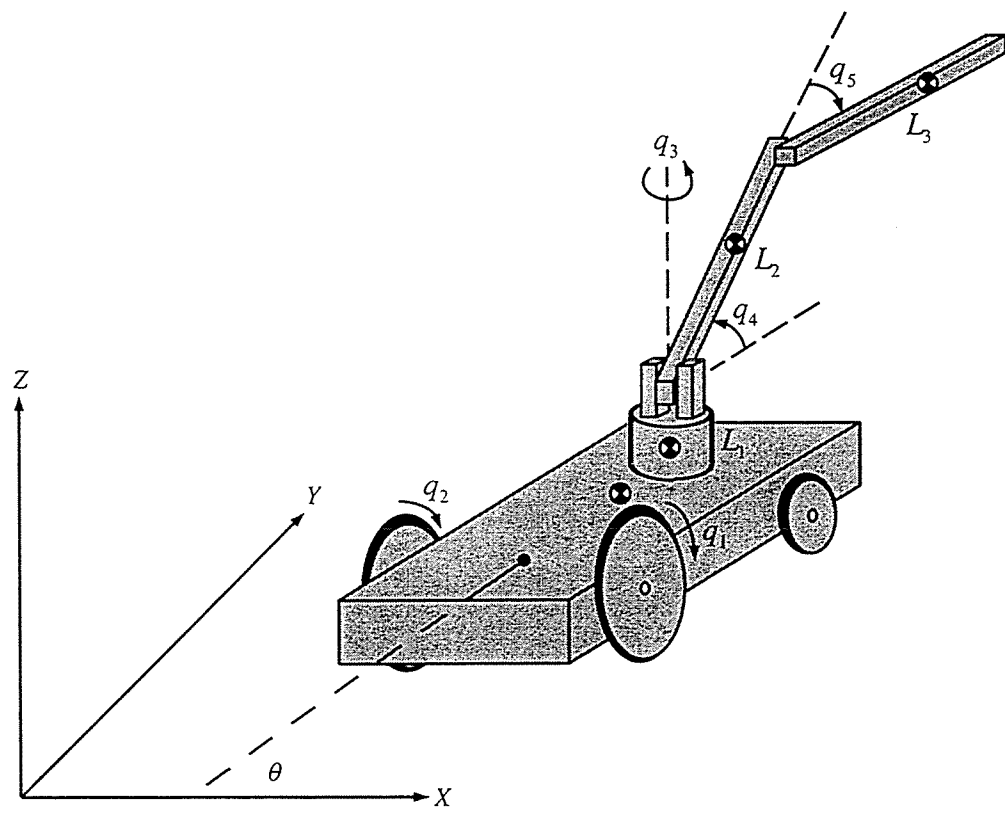


Figure 4.1: The redundant mobile manipulator

In other words, a constant nominal configuration is specified for the manipulator so that there are no singularities or joint limits close to the nominal configuration. The selection of the configuration can be based on engineering judgement or by, for example, maximizing manipulability or available joint range. Yamamoto and Yun (1994) adopted a similar redundancy resolution technique suggested by Egeland and Sagli (1993) and applied it to a planar mobile manipulator subject to nonholonomic constraints. The main drawback of their coordination schemes is that if the manipulator reaches up to perform tasks in vertical coordinates, any motion from the mobile platform will not be able to bring the manipulator into the constant nominal configuration.

The approach demonstrated in Egeland and Sagli (1993) is still useful in resolving the redundancy of the system created by combining a platform with a multi-linked manipulator. A simple approach to the problem above is to bring the mobile platform to the predetermined nominal configuration of the manipulator for the planar model. That is, the mobile platform is moved to the position directly below the end-effector.

## 4.2 Decentralization of Mobile Manipulator

Mobile manipulators consist of two primary subsystems; the mobile platform and the multi-link manipulator. The two subsystems differ substantially in their task assignments, dynamic characteristics and controller requirements. According to the coordination scheme proposed in the previous section, the mobile platform is respon-

sible for positioning the manipulator at a specified point in the workspace. This physical interpretation leads to the decomposition of the model into the mobile platform and the manipulator subsystems and motivates the application of decentralized control to mobile manipulators.

The fixed-base manipulator typically consists of three degrees-of-freedom and can locate the end-effector at any point within the three-dimensional workspace. The second and third degrees-of-freedom specify the position of the end-effector in a plane, while the first degree-of-freedom orients the plane. Consequently, a manipulator with fewer than three degrees-of-freedom restricts the reachable positions to a plane or line, and a manipulator with more than three degrees-of-freedom results in a redundant system. Therefore, in order to avoid further redundancy and to facilitate the control of the mobile manipulator, a three degrees-of-freedom manipulator is used.

### 4.3 Modeling of the Mobile Manipulator

The redundant mobile manipulator shown in Figure 4.1 is considered. The wheeled platform is modeled as a nonholonomic system as in the previous chapter. Because the configuration of the redundant model is similar to the one of the non-redundant model, only additional notation is introduced as follows:

$q_3$ : the joint angle of link 1,

$q_4$ : the joint angle of link 2,

- $q_5$ : the joint angle of link 3,  
 $m_1$ : the mass of link 1,  
 $m_2$ : the mass of link 2,  
 $m_3$ : the mass of link 3,  
 $I_1$ : the moment of inertia of link 1,  
 $I_2$ : the moment of inertia of link 2, and  
 $I_3$ : the moment of inertia of link 3.

The kinetic energy of the multi-link manipulator can be formulated as follows:

$$\begin{aligned}
 T_m = & \sum_{i=1}^3 \left( \frac{1}{2} m_i v_i^2 + \right. \\
 & \left. \frac{1}{2} [I_{x_i} \omega_{x_i}^2 + I_{y_i} \omega_{y_i}^2 + I_{z_i} \omega_{z_i}^2 - 2I_{xz_i} \omega_{x_i} \omega_{y_i} - 2I_{xz_i} \omega_{x_i} \omega_{y_i} - 2I_{yz_i} \omega_{y_i} \omega_{z_i}] + \right. \\
 & \left. m_i [v_{x_i} (\omega_{y_i} \bar{z}_i - \omega_{z_i} \bar{y}_i) + v_{y_i} (\omega_{z_i} \bar{x}_i - \omega_{x_i} \bar{z}_i) + v_{z_i} (\omega_{x_i} \bar{y}_i - \omega_{y_i} \bar{x}_i)] \right) \quad (4.1)
 \end{aligned}$$

where

$$I_{x_1} = I_{y_1} = 0, I_{z_1} = I_1,$$

$$\bar{x}_1 = \bar{y}_1 = 0, \bar{z}_1 = L_{c_1},$$

$$\omega_{x_1} = \omega_{y_1} = 0, \omega_{z_1} = \dot{\theta} + \dot{q}_1,$$

$$I_{x_2} = I_2, I_{y_2} = 0, I_{z_2} = I_2,$$

$$\bar{x}_2 = 0, \bar{y}_2 = L_{c_2}, \bar{z}_2 = 0,$$

$$\omega_{x_2} = \dot{q}_2, \omega_{y_2} = (\dot{\theta} + \dot{q}_1) \sin q_2, \omega_{z_2} = (\dot{\theta} + \dot{q}_1) \cos q_2,$$

$$I_{x_3} = I_3, I_{y_3} = 0, I_{z_3} = I_3,$$

$$\bar{x}_3 = 0, \bar{y}_3 = L_{c3}, \bar{z}_3 = 0,$$

$$\omega_{x_3} = \dot{q}_2 + \dot{q}_3, \omega_{y_3} = (\dot{\theta} + \dot{q}_1) \sin(q_2 + q_3), \text{ and } \omega_{z_3} = (\dot{\theta} + \dot{q}_1) \cos(q_2 + q_3).$$

The potential energy is written as

$$V = m_1 g (r_w + e + L_1 + L_2 \sin q_4 + L_{c3} \sin q_5). \quad (4.2)$$

Apparently, the Lagrangian for the mobile manipulator is  $L(q, \dot{q}) = T_p(q, \dot{q}) + T_m(q, \dot{q}) - V(q)$ .

Now, the generalized coordinates are defined as

$$q = \begin{bmatrix} x_w \\ y_w \\ q_1 \\ q_2 \\ q_3 \\ q_4 \\ q_5 \end{bmatrix} \quad (4.3)$$

and  $C(q)$  is given by

$$C(q) = [C_c(q) \ C_u(q)] \quad (4.4)$$

where

$$C_u(q) = \begin{bmatrix} 0 & 0 & 0 & 0 & 0 \\ \frac{1}{2}r_w & \frac{1}{2}r_w & 0 & 0 & 0 \end{bmatrix} \text{ and} \quad (4.5)$$

$$C_c(q) = \begin{bmatrix} -\sin \theta & \cos \theta \\ -\cos \theta & -\sin \theta \end{bmatrix}. \quad (4.6)$$

Then, we can obtain the motion equations of the mobile manipulator by simply substituting the Lagrangian  $L(q, \dot{q})$  into the Lagrange-d'Alembert formulation

$$\left( \frac{d}{dt} \frac{\partial L}{\partial \dot{q}_u} - \frac{\partial L}{\partial q_u} - \tau_u \right) - C_u^T C_c^{-T} \left( \frac{d}{dt} \frac{\partial L}{\partial \dot{q}_c} - \frac{\partial L}{\partial q_c} - \tau_c \right) = 0 \quad (4.7)$$

where  $q_u = (q_1 \ q_2 \ q_3 \ q_4 \ q_5)$  and  $q_c = (x_w \ y_w)$ .

## 4.4 Manipulability

Singularities usually correspond to points on the boundary of the manipulator workspace, that is, to points of maximum reach of the manipulator. At singularities or singular configurations, the rank of the Jacobian decreases, which may mean that certain directions of motion are unattainable. In some sense, the farther the manipulator is away from singularities, the better able it is to move uniformly and apply forces uniformly in all directions. Several measures have been suggested for quantifying this effect.

Since singular configurations are given by

$$\det(J(\theta)) = 0, \quad (4.8)$$

it is natural to use the determinant of the Jacobian in a measure of manipulator dexterity. The manipulability measure,  $w$  is defined as

$$w = \sqrt{\det(J(q)J^T(q))}, \quad (4.9)$$

which for a non-redundant manipulator reduces to

$$w = |\det(J(q))|. \quad (4.10)$$

Consider the mobile manipulator shown in Figure 4.1. The Jacobian matrix is  $3 \times 3$  square matrix  $J_m$  whose elements are

$$J_m(1, 1) = -L_2 \cos q_4 \sin q_3 - L_3 \cos(q_4 + q_5) \sin q_3,$$

$$J_m(1, 2) = -L_2 \cos q_3 \sin q_4 - L_3 \cos q_3 \sin(q_4 + q_5),$$

$$J_m(1, 3) = -L_3 \cos q_3 \sin(q_4 + q_5),$$

$$J_m(2, 1) = L_2 \cos q_3 \cos q_4 + L_3 \cos q_3 \cos(q_4 + q_5),$$

$$J_m(2, 2) = -L_2 \sin q_3 \sin q_4 - L_3 \sin q_3 \sin(q_4 + q_5),$$

$$J_m(2, 3) = -L_3 \sin q_3 \sin(q_4 + q_5),$$

$$J_m(3, 1) = 0,$$

$$J_m(3, 2) = L_2 \cos q_4 + L_3 \cos(q_4 + q_5), \quad \text{and}$$

$$J_m(3, 3) = L_3 \cos(q_4 + q_5).$$

Then, the manipulability measure of the manipulator is

$$w = L_2 L_3 |(L_2 \cos q_4 + L_3 \cos(q_4 + q_5)) \sin q_5|. \quad (4.11)$$

It can be seen that  $w$  is not related to  $q_3$ . Also, for the given link length  $L_1$ ,  $L_2$ , and  $L_3$ , the following relation is obtained by assuming  $\sin q_5 \neq 0$  and using  $\partial w / \partial q_4 = 0$ :

$$\tan q_4 = -\frac{L_3 \sin q_5}{L_2 + L_3 \cos q_5}. \quad (4.12)$$

This means that the tip of the manipulator should be at the same height as the second joint. This can further be interpreted as maximizing the contribution of the angular velocity of the first joint to the manipulability measure.

Substituting Eq. (4.12) into Eq. (4.11) yields

$$w = L_2 L_3 \sqrt{L_2^2 + L_3^2 + 2L_2 L_3 \cos q_5} |\sin q_5|. \quad (4.13)$$

The value of  $q_5$  that maximizes  $w$  is given by

$$\cos q_5 = \frac{\sqrt{(L_2^2 + L_3^2)^2 + 12L_2^2 L_3^2} - (L_2^2 + L_3^2)}{6L_2 L_3}. \quad (4.14)$$

If the manipulator is regarded as a two-link mechanism consisting of  $q_4$  and  $q_5$ , the optimal angle for  $q_5$  is  $90^\circ$ . For the three degrees-of-freedom manipulator as shown in Figure 4.1, however, the optimal  $q_5$  is smaller than  $90^\circ$  because the contribution of  $q_3$  to  $w$  can be made larger by placing the end point of the manipulator farther from the first joint axis.

## 4.5 Nonlinear Controllers

The technique of feedback linearization relies on exact mathematical cancellation of linear or nonlinear terms from the equations of motion. Therefore, the control law using feedback linearization requires the parameters in the dynamic model of the system to be known precisely. In practice, the exact model of the nonlinear system is not available in performing feedback linearization. Then, given uncertainty in the dynamic model, the performance and stability of the system can be compromised. This

uncertainty will typically arise from different manipulator loadings which will affect the parameters in the system. The feedback linearization design utilizes a nominal robot model which differs from the actual. This modeling error will obviously cause the actual system to deviate from the dynamics predicted by the motion equation.

There is only limited literature available on the adaptive control of feedback-linearizable systems. Sastry and Isidori (1989) and Marino and Tomei (1995) developed adaptive control designs for output-feedback stabilization of nonlinear systems. However, they only considered single-input single-output nonlinear systems. Kanelakopoulos et al. (1992) proposed a design method of adaptive feedback-linearizable controllers for single-input, single-output nonlinear systems, and later expanded it to multi-input, multi-output systems using similar design techniques. However, two restrictive conditions were imposed on the control design. They require that the nonlinear system be input-to-state linearizable and be transformable into the so-called parametric-pure-feedback form. Unfortunately, the mobile manipulator is not input-to-state linearizable due to the nonholonomic constraints and cannot be transformed into the pure-feedback form because it violates the assumption of linear parametrization.

There are two major approaches to dealing with model uncertainty - robust control and adaptive control. The typical structure of a robust controller is composed of a nominal part, similar to a feedback linearizing or inverse control law, and of additional terms aimed at dealing with model uncertainty. The adaptive controller is similar,

but in addition the model is actually updated during the operation, based on the measured performance. In the next subsection, robust adaptive robot control theory and nonlinear PD control theory based on the input-output linearized system are introduced and are applied to the control of the mobile manipulator.

#### 4.5.1 Robust Adaptive Control of Robotic Manipulator

The dynamics of a rigid  $n$ -joint manipulator (with the load considered as part of the last link) can be written as

$$M(q)\ddot{q} + C(q, \dot{q})\dot{q} + G(q) = \tau \quad (4.15)$$

where  $q$  is an  $n$  vector of robotic joint angles,  $M(q)$  is the symmetric positive-definite (*s.p.d*) manipulator inertia matrix,  $C(q, \dot{q})$  is an  $n \times n$  matrix such that  $C(q, \dot{q})\dot{q}$  are the Coriolis and centripetal torques. The  $kj$ th element of the matrix  $C(q, \dot{q})\dot{q}$  is defined as

$$c_{kj} = \sum_{i=1}^n \frac{1}{2} \left( \frac{\partial d_{kj}}{\partial q_i} + \frac{\partial d_{ki}}{\partial q_j} - \frac{\partial d_{ij}}{\partial q_k} \right). \quad (4.16)$$

The  $n$  vector  $G(q)$  represents the gravitational torques. In the physical system, the dynamics have an important passivity property, which ensures that, by proper choice of  $C$  in the above parametrization,

$$s^T(\dot{M} - 2C)s = 0 \quad (4.17)$$

for any  $s \in \mathbb{R}^n$ . This physically significant fact, together with the positive definite nature of  $M$ , is fundamentally incorporated into the structure of the control

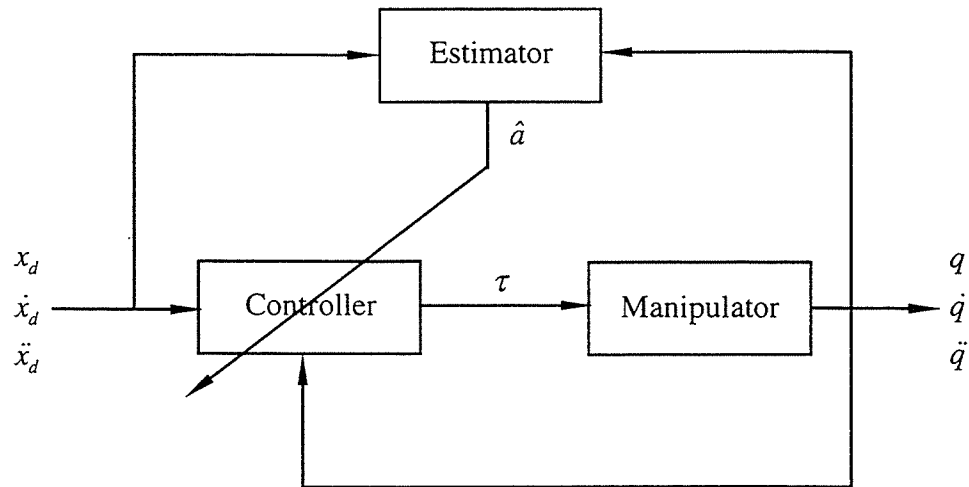


Figure 4.2: The adaptive controller

law below, permitting a physically motivated simplification of an otherwise complex multivariable control problem.

To develop a direct adaptive control law for the system, the tracking error metric is generalized to  $n$  dimensions, by defining

$$s(t) = \ddot{\tilde{q}} + \Lambda \dot{\tilde{q}}(t) \quad (4.18)$$

where  $\Lambda = \Lambda^T > 0$ ,  $\tilde{q}(t) = q(t) - q_d(t)$ , and  $q_d(t)$  is the trajectory the coordinates  $q$  are required to follow, it is assumed to be bounded and at least twice continuously differentiable, with bounded first and second derivatives. It is also convenient to rewrite Eq. (4.18) as  $s(t) = \dot{q} - \dot{q}_r(t)$  where

$$\dot{q}_r(t) = \dot{q}_d(t) - \Lambda \tilde{q}(t). \quad (4.19)$$

Note that this algebraic definition of the error metric  $s$  also has a dynamic inter-

pretation: the actual tracking errors  $\tilde{q}$  are the output of an exponentially stable linear filter driven by  $s$ . Thus, a controller capable of maintaining the condition  $s = 0$  will produce exponential convergence of  $\tilde{q}$  to zero, and hence exponential convergence of the actual joint trajectories to the desired trajectory  $q_d(t)$ .

The state vector for the process is specified in terms of the coordinates  $q$  and their derivatives so that  $x^T = [q^T, \dot{q}^T] \in \mathbb{R}^{2n}$ . With perfect knowledge of  $M$ ,  $C$ , and  $G$  and exact measurement of the state vector, the above derived signals can be used to design an effective nonlinear tracking control algorithm for Eq. (4.15). Indeed, the control law

$$\tau = -K_D s + \tau_n, \quad (4.20)$$

where  $K_D$  is a symmetric positive definite matrix and nonlinear components are given by

$$\tau_n = M(q)\ddot{q}_r + C(q, \dot{q})\dot{q}_r + G(q) \quad (4.21)$$

will produce asymptotically convergent closed-loop tracking of any smooth desired trajectory  $q_d$ , with asymptotically stable closed-loop tracking error dynamics given by

$$M\dot{s} + Cs + K_D s = 0. \quad (4.22)$$

Since a practical controller implementation has at best partial information about the exact structure of the dynamics, the required nonlinear terms are usually not

known exactly. To compensate adaptively for this uncertainty requires first obtaining a factorization of the nonlinear components of the control law:

$$\tau_n = Y(q, \dot{q}, \ddot{q}_r, \ddot{q}_r) a. \quad (4.23)$$

Prior knowledge about the system dynamics must be exploited to separate the (assumed known) nonlinear functions comprising the elements of  $M$ ,  $C$ , and  $G$ , from the (unknown but constant) physical parameter  $a$ . Such a factorization is always possible for the rigid body dynamics of a fixed-based manipulator, when the physical uncertainty is on the mass properties of the individual manipulator links (Khosla and Kanade, 1985) and arises naturally from the structure of the Lagrangian equations of motion.

Using this factorization, but perhaps lacking exact knowledge of the mass properties of the manipulator, the nonlinear components can be implemented using estimates,  $\hat{a}$ , of the true physical parameters,  $a$  as

$$\tau = -K_D s + Y \hat{a}. \quad (4.24)$$

Such a controller results in the closed-loop dynamics

$$M \dot{s} + C s + K_D s = Y \tilde{a} \quad (4.25)$$

where  $\tilde{a} = \hat{a} - a$ , and the model error  $Y \tilde{a}$  acts as a perturbation on the otherwise asymptotically stable closed-loop dynamics. The effects of these perturbations can be asymptotically eliminated by continuously tuning the estimates of the physical

parameters according to the adaptation law

$$\dot{\hat{a}} = -\Gamma Y^T s \quad (4.26)$$

where  $\Gamma$  is a constant, symmetric, positive definite matrix controlling the rate of adaptation. The formal analysis in Slotine and Li (1989) shows that the coupled learning and control strategy, Eqs. (4.24) and (4.26), ensures globally stable operation and asymptotically perfect tracking of any sufficiently smooth desired trajectory.

In practice, the model of the robotic manipulator is always subject to some kind of modeling uncertainties. Among those are the external disturbances. Consideration of disturbances is particularly important in designing the robust controller of the mobile manipulator because the coupling terms appear in the motion equation of each subsystem. Therefore, achieving robustness to the motion disturbances might be crucial. This motivates the design of robust adaptive controller in the presence of disturbances (Reed and Ioannou, 1989).

It is supposed that the model of the robotic manipulator with disturbances is described as

$$M(q)\ddot{q} + C(q, \dot{q})\dot{q} + G(q) = \tau + \tau_d \quad (4.27)$$

where

$$\|\tau_d\| < \infty. \quad (4.28)$$

When the physical parameters are assumed to be unknown, the following robust

adaptive law is proposed:

$$\dot{\hat{a}} = -\sigma\Gamma\hat{a} - \Gamma Y^T s \quad (4.29)$$

and the switching parameter  $\sigma$  is chosen as

$$\sigma = \begin{cases} 0, & \text{for } \|\hat{a}\| < a_0 \\ \sigma_0 \left( \frac{\|\hat{a}\|}{a_0} - 1 \right), & \text{for } a_0 < \|\hat{a}\| < 2a_0 \\ a_0, & \text{for } \|\hat{a}\| > 2a_0 \end{cases} \quad (4.30)$$

The positive scalar  $\sigma_0$  is a design parameter and  $a_0$  is chosen such that  $a_0 > \|a\|$ .

Examining Eqs. (4.24) and (4.26), the joint-space adaptive controller can be interpreted as using only reference velocity and acceleration as input signals and guaranteeing convergence only to these. It is then the definition of the reference velocity in Eq. (4.19) that guarantees the actual convergence to the desired trajectory. Because in the case of Cartesian motion a desired joint trajectory is not given, we now proceed by redefining the joint reference velocity in terms of its Cartesian counterpart. More precisely, the Cartesian reference velocity and acceleration are defined as

$$\dot{x}_r = \dot{x}_d - \Lambda\tilde{x}, \quad \text{and} \quad (4.31)$$

$$\ddot{x}_r = \ddot{x}_d - \Lambda\dot{\tilde{x}}. \quad (4.32)$$

They are related to the joint reference velocity and acceleration by the Jacobian of the mapping  $f : q \mapsto x$ , under the assumption that  $f$  is smooth and invertible,

$$J(q) = \frac{\partial f}{\partial q}, \quad (4.33)$$

$$\dot{x}_r = J(q)\dot{q}_r, \text{ and} \quad (4.34)$$

$$\ddot{x}_r = J(q)\ddot{q}_r + \dot{J}(q)\dot{q}_r \quad (4.35)$$

where  $J(q)$  is a jacobian mapping matrix.

To compute the joint quantities, the above equations are simply inverted. Then, joint reference velocity and acceleration are defined as

$$\dot{q}_r = J^{-1}\dot{x}_r \text{ and} \quad (4.36)$$

$$\ddot{q}_r = J^{-1}\ddot{x}_r - J^{-1}\dot{J}J^{-1}\dot{x}_r. \quad (4.37)$$

This approach will guarantee convergence of Cartesian motion to the desired trajectory, similar to the joint space case, as long as singularities are avoided. Thus, the actual inverse kinematic solution for the desired joint position is not computed directly but rather determined by the dynamics of the system.

## 4.5.2 Nonlinear PD Control of Mobile Platform

A simple approach to controller synthesis for nonlinear systems is to design a linear controller based on the linearization of the system about an operating point. Since the linearization of a system locally determines the stability of the full system, this class of controllers is guaranteed to be locally stable. In many situations, it is possible to prove global stability for a linear controller by explicit construction of a Lyapunov function.

An example of this design methodology is a proportional plus derivative (PD) control law. In its simplest form, a PD control law has the form

$$\tau = -K_p \tilde{q} - K_d \dot{\tilde{q}} \quad (4.38)$$

where  $\tilde{q} = q - q_d$  is the position error and  $K_p$ ,  $K_d$  are diagonal matrices of positive proportional and derivative gains, respectively. Since this control law has no feedforward term, it can never achieve exact tracking for nontrivial trajectories. However, the application of nonlinear PD control is very effective for the set-point control of the mobile platform which is responsible for positioning the manipulator in task space.

## 4.6 Interaction Control

In general, the manipulator cannot follow the desired trajectory without the help of the mobile platform which also positions in the horizontal plane the manipulator to avoid singular configurations. In the previous section, the nonlinear controller for each subsystem of the mobile manipulator was briefly described. In this section, we develop the nonlinear interaction controller based on the redundancy resolution scheme suggested in Sec.4.1. The interaction controller is represented by the block diagram of Figure 4.3.

The desired trajectory of the mobile manipulator is given in the global frame. The manipulator is commanded to move in the local frame fixed on the first joint axis. Subsequently, the base of the manipulator, which is located on the platform,

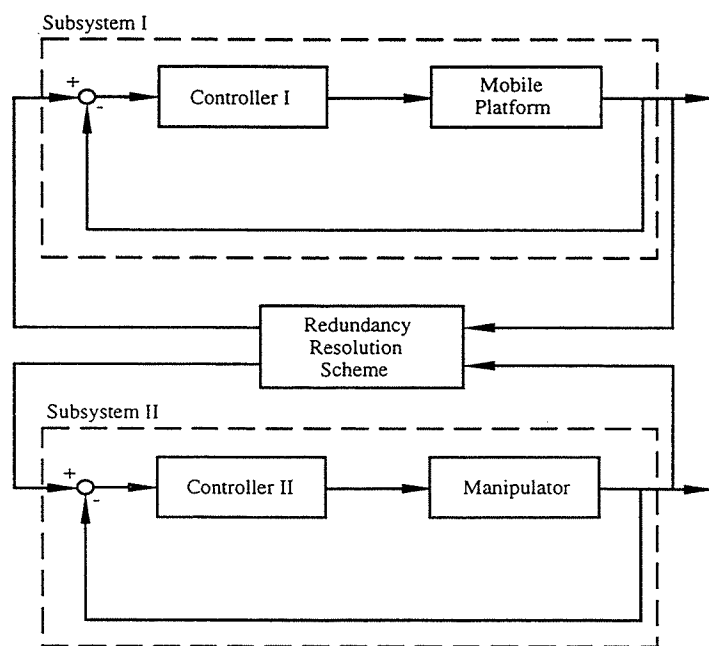


Figure 4.3: The interaction control

is followed by the mobile platform in such a way that it can track the trajectory transformed into the local frame.

The transformation of the desired trajectory  $X_d$  can be performed using the rotation matrix  $R_z(\theta)$  about the z-axis:

$$x_d = R_z^{-1}(X_d - X_w) \quad (4.39)$$

where  $x_d$  is the desired trajectory in the local frame,

$$R_z(\theta) = \begin{bmatrix} \cos \theta & -\sin \theta & 0 \\ \sin \theta & \cos \theta & 0 \\ 0 & 0 & 1 \end{bmatrix}, \quad (4.40)$$

and  $X_w = [x_w, y_w]$  is the mid-point of the wheel base line.

Therefore, the position error  $e_m$  and the velocity error  $\dot{e}_m$  used in the robust adaptive control law are modified to

$$e_m = x_e - R_z^{-1}(\theta)(X_d - X_w) \quad \text{and} \quad (4.41)$$

$$\dot{e}_m = \dot{x}_e - \dot{x}_d \quad (4.42)$$

where  $\dot{x}_d$  is the desired velocity trajectory in the local frame and can be written as

$$\dot{x}_d = \dot{R}_z^{-1}(\theta)(X_d - X_w) + R_z^{-1}(\theta)(\dot{X}_d - \dot{X}_w) \quad (4.43)$$

Now, the Cartesian reference velocity and acceleration are redefined as

$$\dot{x}_r = \dot{x}_d - \Lambda e_m \quad (4.44)$$

$$\ddot{x}_r = \ddot{x}_d - \Lambda \dot{e}_m \quad (4.45)$$

where the desired acceleration in the local frame  $\ddot{x}_d$  is written as

$$\ddot{x}_d = \ddot{R}_z^{-1}(X_d - X_w) + 2\dot{R}_z^{-1}(\dot{X}_d - \dot{X}_w) + R_z^{-1}(\ddot{X}_d - \ddot{X}_w). \quad (4.46)$$

Consider the linear parametrization according to Eq. (4.23). The elements of the parameter vector  $a$  are defined as follows:

$$a = \begin{bmatrix} I_1 \\ I_2 \\ I_3 \\ L_2^2 m_3 \\ L_{c_3} L_2 m_3 \\ L_{c_2} m_2 g \\ L_2 m_3 g \\ L_{c_3} m_3 g \end{bmatrix}. \quad (4.47)$$

Then, it can be shown that each term on the left-hand side of Eq. (4.23) can be put into the form of Eq. (4.27) by a proper parametrization and the control and adaptation laws can be written explicitly as

$$\tau = Y(q, \dot{q}, \ddot{q}, \dot{q}_r, \ddot{q}_r) \hat{a} - K_D s \quad (4.48)$$

where  $Y$  is the parameterized equations of motion in matrix form and its elements are defined as

$$Y(1, 1) = \ddot{q}_{r_3},$$

$$Y(1, 2) = \frac{1}{2}(\ddot{q}_{r_3} + \ddot{q}_{r_3} \cos(2q_4) - \dot{q}_4 \dot{q}_{r_3} \sin(2q_4) - \dot{q}_3 \dot{q}_{r_4} \sin(2q_4)),$$

$$Y(1, 3) = \frac{1}{2}(\ddot{q}_{r_3} + \ddot{q}_{r_3} \cos(2(q_4 + q_5)) - \dot{q}_4 \dot{q}_{r_3} \sin(2(q_4 + q_5)) - \dot{q}_5 \dot{q}_{r_3} \sin(2(q_4 + q_5)) - \dot{q}_3 \dot{q}_{r_4} \sin(2(q_4 + q_5)) - \dot{q}_3 \dot{q}_{r_5} \sin(2(q_4 + q_5))),$$

$$Y(1, 4) = \frac{1}{2}(\ddot{q}_{r_3} + \ddot{q}_{r_3} \cos(2q_4) - \dot{q}_4 \dot{q}_{r_3} \sin(2q_4) - \dot{q}_3 \dot{q}_{r_3} \sin(2q_4)),$$

$$Y(1, 5) = \ddot{q}_{r_3} \cos q_5 + \ddot{q}_{r_3} \cos(2q_4 + q_5) - \dot{q}_5 \dot{q}_{r_3} \cos q_4 \sin(q_4 + q_5) - \dot{q}_3 \dot{q}_{r_5} \cos q_4 \sin(q_4 + q_5) - \dot{q}_4 \dot{q}_{r_3} \sin(2q_4 + q_5) - \dot{q}_3 \dot{q}_{r_4} \sin(2q_4 + q_5),$$

$$Y(2, 1) = \ddot{q}_{r_4} + \frac{1}{2} \dot{q}_3 \dot{q}_{r_3} \sin(2q_4),$$

$$Y(2, 2) = 0,$$

$$Y(2, 3) = \ddot{q}_{r_4} + \ddot{q}_{r_5} + \frac{1}{2} \dot{q}_3 \dot{q}_{r_3} \sin(2(q_4 + q_5)),$$

$$Y(2, 4) = \frac{1}{2}(\ddot{q}_{r_4} - \ddot{q}_{r_4} \cos(2q_4) + \dot{q}_3 \dot{q}_{r_3} \sin(2q_4) + \dot{q}_4 \dot{q}_{r_4} \sin(2q_4)),$$

$$Y(2, 5) = \ddot{q}_{r_4} \cos q_5 + \frac{1}{2} \ddot{q}_{r_5} \cos q_5 - \ddot{q}_{r_4} \cos(2q_4 + q_5) - \frac{1}{2} \ddot{q}_{r_5} \cos(2q_4 + q_5) + \dot{q}_5 \dot{q}_{r_4} \cos(q_4 + q_5) \sin q_4 + \dot{q}_4 \dot{q}_{r_5} \cos(q_4 + q_5) \sin q_4 + \dot{q}_5 \dot{q}_{r_5} \cos(q_4 + q_5) \sin q_4 + \dot{q}_3 \dot{q}_{r_3} \sin(2q_4 + q_5) + \dot{q}_4 \dot{q}_{r_4} \sin(2q_4 + q_5),$$

$$Y(2, 6) = \cos q_4,$$

$$Y(2, 7) = \cos q_4,$$

$$Y(2, 8) = \cos(q_4 + q_5),$$

$$Y(3, 1) = 0,$$

$$Y(3, 2) = 0,$$

$$Y(3, 3) = \ddot{q}_{r_4} + \ddot{q}_{r_5} + \frac{1}{2}\dot{q}_3\dot{q}_{r_3} \sin(2(q_4 + q_5)),$$

$$Y(3, 4) = 0,$$

$$Y(3, 5) = \frac{1}{2}\ddot{q}_{r_4} \cos q_5 - \frac{1}{2}\ddot{q}_{r_4} \cos(2q_4 + q_5) + \dot{q}_3\dot{q}_{r_3} \cos q_4 \sin(q_4 + q_5) + \dot{q}_4\dot{q}_{r_4} \cos q_4 \sin(q_4 + q_5),$$

$$Y(3, 6) = 0,$$

$$Y(3, 7) = 0, \text{ and}$$

$$Y(3, 8) = \cos(q_4 + q_5).$$

We restate the velocity constraint equations obtained in the previous chapter as follows:

$$\dot{x}_w = d_1 h(\dot{q}_1 + \dot{q}_2) \cos \theta \quad \text{and} \quad (4.49)$$

$$\dot{y}_w = d_1 h(\dot{q}_1 + \dot{q}_2) \sin \theta. \quad (4.50)$$

Then, the Jacobian mapping matrix of the mobile platform is defined as

$$J_p = \frac{r_w}{2d_1} \begin{bmatrix} d_1 \cos \theta & d_1 \cos \theta \\ d_1 \sin \theta & d_1 \sin \theta \end{bmatrix}. \quad (4.51)$$

When the mid-point of the wheel base line is selected as the output, it is easily verified that the system is not controllable. This lack of controllability results simply because the mobile platform cannot move along the wheel axis instantaneously. However, full feedback linearization can still be made possible by using the so-called dynamic

extension algorithm (Isidori, 1995). The idea of this algorithm is to delay some combinations of inputs simultaneously affecting several outputs, via the addition of integrators, in order to enable other inputs to act in the meantime and therefore hopefully to obtain an extended decoupled system. Instead, the reference point  $X_p$  directly under the end-point of the manipulator in an optimal configuration is chosen as the output. Then, the Jacobian is written as

$$J_p = \frac{r_w}{2d_1} \begin{bmatrix} d_1 \cos \theta - p \sin \theta & d_1 \cos \theta + p \sin \theta \\ d_1 \sin \theta + p \cos \theta & d_1 \sin \theta - p \cos \theta \end{bmatrix} \quad (4.52)$$

where  $p$  is the distance from the mid-point of the wheel base line to the reference point. Now, the mobile platform is controllable because  $J_p$  is not singular. Also, the system is input-output linearizable by using a nonlinear feedback.

As described in Sec. 4.1 and Sec. 4.5, the mobile platform is responsible for positioning the manipulator at the desired position in the global frame. In the nonlinear PD control law, the position error has the form

$$e_p = X_e - X_p \quad (4.53)$$

where  $X_e$  and  $X_p$  are the position coordinates of the end point of the manipulator and the reference point of the platform respectively. They can be written as

$$X_e = \begin{bmatrix} x_w + x_e \cos(\theta + q_3) + d_3 \cos \theta \\ y_w + y_e \sin(\theta + q_3) + d_3 \sin \theta \end{bmatrix} \quad \text{and} \quad (4.54)$$

$$X_p = \begin{bmatrix} x_w + p \cos \theta \\ y_w + p \sin \theta \end{bmatrix}. \quad (4.55)$$

In most control schemes, including the feedback linearizing control and the interaction control which were developed in this work, the measurement of state variables is required to provide the necessary information for feedback control. The most commonly used sensors are the angular position sensors, the angular velocity sensors, and the angular acceleration sensors. In Appendix A, measurement devices used in robotic manipulators and wheeled mobile robots are presented.

## 4.7 Simulations

In this section, computer simulation is carried out to test the performance of the nonlinear interaction controller developed throughout this chapter. The mobile manipulator shown in Figure 4.1 is used in the simulation and the following parameters are used:

$$m_p = 90kg, m_w = 5kg, m_1 = 2kg, m_2 = 5kg, m_3 = 5kg,$$

$$I_p = 9kg \cdot m^2, I_w = 0.5kg \cdot m^2, I_m = 0.1kg \cdot m^2,$$

$$I_1 = 0.15kg \cdot m^2, I_2 = 0.25kg \cdot m^2, I_3 = 0.25kg \cdot m^2,$$

$$L_1 = 0.4m, L_2 = 0.4m, L_3 = 0.4m,$$

$$L_{c1} = 0.2m, L_{c2} = 0.2m, L_{c3} = 0.2m,$$

$$e = 0.0375m, r_w = 0.075m, d_1 = 0.2m, d_2 = 0.35m, \text{ and } g = 9.8m/sec^2.$$

For each simulation, the mobile manipulator is initially at rest and the heading angle is set to be zero. For the PD controller, the feedback gains are arbitrarily initialized to  $K_p = \text{diag}(35, 35)$  and  $K_d = \text{diag}(25, 25)$ . The actual parameters used in the simulation are

$$a = (0.15, 0.25, 0.25, 0.8, 0.4, 9.8, 19.6, 9.8)^T.$$

The adaptation gains and the feedback gain matrix are arbitrarily assigned. The adaptation gains  $\Gamma$  and  $\Lambda$  are chosen respectively as

$$\Gamma = \text{diag}(0.15, 0.15, 0.15, 0.15, 0.15, 0.25, 0.25, 0.25) \quad \text{and}$$

$$\Lambda = \text{diag}(20, 35, 45)$$

The gain matrix  $K_D$  is set to  $\text{diag}(10, 15, 5)$ .

Three different desired trajectories are applied in simulation to the redundant mobile manipulator. The desired trajectories are chosen as follows:

#### Simulation I

$$x_d(t) = 1.0528 + t/10$$

$$y_d(t) = 0$$

$$z_d(t) = 0.5125 + 0.1 \sin\left(\frac{\pi}{6}t\right)$$

#### Simulation II

$$x_d(t) = 1.0548 + t/10$$

$$y_d(t) = 0.1 \sin\left(\frac{\pi}{6}t\right)$$

$$z_d(t) = 0.5115 + 0.1 \sin\left(\frac{\pi}{6}t\right)$$

### Simulation III

$$x_d(t) = 1.1028 + 0.2(1 - \cos\left(\frac{\pi}{6}t\right))$$

$$y_d(t) = 0.2 \sin\left(\frac{\pi}{6}t\right)$$

$$z_d(t) = 0.5125 + 0.1 \sin\left(\frac{\pi}{6}t\right)$$

Sinusoidal trajectories are used in all simulations. At the beginning of each simulation, the manipulator is controlled to follow the desired trajectory while the platform remains stationary. Then, the platform is commanded to track the set-point located on the horizontal plane directly below the end-point in such a way that the manipulator can avoid a singular configuration. Initially, the end point is not on the specified initial position in each simulation. The position error of the end point, the heading angle, the angular displacement of each wheel, the angular displacement of each joint, the position of the mobile platform, and the control inputs are plotted in Figure 4.4 - 4.24.

Only partial information of the actual parameters ( $\hat{a}(0) = 0.75a$ ) is given to the controller at the beginning. Due to this uncertainty on the mass properties of the system,  $z$  position error is relatively large for the first few seconds of transient period as can be seen in Figure 4.4, 4.11, and 4.18. However, the tracking errors improve as the robust adaptive controller extracts parameter information from the tracking

errors.

Figure 4.7, 4.14, and 4.21 depict the angular displacement of each joint of the manipulator. From these plots, it is observed that the joint angles drift for the first few seconds while the end-point is tracking the desired trajectory with relatively large initial errors due to the mass uncertainty imposed on the controller. As the tracking errors improve, each joint repeats similar patterns of configurations without drift.

Figure 4.9, 4.16, and 4.23 show the actual trajectory of the mid-point of the wheel base line. Note that the reference point located ahead of the platform is chosen as the output of the set-point control of the platform. Therefore, the trajectory of the mid-point of the wheel base line does not necessarily look close to the desired trajectory. This can be seen from Figure 4.23 in which the platform appears to deviate from the circular trajectory. However, the heading angle and the tracking errors, as shown in Figure 4.24 and 4.18 reveal accurate set-point tracking performance of the platform controller.

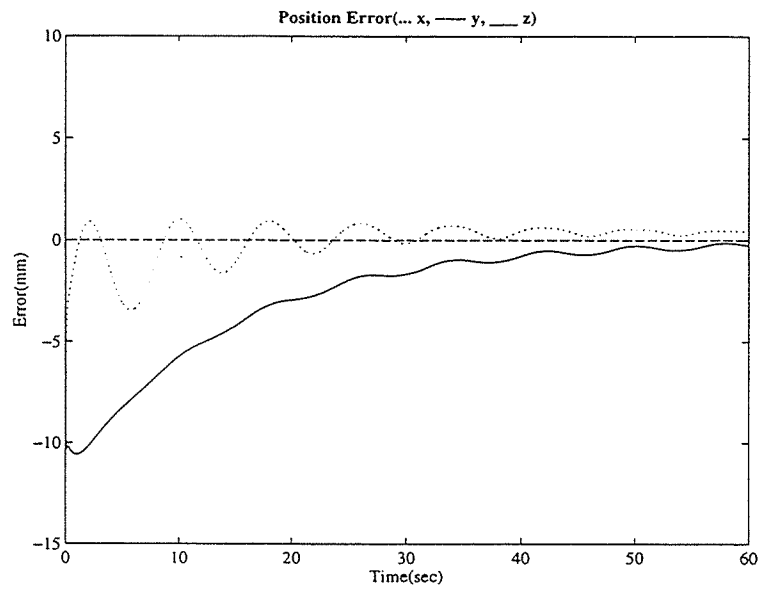


Figure 4.4: Simulation I - position error in task space

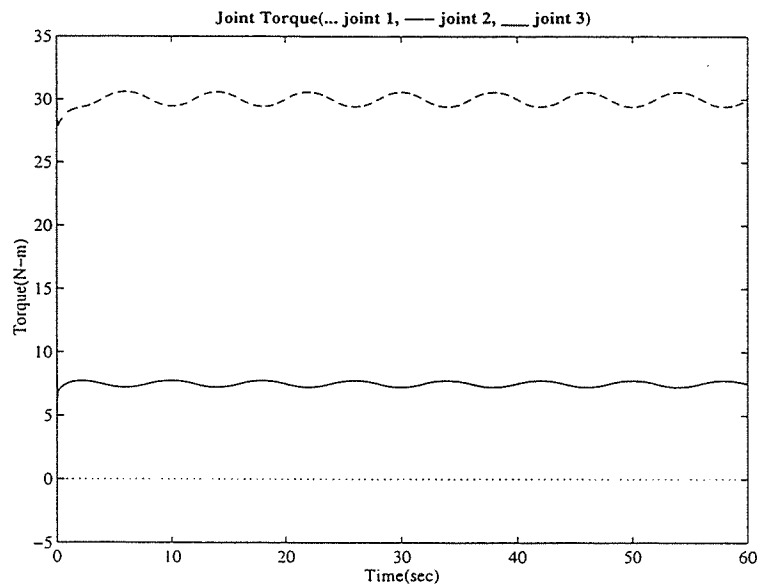


Figure 4.5: Simulation I - actuator torque of each joint of the manipulator

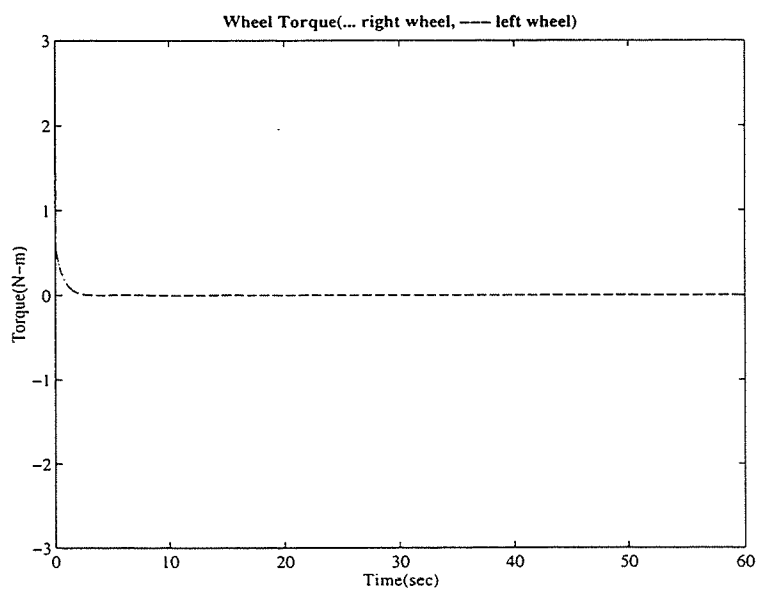


Figure 4.6: Simulation I - actuator torque of each wheel of the mobile platform

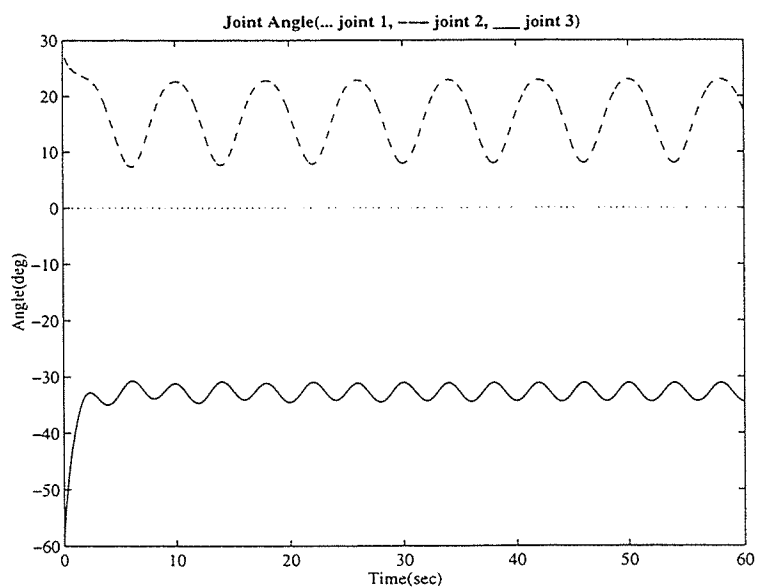


Figure 4.7: Simulation I - angular displacement of each joint

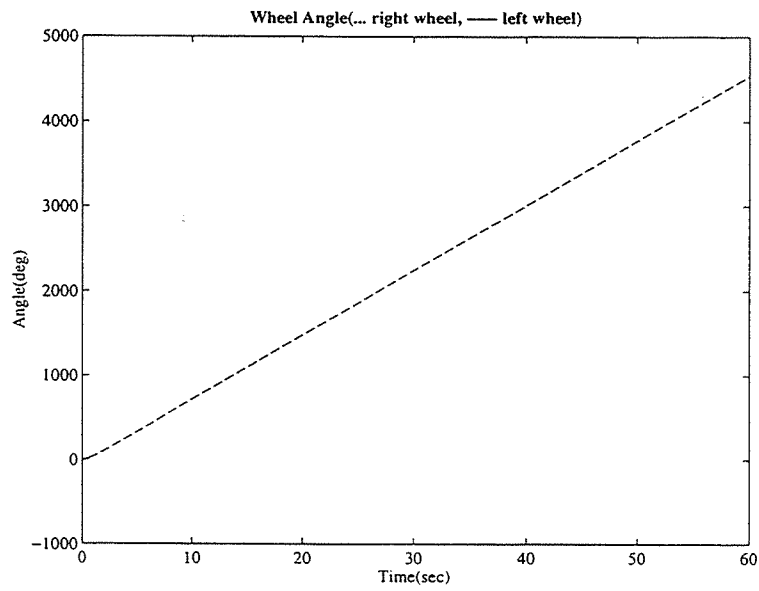


Figure 4.8: Simulation I - angular displacement of each wheel

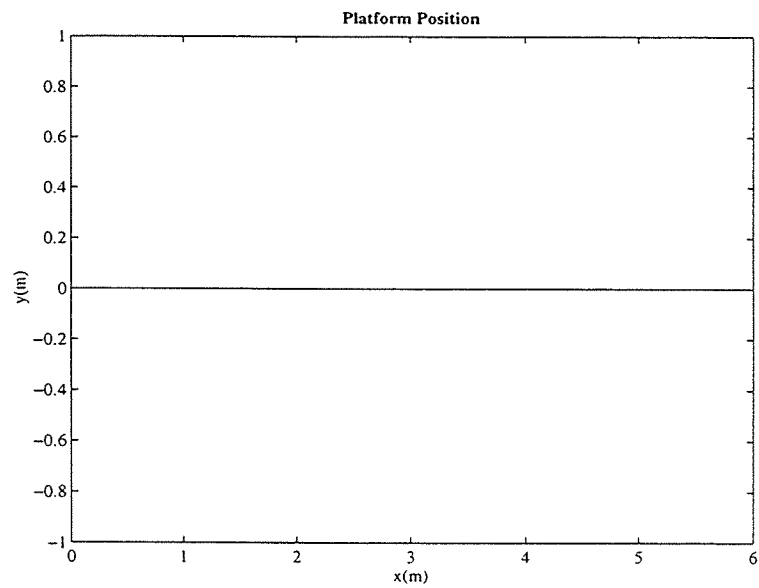


Figure 4.9: Simulation I - xy position of the platform

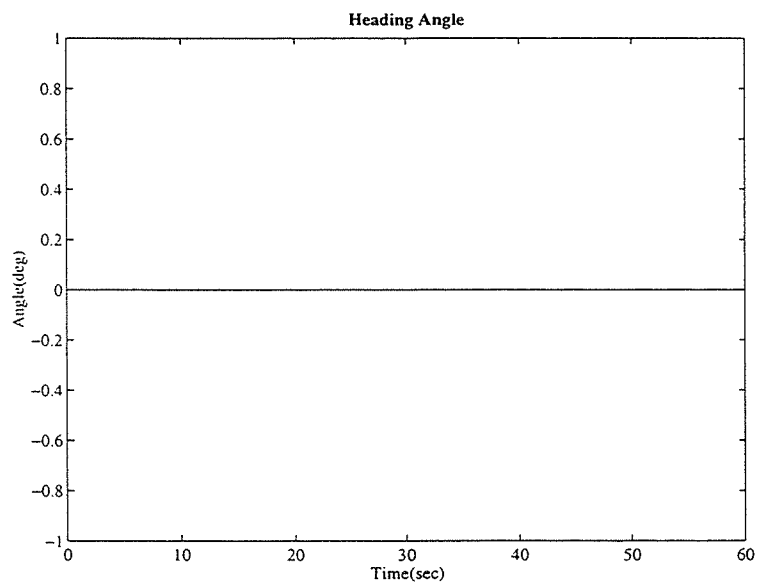


Figure 4.10: Simulation I - heading angle of the platform

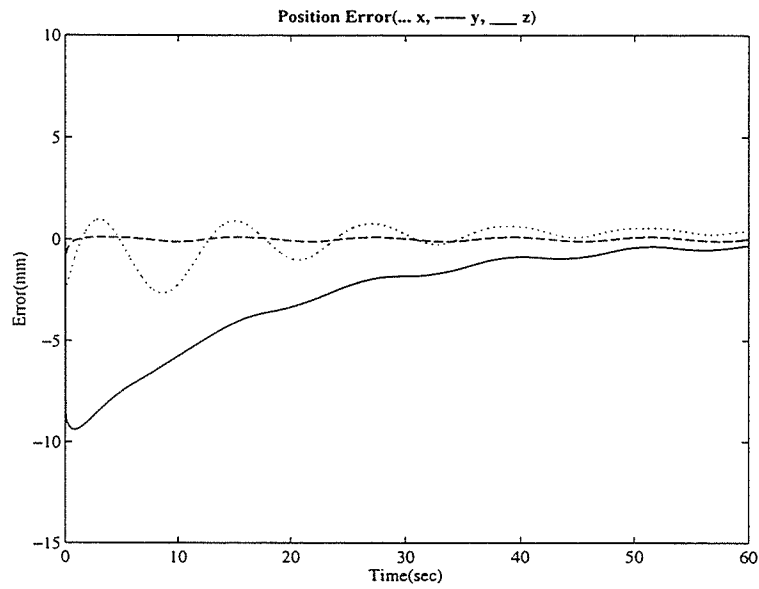


Figure 4.11: Simulation II - position error in task space

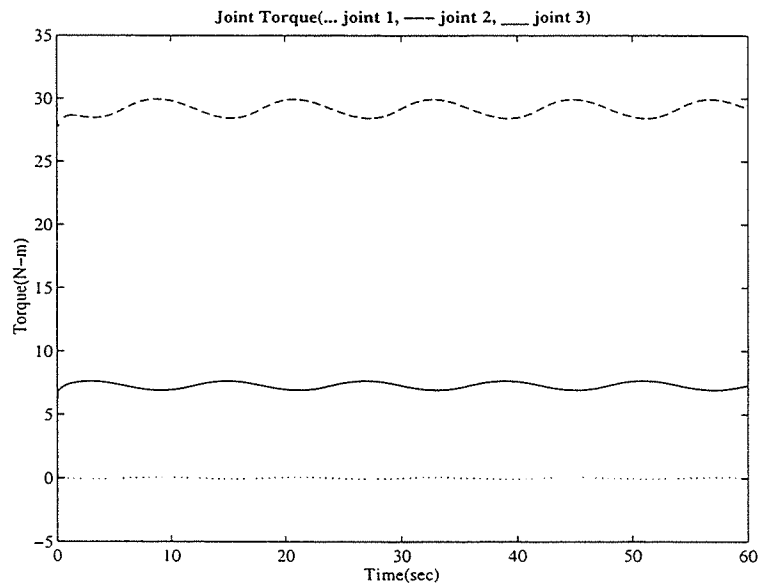


Figure 4.12: Simulation II - actuator torque of each joint of the manipulator

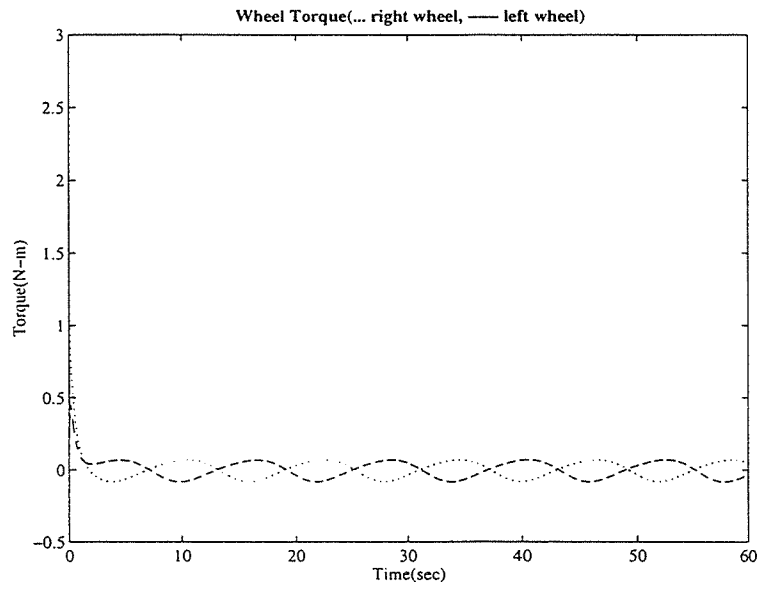


Figure 4.13: Simulation II - actuator torque of each wheel of the mobile platform

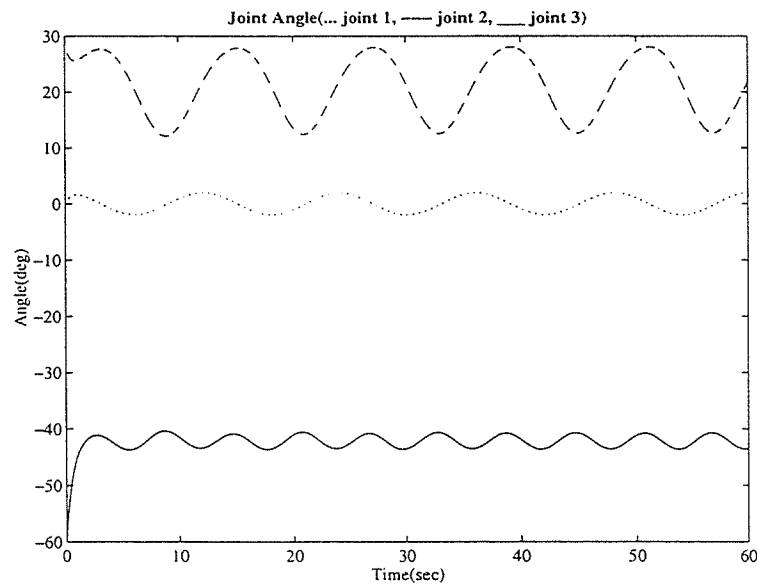


Figure 4.14: Simulation II - angular displacement of each joint

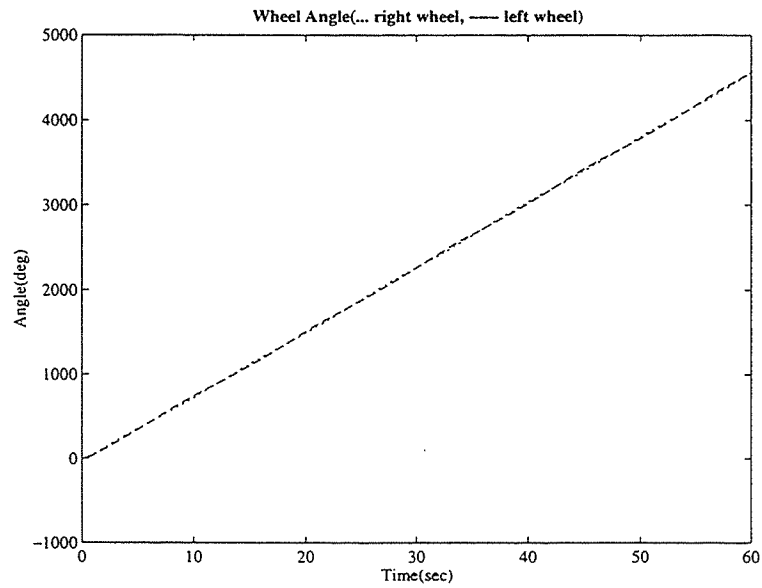


Figure 4.15: Simulation II - angular displacement of each wheel

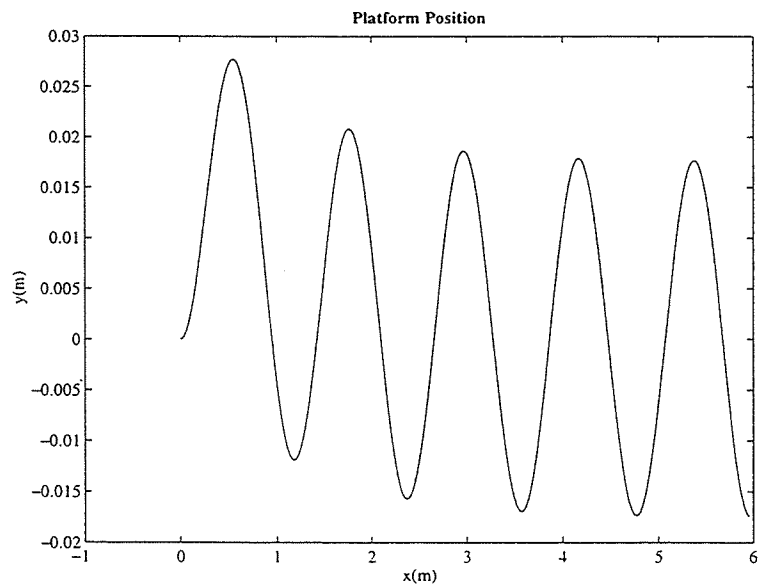


Figure 4.16: Simulation II - xy position of the platform

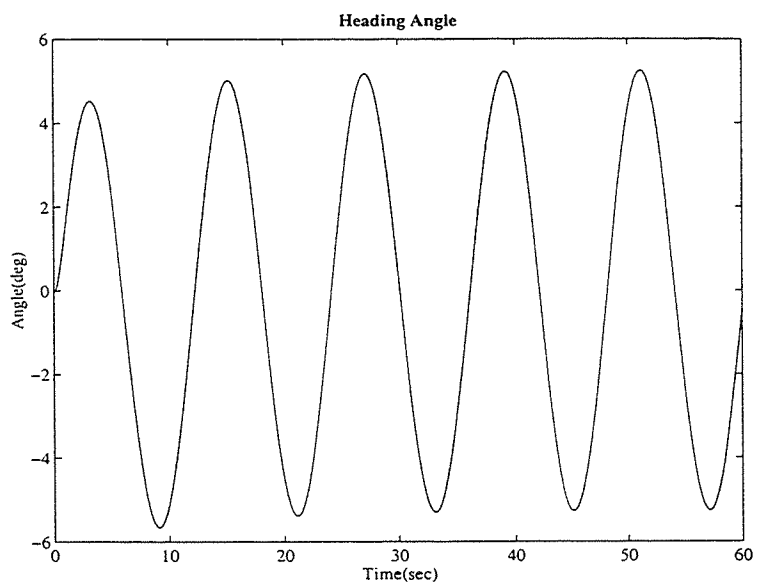


Figure 4.17: Simulation II - heading angle of the platform

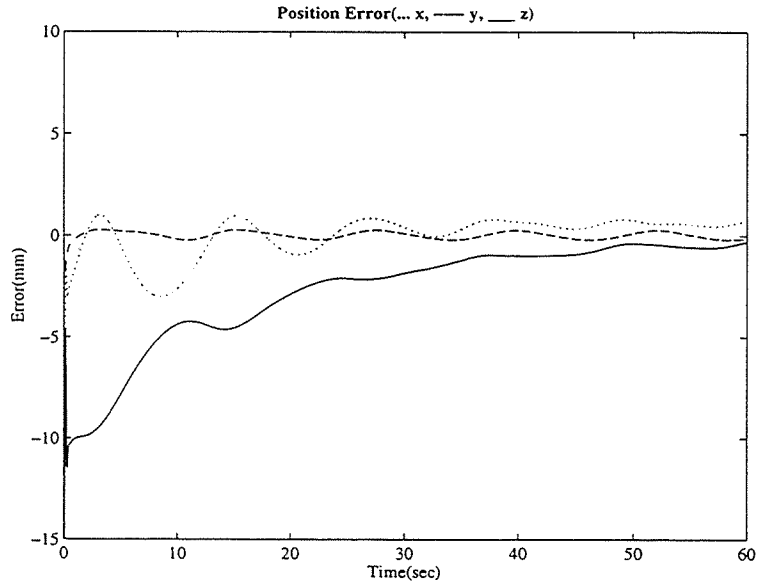


Figure 4.18: Simulation III - position error in task space

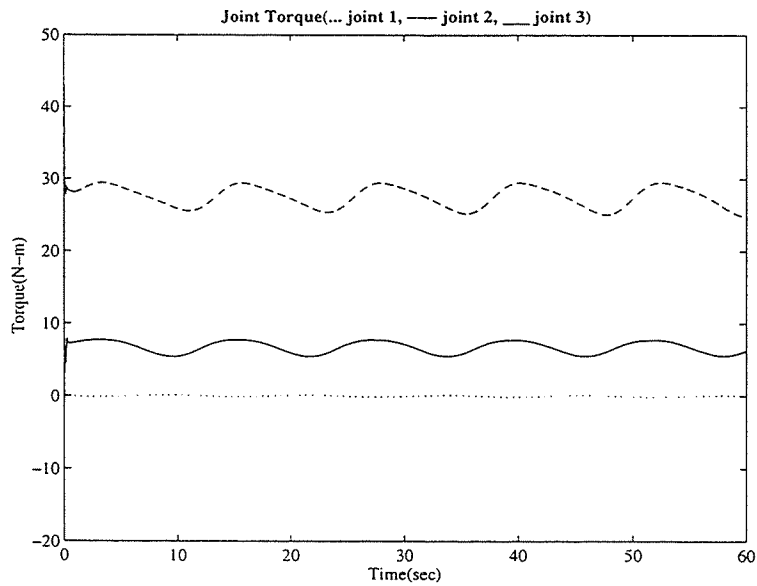


Figure 4.19: Simulation III - actuator torque of each joint of the manipulator

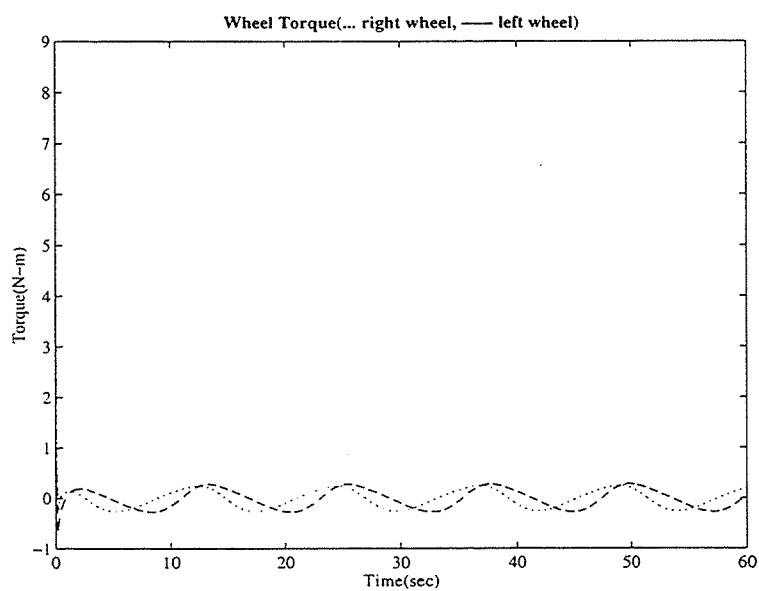


Figure 4.20: Simulation III - actuator torque of each wheel of the mobile platform

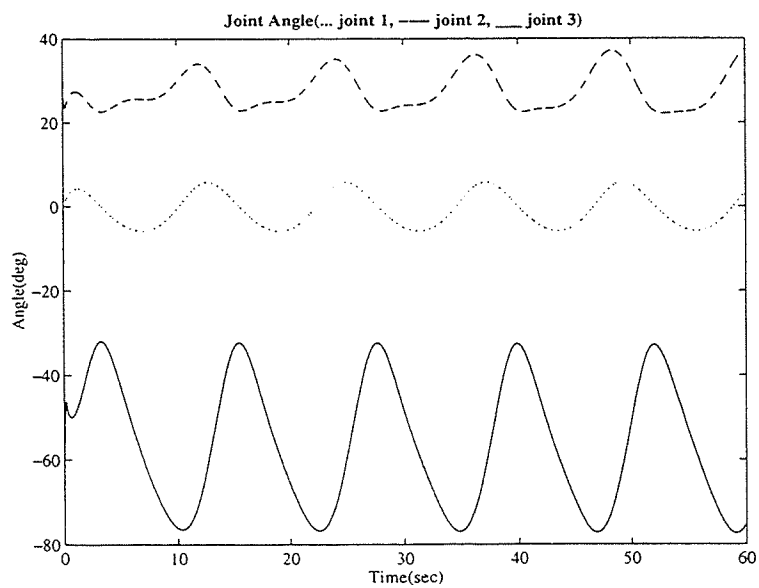


Figure 4.21: Simulation III - angular displacement of each joint

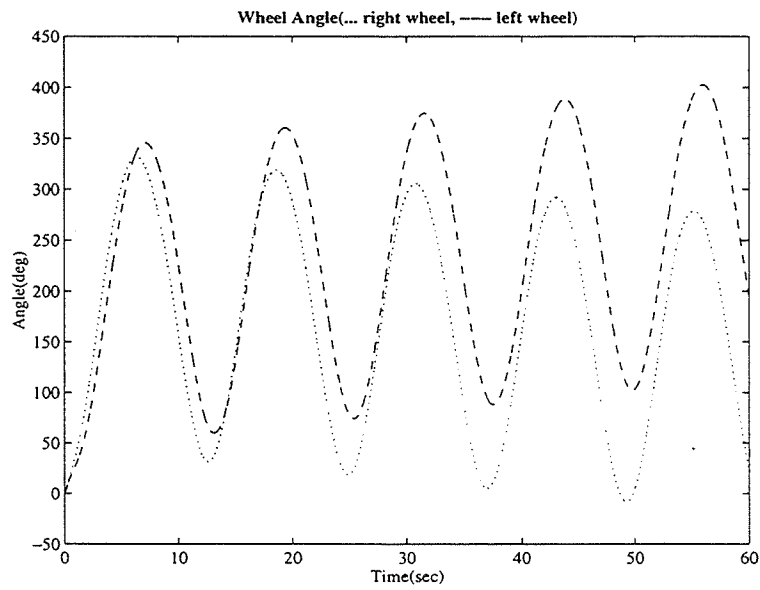


Figure 4.22: Simulation III - angular displacement of each wheel

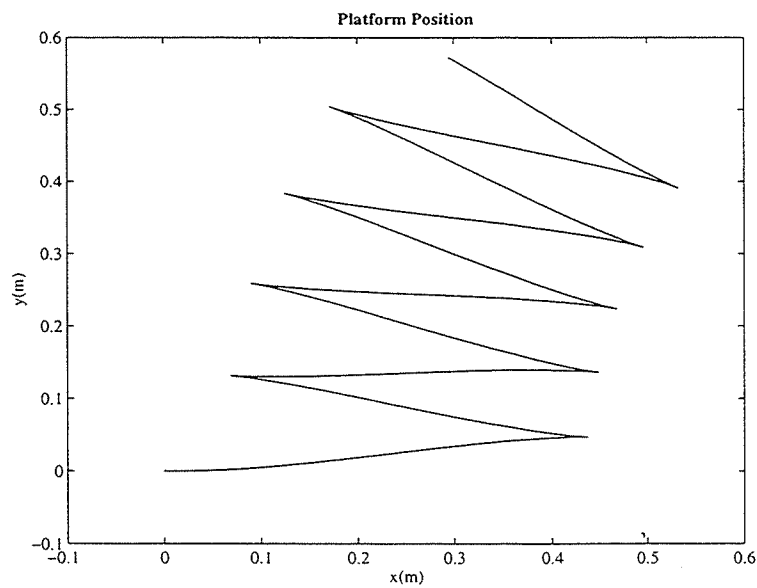


Figure 4.23: Simulation III - xy position of the platform

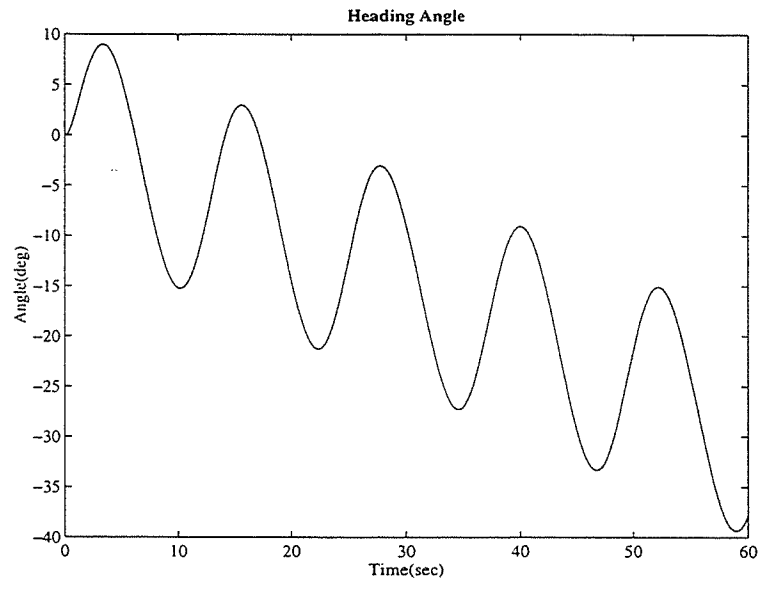


Figure 4.24: Simulation III - heading angle of the platform

## Chapter 5

# Violation of Ideal Constraints

In Chapter 3 and 4, the motion equations of the mobile manipulator were derived based on the assumption that the pure rolling and the non-slipping conditions are satisfied at the contact point of each wheel with the ground. In Chapter 4, the novel interaction control scheme was developed for the kinematic model of the redundant mobile manipulator which operates under no-slip condition and very accurate trajectory tracking was achieved. However, as the mobile manipulator is employed to perform heavy duty work under very high speeds, the impact of wheel slip on the tracking performance of the interaction controller is expected to be substantial.

Recently, Boyden and Velinsky (1994) investigated the importance of dynamic modeling of wheeled mobile robots for high load applications such as highway maintenance and construction. They claimed that use of the kinematic model must be limited to lightweight vehicles which operate under very low speeds, very low accel-

erations, and under lightly loaded conditions. This results motivate the investigation of the tracking performance of the interaction controller for the mobile manipulator subject to wheel slip. First, the dynamic equations of the wheeled mobile robot is derived using Newton's second law. Then, the robustness of the interaction controller is investigated through simulations and a suitable control method is suggested for high load applications as a part of future work.

## 5.1 Dynamic Modeling of Wheeled Mobile Robots

When ideal kinematic constraints are violated due to wheel slippage, modeling of wheeled mobile robots using the Lagrange-d'Alembert formulation is not valid. The equations of motion of the wheeled mobile robot shown in Figure 5.1 can be derived using Newton's second law. Again, note that this is a planar wheeled mobile robot model with three degrees-of-freedom. The detailed derivation of the dynamic equations of wheeled mobile robots can be found in Boyden and Velinsky (1994) and Zhang and Velinsky (1994).

The force and moment equations for the mobile platform can be expressed as

$$\sum F_x = m_p(\dot{u} - v\omega) = F_{ul} + F_{ur}, \quad (5.1)$$

$$\sum F_y = m_p(\dot{v} + u\omega) = F_{vl} + F_{vr}, \quad \text{and} \quad (5.2)$$

$$\sum M_z = I_p\dot{\omega} = d_1(F_{ul} - F_{ur}) - d_2(F_{vl} + F_{vr}). \quad (5.3)$$

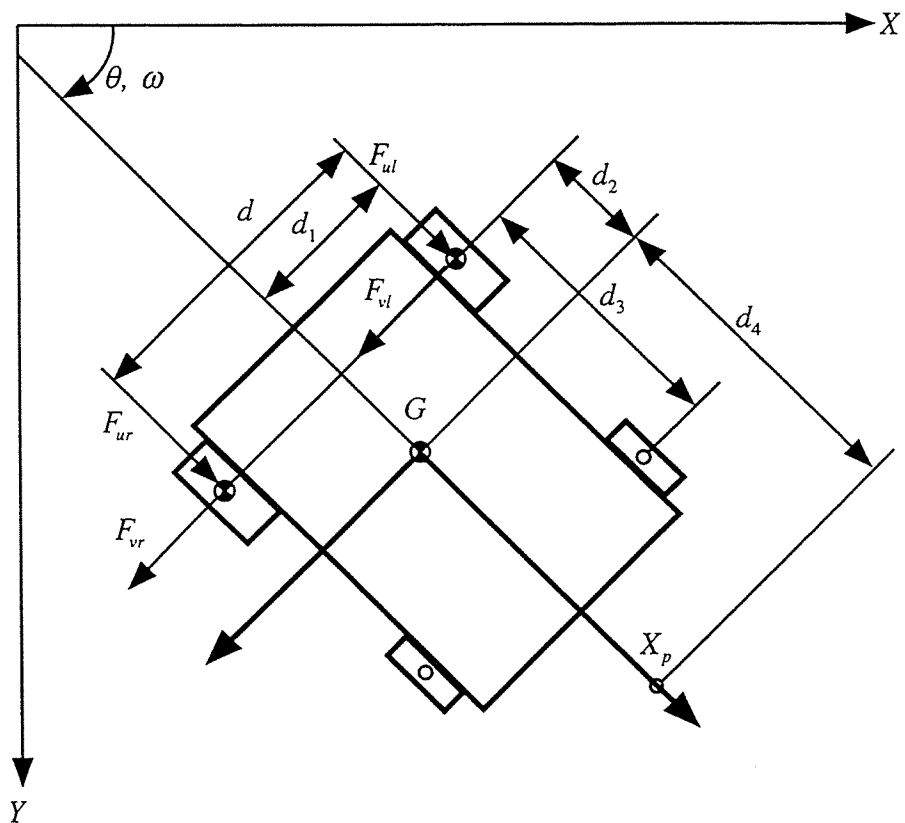


Figure 5.1: Wheeled mobile robot

where  $m_p$  is the mass of the platform,  $I_p$  is the moment of inertia of the platform about z axis,  $I_w$  is the moment of inertia of the combined mass of the wheel and the actuator system about the wheel axis. The velocity constraints of the system are written as

$$u = \frac{1}{2}(u_l + u_r), \quad (5.4)$$

$$v = \frac{d_2}{d_1}(u_l - u_r) + v^s, \quad \text{and} \quad (5.5)$$

$$\omega = \frac{1}{2}(u_l - u_r) \quad (5.6)$$

where  $u$  is the longitudinal velocity,  $v$  is the lateral velocity,  $\omega$  is the yaw rate,  $v^s$  is the lateral slip velocity, and  $u_l$  and  $u_r$  are the longitudinal velocities of the wheel centers. The longitudinal velocities of the wheel centers can be described as follows:

$$u_l = r_w \omega_l - u_l^s \quad \text{and} \quad (5.7)$$

$$u_r = r_w \omega_r - u_r^s \quad (5.8)$$

It is not difficult to show that the motion of the reference point  $X_p$  are described by the following equations:

$$\dot{x} = u \cos \theta - (v + d_4 \omega) \sin \theta, \quad (5.9)$$

$$\dot{y} = u \sin \theta - (v + d_4 \omega) \cos \theta, \quad \text{and} \quad (5.10)$$

$$\dot{\theta} = \omega \quad (5.11)$$

Then, the equations of motion of the mobile platform can be written as

$$\dot{u} = \frac{F_{ul} + F_{ur}}{m_p} + v\omega, \quad (5.12)$$

$$\dot{v} = \frac{F_{vl} + F_{vr}}{m_p} - u\omega, \quad (5.13)$$

$$\dot{\omega} = \frac{1}{I_p} [d_1(F_{ul} - F_{ur}) - d_2(F_{vl} + F_{vr})], \quad (5.14)$$

$$\dot{\omega}_l = \frac{1}{I_w} (\tau_l - F_{ul}), \quad \text{and} \quad (5.15)$$

$$\dot{\omega}_r = \frac{1}{I_w} (\tau_r - F_{ur}) \quad (5.16)$$

where  $\tau_r$  and  $\tau_l$  are the controls. Note that the equations of motions are not in the closed form. The longitudinal and lateral forces on the wheels are calculated by Dugoff's tire friction model (Dugoff et al., 1970).

To see how wheel slip is modeled as the disturbance to the system, we rewrite Eqs. (5.9), (5.10), and (5.11) as

$$\dot{x} = u \cos \theta - d_4 \omega \sin \theta - \delta_x, \quad (5.17)$$

$$\dot{y} = u \sin \theta + d_4 \omega \cos \theta + \delta_y, \quad \text{and} \quad (5.18)$$

$$\dot{\theta} = \omega \quad (5.19)$$

where

$$\delta_x = -v^s \sin \theta \quad \text{and} \quad (5.20)$$

$$\delta_y = v^s \cos \theta. \quad (5.21)$$

Now, the state variables are defined as

$$\eta = \begin{bmatrix} x \\ y \\ \theta \\ u \\ \omega \end{bmatrix}. \quad (5.22)$$

Then, the equations of motion can be written in the state space form as

$$\dot{\eta} = f(\eta) + g(\eta)\tau + \delta \quad (5.23)$$

where

$$f(\eta) = \begin{bmatrix} u \cos \theta - d_4 \omega \sin \theta \\ u \sin \theta + d_4 \omega \cos \theta \\ \omega \\ \frac{d_2 m_p r_w^2}{\chi_u} \omega^2 \\ -\frac{2d_2 m_p r_w^2}{\chi_\omega} u \omega \end{bmatrix}, \quad (5.24)$$

$$g(\eta) = \begin{bmatrix} 0 & 0 \\ 0 & 0 \\ 0 & 0 \\ \frac{2r_w}{\chi_u} & 0 \\ 0 & \frac{4r_w d_2}{\chi_\omega} \end{bmatrix} \begin{bmatrix} \tau_u \\ \tau_\omega \end{bmatrix}, \quad (5.25)$$

$$\delta = \begin{bmatrix} \delta_x \\ \delta_y \\ 0 \\ 0 \\ 0 \end{bmatrix}, \quad (5.26)$$

$$\tau_u = \frac{1}{2}(\tau_l + \tau_r), \quad (5.27)$$

$$\tau_\omega = \frac{1}{2}(\tau_l - \tau_r), \quad (5.28)$$

$$\chi_u = m_p r_w^2 + 2I_w, \quad \text{and} \quad (5.29)$$

$$\chi_\omega = 4I_w d_1^2 + 2r_w(I_p + m_p d_2^2). \quad (5.30)$$

## 5.2 Simulations

With the ideal velocity constraints, it is possible to design the nonlinear PD controller of the mobile platform based on the feedback-linearized system in which

the platform Jacobian exists. However, in real case, the Jacobian mapping does not exist any more because of the wheel slip. Therefore, the platform dynamics cannot be linearized by nonlinear state feedback, which rules out the direct application of the well known nonlinear control algorithms such as feedback linearization and nonlinear PD control. One way to deal with this situation is to use the model of the mobile manipulator subject to the ideal velocity constraints and consider the wheel slip as the disturbance to the system. In this report, we are interested only in investigating the robustness of the interaction controller when wheel slip is introduced to the mobile platform. Another approach to the problem is to design a robust controller for the platform. So far, there is only one literature available on robust control of wheeled mobile platforms which operate under highly loaded conditions. Feng and Velinsky (1996) showed that position tracking control using pulse width modulation is invariant to the external forces and wheel slip. Thus, the interaction control utilizing pulse width modulated control may prove to be very important for high load applications of the mobile manipulator. The design of the robust controller is left to future work.

The same dimensions, physical parameters, and control parameters as with the simulation in the previous chapter are used here with the addition of the parameters in Dugoff's tire friction model:

longitudinal tire stiffness  $C_x = 40034 \text{ N/rad}$

lateral tire stiffness  $C_y = 40034 \text{ N/rad}$

friction coefficient  $\mu = 0.8$

The following desired trajectory used in simulation I in Chapter 5 is applied here in simulation to the redundant mobile manipulator subject to wheel slip:

$$x_d(t) = 1.0528 + t/10$$

$$y_d(t) = 0$$

$$z_d(t) = 0.5125 + 0.1 \sin\left(\frac{\pi t}{6}\right)$$

The position error of the end point, the heading angle, the angular displacement of each wheel, the angular displacement of each joint, the position of the mobile platform, and the control inputs are plotted in Figure 5.2 - 5.7. In addition to the uncertainty on the mass properties of the system, wheel slip is considered as a disturbance to the system as described in the previous section. As shown in Figure 5.2, the results of this simulation indicate that the tracking errors does not seem to improve reasonably fast as in the ideal case owing to the fact that wheel slip acts as a disturbance to the system. Also, Figure 5.5 shows that the joint angles drift for a long period of time. It is expected that the harmful effects of wheel slip can be weakened by a robust controller for the platform (Feng and Velinsky, 1996). This would provide challenging problems such as the tracking performance and stability of the interaction controller.

In this chapter, motivated by the work in Boyden and Velinsky (1994), we explored the robustness problem of the interaction control scheme in the presence of wheel slip. Our intention was to open up some potential problems of the interaction controller for high load and high speed applications of the mobile manipulator and suggest a suitable control design for the platform as a part of future work.

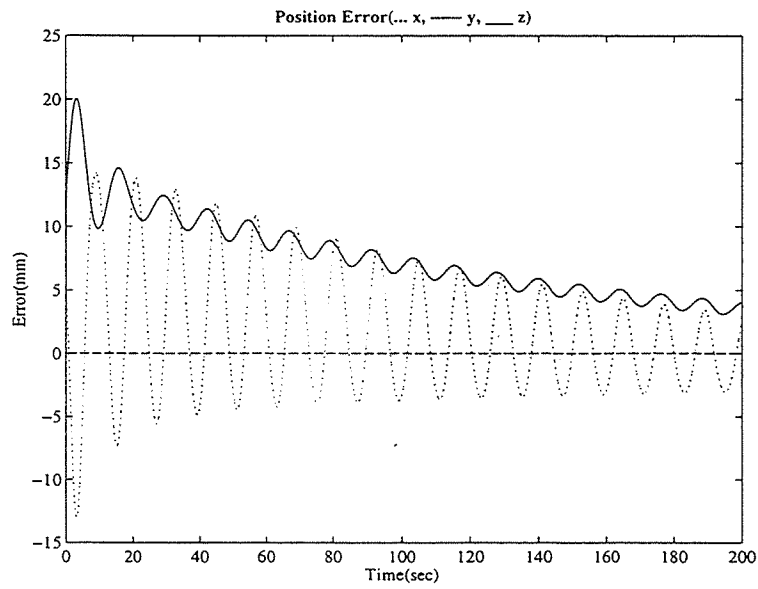


Figure 5.2: Position error in task space

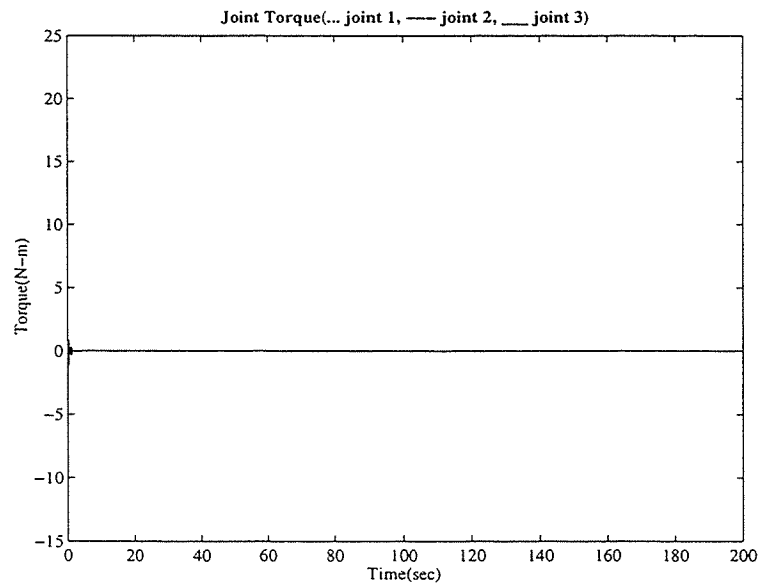


Figure 5.3: Actuator torque of each joint of the manipulator

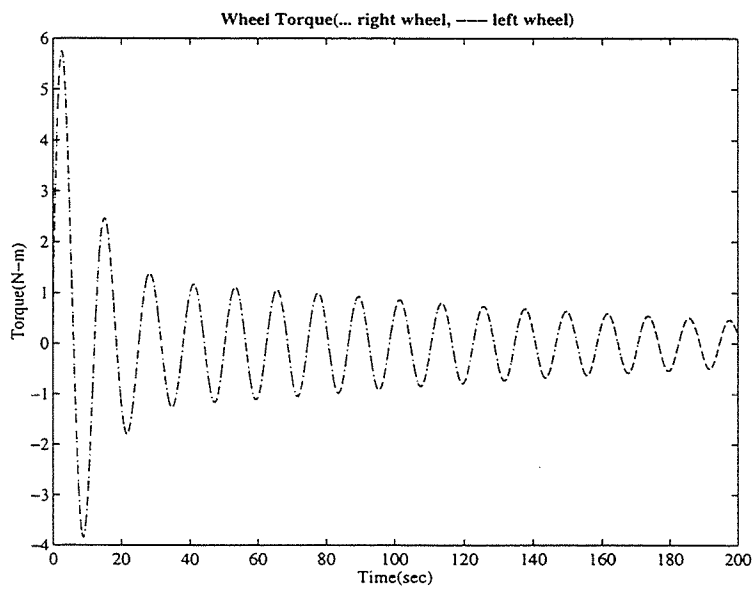


Figure 5.4: Actuator torque of each wheel of the mobile platform

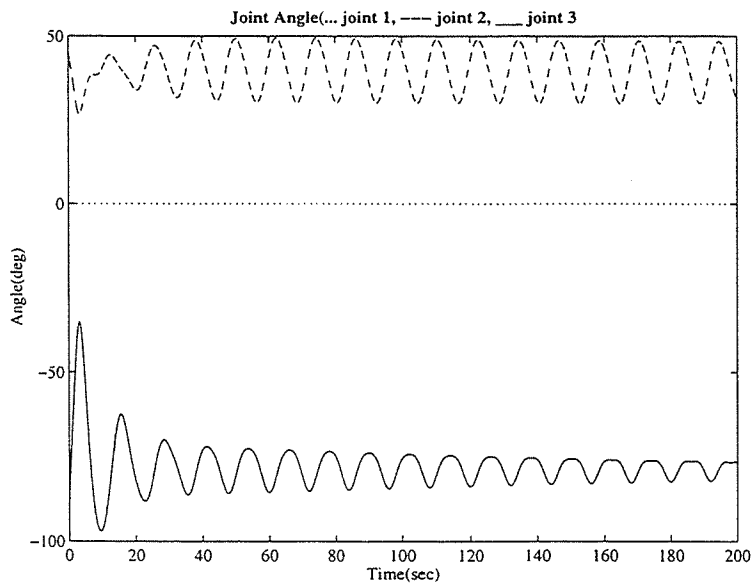


Figure 5.5: Angular displacement of each joint of the manipulator

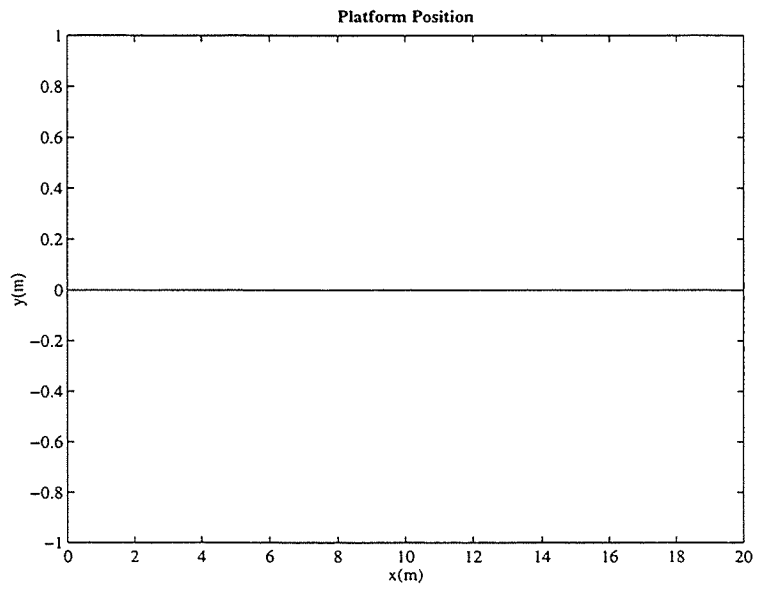


Figure 5.6: XY position of the platform

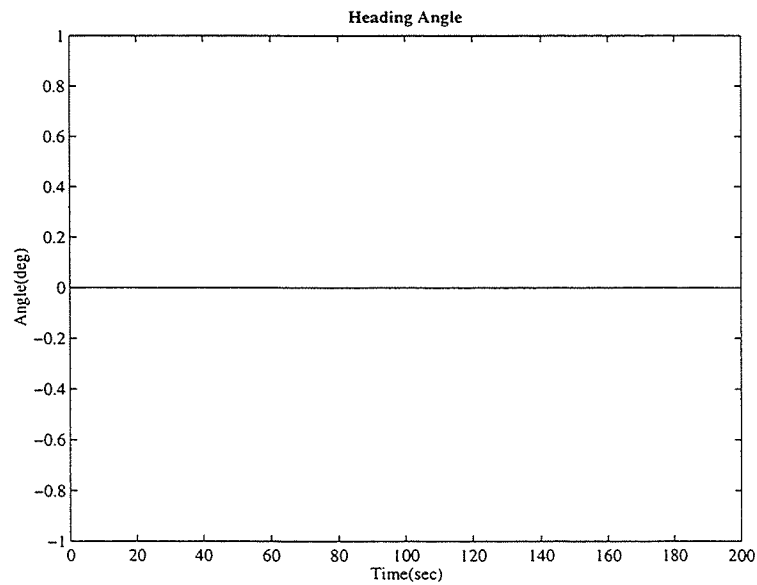


Figure 5.7: Heading angle of the platform

## Chapter 6

### Conclusion

The contributions of this thesis to the area of the modeling and control of mobile manipulators are given in this chapter. Then, future work based on the developments in this thesis is discussed.

#### 6.1 Contributions of this Thesis

Mobile manipulators are expected to play very important roles in the future in many applications. In fact, interest in the area of mobile manipulators has increased significantly because of their combined mobility and dexterity.

The primary goal of this research is to develop new control algorithms for a spatial mobile manipulator subject to nonholonomic constraints and kinematic redundancy. To achieve the goal, the actual research starts with the non-redundant mobile manipulator model in Chapter 3.

A wheeled mobile robot introduces nonholonomic constraints to the equations of motion when wheel slip is neglected. Therefore, the mobile manipulator which consists of a wheeled mobile platform and a robotic manipulator is also subject to nonholonomic constraints. In Chapter 3, the solvability of tracking problem is investigated for the non-redundant mobile manipulator subject to nonholonomic constraints. First, the Lagrange-d'Alembert formulation is used to obtain a concise description of the system dynamics which is in a form well suited for closed-loop control. Then, a nonlinear control law is derived based on static input-output linearization, and the efficacy of the proposed control scheme is verified by simulations.

In Chapter 4, the complexity of the model is increased by introducing kinematic redundancy which is created when a multi-linked manipulator is used. The kinematic redundancy is resolved by decomposing the mobile manipulator into two subsystems; the mobile platform and the manipulator. According to the redundancy resolution scheme, the manipulator is commanded to follow the desired trajectory given in task space and the platform is responsible for positioning the manipulator at a specified point in the workspace to avoid singular configurations of the manipulator. This motivates the development of the interaction control algorithm in which two nonlinear controllers are designed for the subsystems based on the redundancy resolution scheme. The interaction controller consists of robust adaptive controller for the manipulator and nonlinear PD controller for the mobile platform. The simulation results demonstrate excellent tracking performance of the interaction controller.

While the interaction control algorithm represents the significant contributions to the area of the control of mobile manipulators subject to nonholonomic constraints and kinematic redundancy, consideration of wheel slip might be crucial for high load applications because wheel slip is expected to act as a disturbance to the system. In Chapter 5, the dynamic equations of the wheeled mobile platform subject to wheel slip are derived. The simulation results show degradation of tracking performance of the interaction controller in terms of convergence speed to the desired error bound. Therefore, the presence of wheel slip motivates the design of a robust controller for the mobile platform subject to wheel slip.

## 6.2 Future Research

In the practical case of a desired trajectory ended by a rest position, it is known that the mobile platform is not stabilizable at the equilibrium point by at least continuous state feedback laws. To deal with this stabilization problem at equilibrium points, we can use a hybrid strategy and switch to a stabilizing time-varying feedback law when the trajectory enters a sufficiently small disk centered at the equilibrium.

The control algorithms for mobile manipulators were developed with the system subjected to ideal constraints. However, in the presence of wheel slip, it was shown that the tracking performance of the interaction controller can degrade. However, we were able to show that the wheel slip can be modeled as a disturbance to the system and satisfies the matching condition because the control variable and the wheel slip

appear in the same equation. This important fact motivates various approaches to the design of the outer loop control to stabilize the nominal system. Then, the additional feedback can minimize the harmful effects of wheel slip.

In this report, we considered one robotic manipulator mounted on a mobile platform. However, one might be interested in multiple manipulators on the same mobile platform. Then, the combined control algorithm of the interaction control and some kind of known coordinated manipulator control can be developed. Certainly, this would provide challenging performance and stability problems.

# Bibliography

- Boyden, F. D. and Velinsky, S. A. (1994). Dynamic modeling of wheeled mobile robots for high load applications. In *Proceedings of IEEE International Conference on Robotics and Automation*, pages 3071–3078.
- Brockett, R. W. (1983). *Asymptotic Stability and Feedback Stabilization*. Number 162 in Differential Geometric Control Theory. Birkhauser.
- Campion, G., d'Andrea Novel, B., and Bastin, G. (1991). *Exponential stabilization of Mobile Robots with Nonholonomic Constraints*. Number 162 in Lecture Notes in Control and Information Science. Springer-Verlag.
- d'Andrea Novel, B., Campion, G., and Bastin, G. (1995). Control of nonholonomic wheeled mobile robots by state feedback linearization. *International Journal of Robotics Research*, 14(6):543–559.
- de Wit, C. C. and Sordalen, O. J. (1992). Exponential stabilization of mobile robots with nonholonomic constraints. *IEEE Transactions on Automatic Control*, 37(11):1791–1797.
- Dubowsky, S. and B.Tanner, A. (1987). A study of the dynamics and control of mobile manipulators subject to vehicle disturbances. In *Proceedings of International Symposium of Robotics Research*, pages 111–117.
- Dugoff, H., Fancher, P., and Segal, L. (1970). An analysis of tire traction properties and their influence on vehicle dynamic performance. *SAE Transactions*, pages 1219–1243.
- Egeland, O. and Sagli, J. R. (1993). Coordination of motion in a spacecraft/manipulator system. *International Journal of Robotics Research*, 12(4):366–379.
- Feng, X. and Velinsky, S. A. (1996). Pulse width modulated control for the dynamic tracking of wheeled mobile robots. To Appear in *Eleventh CISM-IFTOMM Symposium on Theory and Practice of Robots and Manipulators*.

- Fernandes, C., Gurvits, L., and Li, Z. (1993). *Optimal nonholonomic motion planning for a falling cat*. Nonholonomic Motion Planning. Kluwer Academic Publishers.
- Ghamsepoor, A. and Sepehri, N. (1995). A measure of machine stability for moving base manipulators. In *Proceedings of IEEE International Conference on Robotics and Automation*, pages 2249–2254.
- Greenwood, D. (1988). *Principles of Dynamics*. Prentice Hall.
- Haug, E. (1989). *Computer-Aided Kinematics and Dynamics of Mechanical Systems*. Allyn and Bacon.
- Hootsmanns, N. A. M. and Dubowsky, S. (1991). The motion control of manipulators on mobile vehicles. In *Proceedings of IEEE International Conference on Robotics and Automation*, pages 2336–2341.
- Isidori, A. (1995). *Nonlinear Control Systems*. Springer-Verlag.
- Jagannathan, S. and Lewis, F. L. (1994). Path planning and control of a mobile base with nonholonomic constraints. *Robotica*, 12:529–539.
- Jang, W. M. and Wiens, G. J. (1994). Passive joint control of dynamic coupling in mobile robots. *International Journal of Robotics Research*, 3:209–220.
- Joshi, J. and Desrochers, A. A. (1986). Modeling and control of a mobile robot subject to disturbances. In *Proceedings of IEEE International Conference on Robotics and Automation*, pages 1508–1513.
- Kane, T. R. (1972). Experimental investigation of an astronaut maneuvering scheme. *Journal of Solids and Structures*, 5:313–320.
- Kane, T. R. and Scher, M. P. (1969). A dynamical explanation of the falling cat phenomenon. *Journal of Solids and Structures*, 5:663–670.
- Kanellakopoulos, I., Kokotovic, P., and Morse, S. (1992). Toolkit for nonlinear feedback design. *Systems and Control Letters*, 18:83–92.
- Kerr, J. and Roth, B. (1986). Analysis of multifingered hands. *International Journal of Robotics Research*, 4(4).
- Khosla, P. and Kanade, T. (1985). Parameter identification of robot dynamics. In *Proceedings of Conference on Decision and Control*.
- Li, Z. and Canny, J. F. (1990). Motion of two rigid bodies with rolling constraint. *IEEE Transactions on Robotics and Automation*, 6(1):62–72.

- Li, Z. and Canny, J. F. (1993). *Nonholonomic Motion Planning*. Kluwer Academic Publishers.
- Liu, K. and Lewis, F. L. (1990). Decentralized continuous robust controller for mobile robots. In *Proceedings of IEEE International Conference on Robotics and Automation*, pages 1822–1827.
- Liu, K. and Lewis, F. L. (1992). Application of robust control techniques to a mobile robot system. *Journal of Robotic System*, 9(7):893–913.
- Longman, R. W., Lindberg, R. E., and Zeed, M. F. (1990). Satellite-mounted robot manipulators - new kinematics and reaction moment compensation. *International Journal of Robotics Research*, 6(3):87–103.
- Marino, R. and Tomei, P. (1995). *Nonlinear Control Design*. Prentice Hall.
- Miksch, W. and Schroeder, D. (1992). Performance-functional based controller design for a mobile manipulator. In *Proceedings of IEEE International Conference on Robotics and Automation*, pages 227–232.
- Murray, R. M., Li, Z., and Sastry, S. S. (1994). *An Mathematical Introduction to Robotic Manipulation*. CRC Press.
- Nakamura, Y. and Mukherjee, R. (1989). Nonholonomic path planning of space robots. In *Proceedings of IEEE International Conference on Robotics and Automation*, pages 1050–1055.
- Nakamura, Y. and Mukherjee, R. (1993). Nonlinear tracking control of autonomous underwater vehicle. In *Proceedings of IEEE International Conference on Robotics and Automation*, pages A4–A9.
- Nenchev, D., Umetani, Y., and Yoshida, K. (1992). Analysis of a redundant free-floating spacecraft/manipulator system. *IEEE Transactions on Robotics and Automation*, 8(1):1–6.
- Papadopoulos, E. (1993). *Nonholonomic behavior in free-floating space manipulators and its utilization*. Nonholonomic Motion Planning. Kluwer Academic Publishers.
- Papadopoulos, E. and Dubowsky, S. (1991). On the nature of control algorithms for free-floating space manipulators. *IEEE Transactions on Robotics and Automation*, 7(6):750–758.
- Pin, F. G. and Culioli, J. C. (1992). Optimal positioning of combined mobile platform-manipulator systems for material handling tasks. *Journal of Intelligent and Robotic Systems*, 6:–.

- Pin, F. G., Culioli, J. C., and Reister, D. B. (1994). Using minimax approaches to plan optimal task commutation configurations for combined mobile platform-manipulator systems. *IEEE Transactions on Robotics and Automation*, 10(1):44–54.
- Pomet, J.-B. (1992). Explicit design of time-varying stabilization control laws for a class of controllable systems without drift. *Systems and Control Letters*, 18:147–158.
- Pomet, J.-B., Thuilot, B., Bastin, and Campion, G. (1992). A hybrid strategy for the feedback stabilization of nonholonomic mobile robots. In *Proceedings of IEEE International Conference on Robotics and Automation*, pages 129–134.
- Reed, J. S. and Ioannou, P. A. (1989). Instability analysis and robust adaptive control of robotic manipulators. *IEEE Transactions on Robotics and Automation*, 5(3):381–386.
- Samson, C. and Ait-Abderrahin, K. (1991). Feedback control of a nonholonomic wheeled cart in cartesian space. In *Proceedings of IEEE International Conference on Robotics and Automation*, pages 1136–1141.
- Sarkar, N., Yun, X., and Kumar, V. (1994). Control of mechanical systems with rolling contacts: Application to dynamic control of mobile robots. *International Journal of Robotics Research*, 13(1):55–69.
- Seraji, H. (1993). An on-line approach to coordinated mobility and manipulation. In *Proceedings of IEEE International Conference on Robotics and Automation*, pages 28–35.
- Slotine, J. J. and Li, W. (1989). Composite adaptive control of robot manipulators. *International Journal of Robotics Research*, 25(4).
- Sordalen, O. J., Dalsmo, M., and Egeland, O. (1993). An exponentially convergent control law for an underwater vehicle with nonholonomic constraints. In *Proceedings of IEEE International Conference on Robotics and Automation*, pages 790–795.
- Sordalen, O. J. and Egeland, O. (1995). Exponential stabilization of nonholonomic chained systems. *IEEE Transactions on Automatic Control*, 40(4):35–49.
- Spofford, J. R. and Akin, D. L. (1990). Redundancy control of a free-flying telerobot. *Journal of Guidance*, 13(3):515–523.
- Umetani, Y. and Yoshida, K. (1989). Resolved motion rate control of space manipulators with generalized jacobian matrix. *IEEE Transactions on Robotics and Automation*, 5(3):303–314.

- Vafa, Z. and Dubowsky, S. (1987). On the dynamics of manipulators in space using the virtual manipulator approach. In *Proceedings of IEEE International Conference on Robotics and Automation*, pages 579–585.
- Walsh, G., Tilbury, D., Sastry, S., Murray, R., and Laumand, J. P. (1994). Stabilization of trajectories for systems with nonholonomic constraints. *IEEE Transactions on Automatic Control*, 39(1):216–222.
- Wang, C.-C. and Kumar, V. (1993). Velocity control of mobile manipulators. In *Proceedings of IEEE International Conference on Robotics and Automation*, pages 713–718.
- Wiens, G. J. (1989). Effects of dynamic coupling in mobile robotic systems. In *Proceedings of SME Robotic Research World Conference*, pages 43–57.
- Yamada, K. (1993). Arm path planning for a space robot. In *Proceedings of International Conference Intelligent Robots and Systems*, pages 2049–2055.
- Yamamoto, Y. and Yun, X. (1994). Modeling and compensation of the dynamic interaction of a mobile manipulator. In *Proceedings of IEEE International Conference on Robotics and Automation*, pages 2184–2192.
- Zhang, Y. and Velinsky, S. A. (1994). Tracking control algorithms for the tethered mobile robot. Technical Report UCD-ARR-94-06-30-01, UCD.

# Appendix A

## Sensors

In many applications of robot control schemes, state variables are used as feedback signals. Many measurement devices and techniques have been developed to meet the needs of accurately measuring state variables. In the following sections, state measurement devices used in robotic manipulators and mobile robot systems are summarized.

### A.1 Angular Position Sensors

Position sensors are installed at each joint of most robotic manipulators. The most commonly used position sensors are encoders, synchros, and resolvers.

### A.1.1 Encoders

By far digital transducers called encoders are in wide use. Three major classes - tachometer, incremental, and absolute - are available commercially. Encoders of all three types can be constructed as contact devices or as noncontacting devices using either magnetic or optical principles. For the finest resolution, optical encoders are generally required.

The encoder is mounted on the servo motor. When the motor rotates certain degrees, the absolute position of that joint can be read from the digital output of encoder. The resolution of the encoder is equal to  $360/2^n$  degree, where  $n$  is the track's number.

### A.1.2 Synchros

Synchros are used to measure and compare the actual angular position with its commanded position. The error voltage is an ac voltage of the same frequency as the excitation and of amplitude proportional to the error angle. When the error angle is zero, the error voltage is zero and thus the system stays at rest. When the error voltage is not equal to zero, the motor will rotate so as to return the actual position to the reference angle.

Synchros are similar in construction to three-phase wound-rotor motors. There are one winding for rotor and three windings for stator. In operation, the rotor is energized with an ac voltage. The voltages induced on the three stator windings are

precisely related to the angle of the rotor. An electronic circuit known as "synchro converter" is used to convert the synchro output voltage to an analog or digital representation of the rotor angle.

### **A.1.3 Resolvers**

Resolvers are small ac rotating machines similar to synchros. In general, they have two stator windings and two rotor windings.

## **A.2 Angular Velocity Sensors**

In principle, the signal from a joint position sensor can be electronically differentiated to obtain joint velocity. However, if the joint position sensor has a noisy output, differentiating the position sensor signal can effectively magnify the noise sufficiently to make the servo system unstable or unreliable. To overcome this difficulty, several velocity sensors can be used to measure the joint velocity directly.

### **A.2.1 DC Tachometer System**

A DC tachometer system consists of a voltage meter and a small DC generator which produces an output voltage roughly proportional to speed. The latter is usually constructed with a permanent magnet stator and a multipole wound armature. The armature is connected directly to the rotating shaft of the servo motor which is used to

drive the manipulator joint. When the small permanent magnet DC generator rotates with the servo motor, its output voltage (when driving a high-impedance load) varies in proportion to the rotation speed of the armature. Voltage output variations can then be translated into speed changes or be used as a feedback signal to control the robotic manipulator.

## A.3 Angular Acceleration Sensors

Gyroscopes and accelerometers are used to measure rate of rotation and acceleration. Measurements are integrated once (or twice) to yield position. These instruments are commercially available in a wide variety of types and ranges to meet correspondingly diverse application requirements.

### A.3.1 Accelerometers

Most of the advanced accelerometers are dual axis angular tilt sensors with high resolution, response speed, and accuracy. These sensors make use of two accelerometers, one oriented along the  $X$ -axis and one oriented along the  $Y$ -axis, to measure the angular tilt of an object with respect to the horizontal. Typical accelerometers are equipped with an on-board microcontroller, A/D converter, and temperature sensor. The combination of temperature sensing and microcontroller yields a system requiring no user calibration. Accuracy of commercially available accelerometers is

typically  $0.1^\circ - 0.5^\circ$ .

### A.3.2 Optical Gyros

The basic optical rotation sensor consists of two laser beams traveling in opposite directions (i.e., counter propagating) around a closed-loop path. The constructive and destructive interference patterns formed by splitting off and mixing parts of the two beams can be used to determine the rate and direction of rotation of the device itself. Recently, the price of highly accurate fiber-optic gyros (also called laser gyros), used in airplane, have come down significantly. With the price tags of \$1,000 to \$5,000, these devices have now become more suitable for many robot applications.